December 2004 • NREL/SR-520-37195

Subcontractor Report

Development of Advanced Deposition Technology for Microcrystalline Si Based Solar Cells and Modules

Final Technical Report
1 May 2002–31 July 2004

Y.M. Li
Energy Photovoltaics, Inc.
Princeton, New Jersey

National Renewable Energy Laboratory
1617 Cole Boulevard, Golden, Colorado 80401-3393
303-275-3000 • www.nrel.gov

Operated for the U.S. Department of Energy
Office of Energy Efficiency and Renewable Energy
by Midwest Research Institute • Battelle

Contract No. DE-AC36-99-GO10337

December 2004 • NREL/SR-520-37195

Development of Advanced Deposition Technology for Microcrystalline Si Based Solar Cells and Modules

Final Technical Report
1 May 2002–31 July 2004

Y.M. Li
Energy Photovoltaics, Inc.
Princeton, New Jersey

NREL Technical Monitor: Bolko von Roedern

Prepared under Subcontract No. ZDJ-2-30630-28

National Renewable Energy Laboratory
1617 Cole Boulevard, Golden, Colorado 80401-3393
303-275-3000 • www.nrel.gov

Operated for the U.S. Department of Energy
Office of Energy Efficiency and Renewable Energy
by Midwest Research Institute • Battelle

Contract No. DE-AC36-99-GO10337

Executive Summary

The objectives of this project, covering the first two phases of an originally anticipated three-phase undertaking, are the development of novel deposition techniques for microcrystalline silicon materials (μc-Si, which is now more appropriately called nanocrystalline Si or nc-Si), and the demonstrations of solar cells with nc-Si absorbers, in single junction and tandem structures, of high efficiencies produced by low-cost, high-throughput, single chamber PECVD method. We have achieved the technical goals set for the end of this project (Phase II), which were: i) nc-Si single junction solar cells of 6% efficiency; ii) a-Si/nc-Si tandem solar cells of 8% post-light-soaking efficiency; iii) nc-Si films produced by HWCVD (at Syracuse University which focused on nc-Si material preparation). The efficiency values confirmed by NREL are 6.5% and 8.7%, respectively, for nc-Si single junction and a-Si/nc-Si tandem solar cells, produced with 'near-the-edge' nc-Si absorbers using mediocre ZnO/Al back contacts. Our nc-Si devices exhibit excellent stability in ambient or under light exposure, and typically show a slight increase in conversion efficiency after long-term illumination. The a-Si/nc-Si tandem solar cells show more notable degradation (~10-15%) under one-sun light soaking than 47-sun accelerated exposure (< 8%).

The significance of our accomplishments under this NREL subcontract is the demonstration, by good solar cell efficiencies, of the viability of nc-Si p-i-n type solar cell processing in a low cost, *single*-reactor (without load-lock), batch type, conventional RF-PECVD machine, using the hydrogen dilution technique (H_2+SiH_4 as supply gas mixture), on readily available SnO_2/glass superstrates, without relying on any exotic laboratory tricks. We are now more confident about the potential and practicality of the nc-Si PV technology than at the beginning of this project.

The most critical element in device processing has been found to be the seeding procedure by which nc-Si absorber (the i-layer) is grown over an amorphous-Si based under-layer or directly on a TCO front contact. We have conducted an extensive search for the best seeding techniques, including i-layer seeding and the novel 'closed chamber' seeding methods. Seeding by boron-doped p-layer, preferably on a ZnO-coated SnO_2, has resulted in superior nc-Si cells. Other highly challenging issues, such as dopant and impurity contamination, reproducibility, and tunnel junction performance for the a-Si/nc-Si tandem cells have been successfully addressed. We have also explored new TCOs in light-trapping structures for advanced optical engineering of devices.

We have established correlations between microstructure and device performance of the nc-Si materials. High-efficiency and high crystallinity of the i-layer are mutually exclusive in nc-Si solar cells. An extremely critical question for device performance and large-area uniformity is why superior nc-Si solar cells are made *only* with nc-Si absorbers grown in the vicinity of the boundary of transition from the nanocrystalline phase to the amorphous phase ('near-the-edge').

Our lower-tier subcontractor at Syracuse University has completed the setup for the 'combined' plasma and hot-wire CVD (HWCVD). Thin films of nano-crystalline silicon and possibly poly-crystalline silicon have been produced by a novel ceramics-HWCVD technique at relatively low temperatures. Microstructural and compositional measurements have been performed to study the crystallinity, structural attributes, and impurity levels. The existence of a second Si phase, other than conventional crystalline Si, is postulated. Infrared photocurrent spectroscopy has been developed for estimating defect density of absorber layers of nc-Si single junction solar cells.

Table of Contents

List of Figures

List of Tables

1. Introduction

This section provides an overview of this subcontract. The original objective of the proposed three-year project was primarily to demonstrate microcrystalline silicon (μc-Si) solar cells and 1 Ft^2 modules prepared by RF-PECVD in a low-cost, high-throughput, non-load-locked, single chamber system at Energy Photovoltaics, Inc. (EPV). A secondary goal, by our subcontractor at Syracuse University (SU), was to prepare μc-Si thin films using hot-wire CVD (HWCVD) in combination with RF-PECVD (the combined hot-wire and plasma method) for high growth rate μc-Si of device quality that cannot be obtained by either deposition method alone. Due to the termination of this subcontract at the end of Phase II, the project goals had been limited to the demonstration of high efficiencies of small area nc-Si single junction and a-Si/nc-Si tandem solar cells without attacking process scale-up issues critical for module fabrication. During Phase I, we recognized the small sizes of crystallites in the Si:H absorbers (~ 10-20 nm), and we began to refer to μc-Si as *nanocrystalline* silicon (nc-Si), which is a more accurate description of this type of materials, in our reports and publications (as is increasingly the practice by other workers). This Final Technical Report covers both Phase I and Phase II of the program. The emphasis here will be on the progresses made and key lessons learnt during the 27-months endeavor.

Background. In the last few years, hydrogenated microcrystalline silicon or nc-Si solar cells have generated great interests as a key component in the next-generation, thin-film silicon based multijunction photovoltaic (PV) devices. The remarkable progress in both solar cells [1] and modules based on nc-Si has led to about 9%, 14%, and 13% efficiencies, respectively, for nc-Si single junction solar cells [2-4], a-Si/nc-Si tandem cells [2-5], and a-Si/nc-Si large area tandem modules [4,5]. More recently, it has been recognized that low-temperature CVD Si:H thin films suitable as solar cell absorbers are actually a collection of Si nanocrystallites (typical sizes 5-20 nm) dispersed in an amorphous 'matrix'. Properties of nc-Si thin films are thickness-dependent (varying with deposition time and generally growth history) and asymmetric, often exhibiting column structures (conglomerates of tiny crystallites surrounded by non-crystalline tissues). The deposition conditions for nc-Si must be carefully tailored to obtain a set of desired properties appropriate for a given application. The prominent features of nc-Si as solar cell absorber are its much improved stability against light soaking, low electronic defect density, good photocarrier transport (collection lengths) allowing for larger absorber thickness, and long-wavelength optical absorption higher than that of crystalline Si which is non-existent for hydrogenated amorphous silicon (a-Si:H, or simply a-Si). The nc-Si approach to multijunction, spectrum-splitting devices can avoid the use of expensive GeH_4 needed to grow low-bandgap a-SiGe i-layers (vs. a-Si), and a simpler solar cell structure. A practical appeal is that high quality nc-Si can be prepared in RF-PECVD equipment similar to those used in the established industrial production of a-Si large-area PV modules. The requirement of thicker i-layer for the nc-Si bottom cell can be expected to significantly reduce shunting problem in the manufacturing of large-area PV modules. The a-Si/nc-Si tandem device is one of the most promising thin film candidates for cost-competitive photovoltaic applications in terms of efficiency improvement, scale-up potential, raw material availability, energy payback time, and performance under real-world, outdoor conditions.

The tasks of optimizing nc-Si solar cell conversion efficiency have largely been a trial-and-error exercise. The most critical requirements for nc-Si growth are: 1) Low impurity contaminations; 2) 'Near the edge' growth conditions (see later); 3) Low ion-bombardment energies for low defect density when using plasma deposition techniques. High growth rate is essential for

manufacturing nc-Si based PV modules due to the far greater thickness required in comparison with a-Si based PV products. Much remains to be learnt in search of a cost competitive implementation of the 'next-generation' hybrid a-Si/nc-Si thin film PV technology. Formidable challenges include, regrettably, the high costs associated with the lengthy deposition and the sophisticated equipment required to maintain good nc-Si uniformity over large areas. A particularly nasty and poorly understood phenomenon underlying the non-uniformity problem of nc-Si cells is the widely observed deterioration of cell performance with *increasing* degree of nano-crystallinity. That is, optimal nc-Si absorber is deposited *only* near the transition from nanocrystalline phase to amorphous phase (the so-called 'near-the-edge' nc-Si).

For a number of years, EPV has been successfully manufacturing 8 Ft^2, p-i-n type, a-Si/a-Si tandem PV modules on commercial SnO_2/glass by RF-PECVD using its proprietary 'box carrier' reactor capable of simultaneously coating 48 stationary plates in a *single* chamber without load-lock [6]. Besides low equipment costs and high throughput, the advantages of EPV's single-reactor, single-chamber PECVD system include high gas utilizations, a controllable low-contamination profile, ease of operation, and low maintenance. In the last two years, supported by the PVMaT program, we have improved the stabilized power of such modules from below 40W to the ~ 43W range [7], with higher yield, better process control, and lower costs. A more recent advance is the implementation of ZnO-enhanced rear reflector, ZnO/Al (versus Al alone), for even higher module power. By replacing the a-Si bottom junction absorber with nc-Si, we anticipate the efficiency of large area a-Si/nc-Si PV modules to reach 8% (on SnO_2/soda-lime glass) against the ~ 5.5% stable efficiency for our present a-Si/a-Si commercial modules (64 watts vs. 44 watts rated power). The low-cost, low-maintenance, easy to use, and high-throughput EPV manufacturing technology for a-Si/a-Si tandem PV devices is an attractive candidate for nc-Si solar cell processing as the large thickness or long deposition time of nc-Si absorber demands high 'effective throughput' (i.e., coated area per unit time, normalized to the capital costs of the equipment). EPV aspires to leverage its vast experiences in low-cost manufacturing of a-Si/a-Si tandem PV modules into the higher output and more stable a-Si/nc-Si modules to meet growing market demands for more efficient PV products at lower costs.

This Project. The key objective of this NREL subcontract is to take the first steps to extend EPV's RF-PECVD manufacturing technology to the promising field of a-Si/nc-Si solar cell fabrication by demonstrating 'proof-of-concept' devices of good efficiencies that previously were believed to be unobtainable in single-chamber reactors owing to contamination problems. A complementary goal is to find a new high-rate deposition method that can conceivably be deployed in large PECVD type reactors. We emphasize that our goal was *not* to produce 'champion' devices of near-record efficiencies, but rather to achieve modestly high efficiencies using a far simpler (cheaper) system, via practical processing methods and materials. To directly attack issues in solar-cell fabrication at EPV, the nc-Si thin films were studied almost *exclusively* in the p-i-n device configuration (as absorbers or i-layers), not as stand-alone films.

Highly efficient, p-i-n type, nc-Si based solar cells are generally grown on expensive, laboratory superstrates, such as custom ZnO/glass of high texture (granular surface) and low absorption [9]. Also standard is the use of a highly effective back reflector ZnO/Ag, where the ZnO can be surface-textured for efficient diffuse reflection [9]. The high-efficiency 'champion' devices made by the PECVD methods [2-4] were invariably prepared in sophisticated (read: expensive), multi-chamber, or at least load-locked deposition systems. The electrode utilization efficiency, defined as the surface area ratio of the powered electrode to that of the substrates, is typically

low at about one (1:1). To evaluate the true potential of nc-Si absorbers for cost-competitive, *commercially* viable manufacturing of large-area PV modules, we have taken a more down-to-earth approach, based on our proven production of a-Si PV modules by a massively-parallel batch process in single chamber RF-PECVD systems [6], to the study of nc-Si solar cells, with the aim of producing high efficiency a-Si/nc-Si solar cells and sub-modules.

Through this program, we have attempted to address some pressing issues facing nc-Si PV technology: 1) Costly UHV type multi-chamber reactors widely assumed to be essential for impurity and/or contamination control; 2) Low deposition rate per unit area of powered-electrode (or per unit volume of the reactor); 3) The use of expensive, specially-made substrates that are ill-suited for production. The work at EPV has focused on nc-Si *device* preparation using conventional RF-PECVD in a single-chamber system. The parallel and largely independent work at our lower-tier subcontractor, Syracuse University (SU) has been devoted to the novel growth technique of combining PECVD with hot-wire CVD (HWCVD), simultaneously in the same reactor, to harvest their complementary virtues for high-rate, high quality nc-Si suitable for solar cells. Some nc-Si solar cells have been characterized at both EPV and SU. In addition, through collaborations between EPV and the New Jersey Institute of Technology (NJIT, Mr. Liwei Li and Professor Roland A. Levy), the microstructures of a number of nc-Si single junction solar cells have been evaluated and correlated with their solar cell parameters [10].

It was highly critical for us, in the early stages of the subcontract, to gain some credibility for our uniquely challenging approach to fabricating nc-Si devices in a truly single reactor, multiple parallel-substrate PECVD system without the gas-dispersing showerhead (facing the substrate) commonly found in conventional PECVD reactors. The routine use of low-cost SnO_2-coated glass as superstrate was an additional obstacle. During Phase I, we tried to lay a solid foundation for advanced research in nc-Si based solar cells by broadly exploring device fabrication recipes and identifying process issues critical to device performance as detailed later. During Phase II, we built on the experiences gained in Phase I, and targeted the critical seeding problem for nc-Si solar cells, the difficult tunnel junction for a-Si/nc-Si dual-junction devices, and the front contact and back contacts including TCOs. At SU, nc-Si and poly-Si thin films were grown and characterized by various methods. The specific tasks carried out during the program include:

- Complete the construction, upgrading, and debugging of the deposition apparatus; make the necessary changes as required by the evolving processing conditions.
- Establish correlations between plasma or CVD processing conditions and nc-Si film growth rate, uniformity, microstructures, optical and transport properties, and solar cell parameters.
- Identify specific requirements for depositing high-efficiency nc-Si solar cells by single-chamber RF-PECVD, including base vacuuming, contamination control, and gas flow rates.
- Study and overcome key roadblocks for efficiency (e.g., seeding problem) and uniformity.
- Demonstrate the feasibility of producing nc-Si cells by the proposed low-cost method by producing devices of good FF, V_{oc}, efficiency, stability, and good reproducibility.
- Observe growth rate and non-uniformity under various processing conditions.
- Study and improve the stability of single junction and tandem solar cells upon light soaking.
- Identify root causes for problems in such areas as reproducibility, uniformity, and efficiency.

- Improve the optical design and implementation of nc-Si cells requiring better light-trapping.
- Demonstrate optimized devices by integrating all the progresses made in different areas.

Key results. Under NREL's support for over two years, starting from scratch, EPV has made great strides in developing nc-Si solar cell technology [8] as reported here. We have achieved the small-area device performance goals set forth in this subcontract. These include very *stable* single junction p-i-n type nc-Si solar cells of near 6% efficiency on untreated SnO_2/glass, and **6.5%** on ZnO-coated SnO_2 without AR (confirmed by NREL), using mediocre ZnO/Al back contacts, by single chamber, non-load-locked, fully stationary RF-PECVD. The best nc-Si single junction cells (i-layer ~ 1.5-2 μm) show FF over 71%, and V_{oc} of 500-530 mV. We have also met the 8% performance target for a-Si/nc-Si tandem solar cells (using SnO_2 front contact and ZnO/Al back contacts without AR), which show initial and light-soaked (500 hours under one-sun) efficiencies of 8.8% and 8.1%, respectively. A post-light-soaking efficiency of **8.7%** has been measured at NREL for an EPV a-Si/nc-Si 'micromorph' tandem cell. The good devices were built on improvements in the seeding procedure, contamination control, and understanding of nc-Si i-layers in the context of solar cell applications. We have also gained valuable insights into the critical tunnel junction issue for tandem devices, optical engineering required for nc-Si based solar cells, non-uniformity of nc-Si growth and limitations on high-rate deposition. At SU, nc-Si and poly-Si(?) thin films have been produced at low temperatures by novel ceramics-HWCVD. These films show a number of interesting properties as described in Section 6.

2. An Extensive Study of Seeding Methods for nc-Si Single Junction Cells

Unless otherwise stated, the nc-Si samples and solar cells discussed in the rest of the report were all produced by the RF-PECVD method at measured at EPV.

2.1 Equipment and solar cell fabrication procedure at EPV

Equipment Description. EPV's R&D system dedicated to this project is a scaled-down version of the much larger, batch-type, single chamber RF-PECVD machines containing 12 powered RF electrodes in parallel to simultaneously manufacture 48 a-Si/a-Si tandem plates of 0.79 m^2 size. This R&D apparatus, with a single RF-power electrode for coating four parallel substrates of 12"x15" in size, was constructed to closely resemble the production equipment for easier process transfer. The reactor is placed in a single-chamber vacuum vessel without any load-lock chamber. External channel strip heaters are placed on the outer side-walls of the chamber for irradiative heating of the interior of the chamber. This is the major limiting factor in the throughput of our reactor as it takes several hours to fully heat up glass plates (superstrates, loosely called substrates here) placed in the center of the reactor. Substrate temperatures are monitored by two thermocouples touching the outer side-walls of the substrate-carrier box, while heating is unconnectedly controlled by thermocouples mounted on the external walls of the vacuum vessel. An Edwards QDP-40 DryStar dry pump is used for plasma processes. Another dry pump (Edwards Scroll pump) is used for roughing down the chamber, and for backing a turbo-molecular pump used to create a base vacuum. The absence of any oil-based pump prevents oil vapor contamination of the system. For reliable pressure measurements, redundant pressure gauges and Baratrons (capacitive manometers) are used on the chamber and in all the

pumping pipelines. RF power at the conventional 13.56 MHz, capacitively coupled (the parallel-plate configuration) to the plasma between two pairs of substrates (one pair placed on each side of the power electrode), was initially supplied by an ENI ACG-6B, and later by a Dressler Cesar 136 power generator. The single chamber design dictates that vacuum is broken after *each* deposition run for substrates removal and loading. Very high vacuum has been unattainable (nor has it been necessary) due to routine atmospheric exposures. An RGA was sometimes used to determine the background impurity compositions before and/or after deposition. We found that, under high gas-flow conditions, the purity of the supply gas (H_2 and SiH_4) is more important than the base vacuum. Earlier in Phase I, severe instability of the ENI automatic RF matching network (model MW-10D) caused plasma ignition delays, plasma instability, hefty power loss outside of the plasma, and RF interferences with other electronic instruments. We solved the problem by building, in-house, a manual RF impedance matching network of excellent stability. For each plasma step, besides forward and reflected power, we monitor the RF *current* which is a more pertinent measure of plasma intensity than the commonly cited RF power value (wattage).

Device Fabrication. The single junction solar cells are of the superstrate, p-i-n diode variety: glass/TCO/p/i/n/b.c., where 'b.c.' stands for back electrical contact which is typically sputtered Aluminum (Al). The default front contact, TCO, is commercial grade SnO_2 on 3-mm thick soda-lime glass (LOF TEC7 or AFG PV-TCO), which has rather poor optical transmission (< 79%) and low haze (< 6-7% near the red-color region) that limits the short-circuit current, J_{sc}, of solar cells. The routine use of sputtered Al as back contacts was for its simplicity and fast device fabrication (for fast feedback on recipe development). In Phase II, sputtered ZnO/Al back contacts of higher reflectivity (than that of Al alone) were often used to obtain higher J_{sc} and cell efficiency. Occasionally, for better device performance called for by the Milestones of the subcontract, the superior and more granular Asahi SnO_2 on 1-mm glass (haze > 10%) was used. In later part of Phase II, a thin ZnO layer (200-300 Å) would be sputtered on to the SnO_2 to protect it against hydrogen-plasma etching and to facilitate Si:H nucleation (faster seeding). Due to the very limited supply of the preferred Asahi SnO_2 as front contacts, we have been unable to tailor our deposition recipes specifically for the higher-textured SnO_2 (with or without the ZnO protective coating). Instead, we have simply reproduced runs on Asahi SnO_2 using recipes developed on the lower-textured commercial SnO_2. We believe that our 'best' devices would have shown higher efficiencies had we been able to optimize recipes directly on Asahi SnO_2.

Most of the nc-Si i-layers (solar cell absorbers) were fabricated, by RF-PECVD method, from gas mixtures of silane (SiH_4) heavily diluted by hydrogen (H_2), at a H_2 to SiH_4 ratio of 20 to 300. This dilution ratio, R, would be even higher for seeding, depending on the choices of RF power level and total chamber ('chemical vapor') pressure. Supplementary argon (Ar) gas dilution was studied briefly as described later. The substrate temperatures were normally seen in the 170-200 °C range, which would typically increase by 10-20 °C during i-layer deposition for a fixed temperature on the external-chamber wall (due to plasma heating and thermal conduction by hydrogen). Boron and phosphorus dopant source gases were respectively trimethylboron (TMB, $[CH_3]_3B$) and phosphine (PH_3) for depositing doped p-layers and n-layers in the *same* reactor (same vacuum chamber) as i-layers, without *any* movement of the substrates and/or the reactor throughout the entire device fabrication. The occasional exception was for a-Si/nc-Si tandem cell fabrication when air-break or complete substrate removal (unloading) was needed as part of the tunnel junction formation process. There was no reactor cleaning between the runs or between individual layers in a given run. The reactor and vacuum chamber were normally cleaned every 3-4 months or after 50-60 deposition runs, thanks to the low-maintenance design

of EPV's plasma reactor. After turbo-molecular pumping for several hours, the base vacuum typically would reach mid- to low-10^{-6} torr before the onset of the nc-Si related deposition processes. Later on, the fabrication of a-Si/nc-Si tandem solar cells would follow the same general procedure for each individual junction, but with added steps between the two separate p-i-n devices (tunnel junction, see later discussion).

For single junction solar cell fabrication, a thin p-type layer (typically a-SiC:H p-layer when *bare* SnO_2 is used as front contact) would be first deposited on the TCO. This was followed by a seeding procedure (which might comprise several steps) to induce crystallization for the Si:H i-layer. Then, the 'bulk' of the nc-Si absorber (i-layer) would be grown. Finally, an a-Si (or nc-Si) n-layer was deposited. When ZnO-coating was used on top of SnO_2, seeding normally would be performed directly on the dual-layer TCO without a thin a-SiC p-layer (protective layer). Al back contacts (or later on, ZnO/Al) would be sputtered using shadow masks for cell definition (with cell areas between 0.16 and 0.25 cm^2). Early on in Phase I, the small area solar cells, near 0.2 cm^2 in size, were often defined by wet-etch (to remove Al film from non-cell areas) after blanket Al deposition without any mask. The wet-etch method tended to produce better cells (compared to shadow-mask cells) but it was more cumbersome to use routinely for the large numbers of solar cells that would be characterized for each device run. Light current-voltage curve (I-V), dark I-V, and spectral response (quantum efficiency, QE) under zero and negative electrical biases were customarily obtained for the solar cells. Device stability was studied for selected samples under one-sun and 47-sun irradiances (accelerated light soaking), and in the dark (ambient storage under partial room light). Microstructures of representative solar cells were probed by Raman scattering, X-ray diffraction (XRD), and atomic force microscopy (AFM) at NJIT. Optical absorption spectra of the nc-Si i-layers of a few solar cells have been studied by the infrared photocurrent spectroscopy technique at Syracuse University to be detailed later.

Device Characterization. To judge if the Si:H i-layer (absorber) in device configuration is amorphous, nanocrystalline, or mixed-phase (containing significant fraction of nanocrystalline phase), we have primarily relied on values of the long-wavelength QE or red-light response (e.g., at 800 nm), and the open circuit voltage, V_{oc}, of the solar cell as yardsticks. With the poorly-reflecting Al back contact, a-Si solar cells show zero QE at 800 nm, while its V_{oc} would be > 800 mV as compared to nc-Si cells (< 550 mV). We have also regarded superior stability of a thick device upon light exposure as being indicative of a substantially nanocrystalline absorber (in stark contrast to the poor stability of thick a-Si cells). Occasional micro-structural examinations by Raman scattering would confirm the 'phase' of the absorber. The complication is that, without proper seeding, many of the thick Si:H layers produced in this subcontract likely started as amorphous and then evolved into mixed-phase, and, under the right conditions with enough time, eventually became nc-Si. Such 'initially-amorphous' devices show higher V_{oc} (> 550 mV) and poor FF than solar cells whose i-layers are substantially nano-crystalline from the very beginning (near the p-layer). We lack sophisticated means to probe Si:H i-layers in their growth direction (in situ or post-deposition). Note that, in the study of various seeding techniques, we were mainly concerned with the *relative* changes of device parameters with recipe variations, not the absolute efficiencies of the devices. Thus, optical engineering of the devices (front TCO and back contacts) were largely 'neglected' until recently.

2.2 Importance of seeding

The performance of nc-Si solar cells depends on many processing details, chief among which are the seeding/nucleation technique to be discussed in this section, and the growth conditions for the bulk of the nc-Si i-layers to be described in Section 3. Here, seeding refers to the enabling procedure for an *abrupt* 'phase transformation' from the initially amorphous-Si (on a-Si alloy base-layer or foreign TCO) to the desired nanocrystalline phase for Si:H i-layer. This seeding step is absolutely crucial, regardless of deposition conditions for the 'bulk' Si:H i-layer, to ensure rapid yet device-friendly amorphous-to-nc structural conversion. Any slow and lengthy phase transition inside the i-layer, which necessarily ensues in the absence of a dedicated and effective seeding step, is a sure formula for 'disaster'. This became apparent from our first runs of nc-Si solar cells which exhibited 'mixed' behavior of a-Si and nc-Si, as those i-layers were initially amorphous and later nanocrystalline. Initial efficiencies and stability of such devices are terrible.

The foremost lesson we learnt during the project can be put this way: the seeding process can 'make or break' any p-i-n nc-Si solar cell. This is the reason why we relentlessly attacked the seeding problem through most of the program period. Device optimization for nc-Si is much more complicated than that for a-Si because, in part, the quality or suitability of the deposition conditions for the bulk i-layer can only be evaluated in the context of a chosen seeding recipe. Seeding determines both the critical p/i interface and the evolving properties of the bulk i-layer. *Both* seeding and nc-Si absorber ('bulk' i-layer) have to be done 'right' (with compatible interface) to obtain high efficiency and stability for p-i-n solar cells (with illumination from the p side). In contrast, the p and i layers in a-Si solar cells can largely be independently optimized. Single junction a-Si solar cells generally consist of the same type of layers (amorphous Si and its alloys, even though nc-Si doped layers can be used for equal but not higher performance), while nc-Si solar cells contain different types of Si:H films that, ideally, should make rapid yet smooth 'phase' transitions. Superior seeding process serves precisely this purpose.

Because the seeding layer should be as thin as possible, the conditions of seeding plasma in the nucleation stage are highly etching with very-low growth rate, substantially different from those for the bulk nc-Si i-layer. More than half of the device runs throughput this project (> 400) were devoted explicitly to the study of seeding effects on nc-Si single junction solar cell performance and absorber layer properties. Bear in mind that, our seeding procedure was severely constrained by three considerations: 1) The use of bare SnO_2 which, until later in Phase II when ZnO thin-film sputtering became available for over-coating SnO_2, precluded the possibility of growing nc-Si seed layer *directly* on the substrate (as SnO_2 is unstable against highly energetic hydrogen-rich plasma), requiring the presence of a 'protective' layer on SnO_2 that introduced notable optical loss and actually retarded seeding; 2) Importantly, in our *single*-reactor, single-chamber system, any seeding process must satisfy the stringent *non-contamination* requirement for nc-Si i-layer growth following the seeding procedure; 3) Seeding must be homogeneous over large substrates. Eventually we overcame the first and the third obstacles by ZnO over-coating of SnO_2, and by dynamic p-seeding using proper combination of pressure, power, and gas flow rates. The second demand has been met by minimizing dopant concentration and seeding time. The use of SnO_2 as the front contact (versus the much more commonly used ZnO at other laboratories) over an extended period had cost us a great deal in technical progress and devotion to other key issues.

The strong interplay between the seeding process and the bulk i-layer growth is one of the major difficulties in obtaining, and reproducing, high efficiency nc-Si solar cells. For a fixed set of i-layer plasma conditions capable of *sustaining* nc-Si growth (when the under-lying Si film is

already nanocrystalline), seeding or incubation (which may comprise several individual steps) *strongly* influences the properties of the Si:H absorber and its device performance. Under the same Si:H i-layer growth conditions using moderately high input RF power and high H_2/SiH_4 dilution, amorphous, mixed-phase, or nanocrystalline absorbers can be obtained, respectively, depending on the seeding history. **Figure 1** below shows distinctive Raman scattering spectra from three Si:H p-i-n devices, whose i-layers were prepared with different seeding procedures, but the 'bulk' i-layers were grown under the same plasma conditions. The strength of Raman signal near 520 cm^{-1} is taken as a measure of nano-crystallinity of the Si:H absorber. For the sample made with weak seeding, evidence of nano-crystallinity is largely absent despite the long deposition time (~3 hours, resulting in ~ 1.5 μm thick Si:H film), as we had found in quite a few the earlier devices (intended to be fully nc-Si). When seeding was intense and prolonged, depending on i-layer recipe, we obtained either a-Si or nc-Si absorber with little 'mixed-phase'. It appears that truly nc-Si cells possess a Raman-derived crystalline volume fraction, X_c (Raman signal strength at 520 cm^{-1} divided by the sum at 520 cm^{-1} and 480 cm^{-1}), of > 65%.

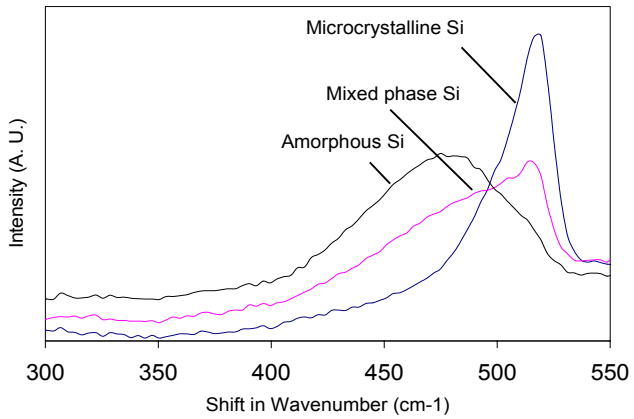

Figure 1 Raman scattering spectra of three Si:H single junction solar cells.

Conceptually, we loosely classify all seeding techniques into two types: 1) *i-seeding*, which is to induce nucleation inside the 'undoped' i-layer (close to the p/i interface for p-i-n solar cells), and the seed layer is part of the PV-active absorber layer; 2) *p-seeding*, which is to generate seeding action entirely inside the p-layer (with moderate or high level of boron doping), hence the seed layer serves both as p-layer and nucleation layer situated on the p-side of the p-i interface (if we ignore trace impurities). In either type of seeding, Si nucleation is assisted by very high H_2/SiH_4 dilution ratio and high RF power. To limit the thickness of the seed (transition) layer, a hydrogen-rich etching plasma (which causes subtraction of film thickness) may be helpful as a precursor (or even as the whole seeding step) to seed layer growth (addition of film). Practically, the demarcation between i-seeding and p-seeding is often blurred, as truly 'undoped' i-layer is hard to come by. We have also tested the combination of i-seeding and p-seeding to harvest their respective advantages for better overall seeding efficacy and higher solar cell performance.

We faced multiple hurdles in the critical seeding processes: high optical losses in the p-type seed layer (p-seeding); likelihood of cross contamination of i-layers by boron-containing seeding plasma, and more seriously by phosphorus that can be released during excessive plasma etching

(in closed-chamber seeding or pre-seeding H-etch processes) in our single-chamber PECVD; poor reproducibility due to contamination and shaky seeding efficacy; unsatisfactory uniformity of seed layer over the 12"x15" substrate area; sensitivity of seeding effectiveness to the texture or roughness of the SnO_2 superstrate; and generally poor compatibility with H-plasma and seeding processes of SnO_2 (which was used throughout most of the project aimed ultimately at the 'micromorph' a-Si/nc-Si tandem devices for which ZnO front contact is not nearly as crucial as for nc-Si single junction cells). These issues are expounded in the following sub-sections.

2.3 Seeding inside the i-layer of p-i-n solar cells (i-seeding)

The i-seeding tactic has not been widely practiced, presumably due to its poor device suitability resulting from the inevitable creation of high levels of defects by the energetic, strongly etching plasma needed for speedy nucleation in the seeding layer (which becomes part of the PV-active absorber). However, i-seeding has been used to produce reasonably efficient n-i-p type nc-Si solar cells [12], where the seeding process would occur near the far-less critical n/i interface instead of the p/i interface as is the case for p-i-n type cells. We have not seen any discussion on i-seeding for superstrate p-i-n type nc-Si cells. The motivation for studying i-seeding includes its suitability for single-chamber systems (where minimal deposition of doped layers is preferred to reduce cross contamination), the absence of optical loss to the 'dead' p-seed layer (as it is very tricky to grow transparent yet effective p-seed layer on SnO_2). We further speculated on the potential for higher V_{oc} when a wider-bandgap a-Si:H 'buffer' layer was deposited on the a-SiC:H p-layer prior to the onset of the i-seeding process. The cross-contamination issue is further described in Section 3. Early in Phase I, we deliberately took a big chance to work on the higher risk, poorly studied i-seeding methods, instead of the 'safer' p-seeding. We have found that the relatively short i-seeding (a small fraction of the total i-layer deposition time) often has an even greater influence on device performance than that of the commonly used p-seeding.

To avoid p/i interface plasma damages, we typically deposited a thin undoped a-Si buffer layer (100–400 Å) on the a-SiC p-layer before the start of i-seeding. Two versions of i-seeding were evaluated. In the simplest form, nucleation was attempted by intense glow-discharge etching, using pure H_2 gas, on the a-Si:H buffer layer (resulting in a reduction of buffer layer thickness). This 'etch seeding', performed at various pressures and durations, produced either amorphous or mixed-phase solar cells with terrible FF (e.g., 20-30%). We concluded that pure hydrogen etching, by itself, is incapable of generating a good 'template' for instantaneous nc-Si growth required for solar cell synthesis. The poor device behavior was partially due to excessive plasma damages on the a-Si:H buffer layer as confirmed by poor device characteristics of a-Si:H control cells deposited on the etched buffer layer. The other, more effective i-seeding method was to deposit a thin Si:H 'incubation' film at very low growth rate from a H_2+SiH_4 gas mixture of extremely high R (H_2 to SiH_4 dilution ratio), followed by an optional step of grading of SiH_4 flow rate (while keeping H_2 flow rate constant) leading to the growth of 'bulk' nc-Si i-layer. The combination of H-plasma etching and subsequent SiH_4 grading (at the beginning of i-layer deposition) has proved to work much better than H-plasma etching alone. **Figure 2** displays the variations with R of V_{oc} and red-response of nc-Si cells produced by i-seeding for a fixed set of bulk i-layer plasma parameters. Insufficient R resulted in largely amorphous and mixed-phase cells. All the solar cells obtained from i-seeding, with or without a subsequent SiH_4 grading leading to steady i-layer growth, exhibit low FF (< 50%), weak red-light response, and rather high V_{oc} (indicating that the initial i-layer was amorphous). The SiH_4 flow-rate grading step, seemingly beneficial in some cases, might be unnecessary if the seeding layers were sufficiently

developed (closer to the nc-phase), as evidenced from a number of experiments using either i-seeding or p-seeding. When marginal seed layers are used, i-layer grading may help to complete the nucleation process. For now, we cannot rule out the utility of i-layer grading, especially as part of an overall seeding formula (e.g., in combination of p-seeding to be presented later).

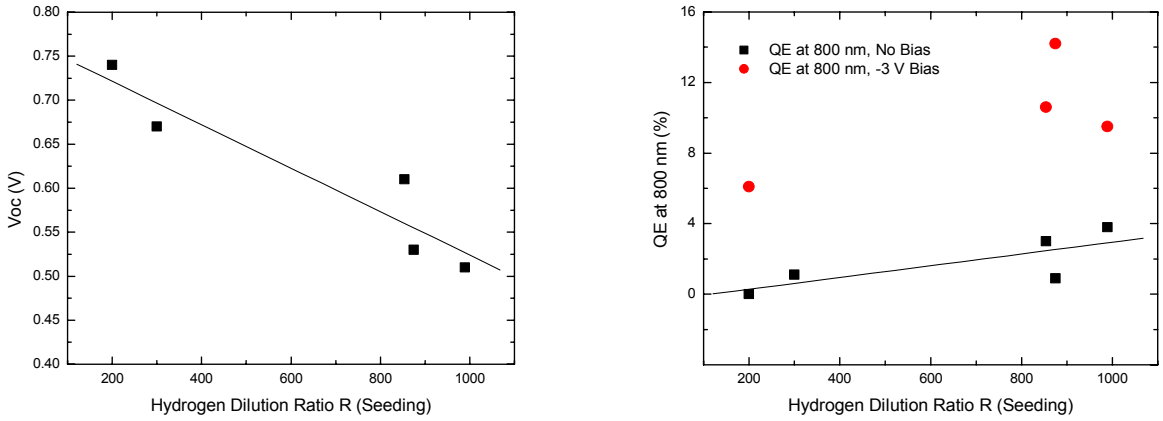

Figure 2 Effect of hydrogen dilution ratio R during i-seeding on V_{oc} (left) and QE at 800 nm (right) of nc-Si solar cells with Al back contacts.

Table 1 lists the PV parameters of representative nc-Si single junction solar cells produced with different seeding techniques, with a few variations in other device aspects as indicated. The nc-Si i-layers, near 1.5 μm thick, were deposited under the same conditions (except R130 at higher power) at a rate of ~ 1.2 Å/sec. The first entry, R130, shows that nc-Si cells can be made by simply etching the p-layer using H-plasma, without actually growing a seed layer. The FFs of such cells, however, tend to be low. Also, higher RF power is needed for the nc-Si i-layer (in part to compensate for the lack of fully-developed seeding), as standard nc-Si i-layers show low efficiencies (both FF & J_{sc}). The next two entries in the table illustrate PV properties of nc-Si solar cells made by the 'i-seeding + SiH_4-grading' on a-Si buffer, which generally show better V_{oc} than those cells attained from p-seeding or i-seeding without the a-Si buffer. In addition to low efficiencies due to both low FF and low J_{sc} (with strong bias-dependence of the QE), these cells show hefty light-induced degradation in efficiency, as expected from initially amorphous, thick absorbers. A complication in interpreting data from the earlier nc-Si devices is that, during the period, both seeding recipes and i-layer growth conditions were being varied (often in the same device), such that bad i-seeding might not be the sole origin for bad device performance.

In Phase II, we endeavored to improve i-seeding after we had gained a lot more insights from studying p-seeding techniques. We simplified our earlier i-seeding routine by eliminating the undoped a-Si 'buffer' layer, and forming i-seed layer directly on the a-SiC p-layer. Because of the powerful plasma used, some etching invariably occurs in the seeding process that would liberate dopants buried in previously deposited doped layers. Hence the distinction between p-seeding and i-seeding is no longer clear in many of the later i-seeding experiments. Surprisingly, this version of i-seeding worked much better despite the concern that direct exposure of the p/i interface to intense H-plasma would be harmful. We also learnt that the degree of i-seeding must be carefully controlled, as 'over-seeding' in i-layer can do more harm than 'under-seeding' for initial device efficiency. Better FFs were realized using direct i-seeding, as exemplified by the

four samples, R262, R247, R271, and R383 in table 1 (the fourth to seventh entries). These solar cells were grown without any grading after i-seeding. Many more runs were made by i-seeding than those listed here, encompassing a variety of seeding recipes. Despite the improvements in FF by i-seeding directly on the a-SiC p-layer versus the case of undoped a-Si buffer, the J_{sc} is still disappointing, and FF still low. The poor blue and low peak QE values, even under reverse electrical bias, placed a major drag on conversion efficiency. The low J_{sc} is not mainly caused by optical loss in the a-SiC p-layer, but is suspected to arise from carrier loss or recombination near the seeding interface (inside or close to the i-incubation layer), since the red-light QEs of such solar cells are relatively healthy and only weakly dependent on electrical bias.

Device I.D.#	Type of Seeding; Other Descriptions (seeding method, bulk i-layer feature)	V_{oc} (V)	J_{sc} mA/cm^2	FF (%)	Effi (%)
R130-1	Pure H-etch on a-SiC p; higher power for nc-Si i-layer	0.50	15.1	57	4.3
R139-1	i-seeding, on thin a-Si:H buffer over a-SiC p-layer	0.51	14.0	50	3.6
R141-1	i-seeding, on thin a-Si buffer over a-SiC p-layer	0.52	14.7	47	3.6
R262-1	i-seeding, without a-Si buffer, moderate power	0.46	15.3	63	4.4
R247-1	i-seeding at higher RF power, modified recipe	0.46	15.2	64	4.5
R271-1	i-seeding, high then low power (2-step), no buffer	0.48	15.0	63	4.5
R383-3	i-seed., no buffer, SiH_4 flow low then high (2-step)	0.47	15.5	55	4.1
R140-1	p-seeding, thick seed-layer (over SnO_2/a-SiC p)	0.50	13.8	70	4.8
R147-3	Closed-chamber (CC) 'static-mode' seeding, 1st trial	0.50	15.5	65	5.0

Table 1 Properties of some nc-Si devices made by i-seeding, and three cells made by alternative seeding methods for comparison (on commercial SnO_2, Al back contact).

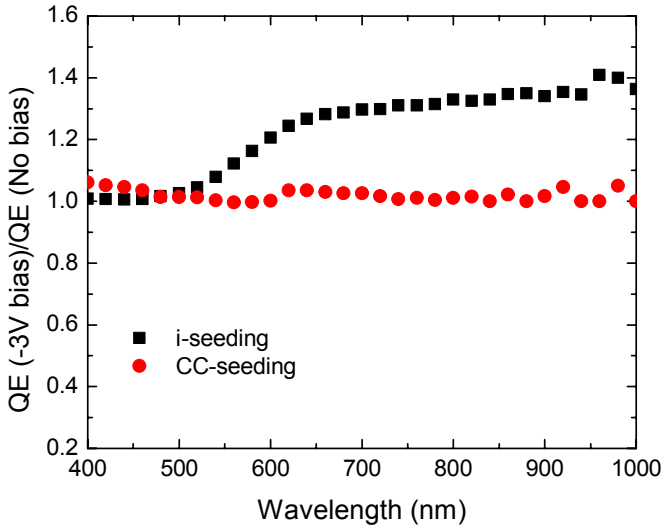

Figure 3 QE ratio spectra (-3 V to zero V electrical bias) of two nc-Si single junction solar cells prepared by i-seeding (R141) and CC-seeding (R147), respectively.

Figure 3 illustrates the carrier collection problem ubiquitously associated with i-seeding process, particularly severe at longer wavelengths, due to high defect density in the phase-transition region near the p-i interface. In contrast, solar cells produced by CC-seeding (or p-seeding) do not show such pronounced bias-dependent QE spectra in the absence of acute contamination.

Excessive i-seeding (longer time and/or higher RF power) resulted in very low V_{oc} and FF, presumably due to the formation of a highly defective seed layer (likely to be mixed-phase or even nanocrystalline) at the p/i interface. The thicker the i-seed layer, the lower the efficiency. Elevated nanocrystallinity has been found to correlate with inferior absorber performance compared to the 'near the edge' nc-Si. This is a major difficulty with i-seeding compared to p-seeding. While highly damaging to J_{sc} (severe optical loss), excessively developed, thick nc-Si p-seed layer (grown by p-seeding method) does not degrade the FF or V_{oc} of the solar cells. We also tried i-seeding with high power and high hydrogen dilution that would minimize the thickness of the highly defective 'incubation layer'. Devices with very low V_{oc} and poor FF resulted from either too little i-seed layer deposition (instead, a large fraction of the p-layer was probably etched off by the seeding plasma), or high density of defects generated by the intense i-seeding plasma. Another possibility was the formation of a highly nanocrystalline i-layer, unsuitable for i-layer purposes, near the p/i interface. For this reason, i-seeding is difficult to optimize and implement as a stand-alone technique for p-i-n type nc-Si solar cells.

We note that the various i-seeding processes have by no means been 'optimized'. Since the later part of Phase I, we decided to focus our limited resources on the more conventional p-seeding and the novel 'closed-chamber' seeding techniques. Although we have not made, by i-seeding techniques, highly efficient nc-Si devices, the experiences that we had acquired from i-seeding experiments proved to be constructive in developing other, more successful seeding techniques.

2.4 A novel seeding technique: 'closed chamber' plasma (static mode)

Since the launch of this project, we paid close attention to the uniformity of all processes over the 12"x15" superstrate areas. Because of the importance of seeding on nc-Si solar cell performance, homogeneous device performance (necessary for good nc-Si related PV modules) demands *both* uniform seeding and uniform i-layer. However, in the earlier periods, conventional 'dynamic' seed layer thickness-uniformity (either i-seeding or p-seeding) had been deemed unsatisfactory in our 'box-carrier' reactor. Further, we had been facing unacceptably large optical losses with p-seeding technique on SnO_2 superstrates to be detailed later. To address these two issues, we have explored an alternative scheme, called 'closed chamber plasma seeding' ('static seeding'), or simply CC-seeding. The hypothesis is that, in an isolated hydrogen-rich plasma confined by silicon-coated walls (including the substrates), etching and re-growth of SiH_x species ultimately would reach near-equilibrium on the surfaces exposed to the plasma, regardless of the initial conditions, because there is neither supply nor removal of species in the isolated environment (neglecting any outgassing, remote deposition of SiH_x species, and minuscule vacuum leaks). If so, the repeated removal and redeposition on a fairly stationary film surface should be conducive to structural conversion. Therefore, it might be *unnecessary* to grow a seeding film of some non-negligible, critical thickness (e.g., $\geq$ 100 Å) in order to secure template effect, as suggested by some publications (see, e.g., [14]). Rather, one can start with an amorphous Si film, perform 'static' plasma treatment, and get a 'restructured' surface (involving sub-surface atomic layers) that can exhibit 'memory' effect of a template for nc-Si growth. This prospect is extremely attractive for maximizing optical transmission through

the p-seed layers which, when deposited by conventional p-seeding, are highly opaque and too sensitive to even mild increase in its thickness, in stark contrast to wide-bandgap a-SiC p-layers.

The 'Closed chamber CVD' idea was previously applied to hydrogen treatment of a-Si layers in preparation of bulk nc-Si films by a cyclic process (alternating a-Si deposition and H-plasma treatment, in a layer-by-layer fashion) [13]. In contrast, our 'closed chamber' plasma technique was strictly intended for *seeding* (nucleation) purposes, and not in any way applied to the actual growth of nc-Si absorbers for solar cells (which would not make sense due to single-chamber cross contamination). Actually, by all device indications, the CC-seeding layers are not quite nanocrystalline. While the concept of 'closed chamber' plasma is not new, this is the first time that such an idea was applied to the task of nucleation specifically for nc-Si solar cells. Further, our purpose is not simply to show the possibility of seeding, but rather to solve the seed-layer *non-uniformity* problem in EPV's box-carrier RF-PECVD reactor. Another crucial distinction to be made is that we have made reasonably efficient nc-Si and a-Si/nc-Si solar cells (not just some stand-alone films to show an exotic deposition technique without making functional devices) in a single chamber, non-load-locked system. Our experiments provide first objective assessments of the potential and the limitations of closed-chamber processes for nc-Si *device* fabrications.

In the most basic CC-seeding scheme, a fairly thick a-SiC p-layer is first deposited on the TCO (SnO_2), just like that for a-Si:H solar cells (except thicker). Then the chamber is filled with either pure H_2 gas, or a mixture of H_2 and SiH_4 and TMB (SiH_4 is < 3%). An energetic plasma is ignited shortly after the vacuum system is put into the 'closed chamber' mode (when all gas inlet and pump-out valves are shut off). During CC-seeding, no gas is introduced into or extracted from the chamber, which maintains about the same pressure (a slight increase can be explained by plasma heating). The RF current tends to vary slightly (within 2-4%) over the CC-seeding period when RF power level is typically kept constant (except in multiple-step seeding runs). The first four entries in **Table 2** are examples of nc-Si single junction solar cells grown by the CC-seeding method (known at EPV as the 'Static Etch-Dep' seeding method).

Run I.D.	Seeding (nucleation) Method	V_{oc}	J_{sc}	FF	Effi.
	(type of TCO/glass front contact; type of back contact)	(V)	mA/cm^2	(%)	(%)
R147	CC-seeding ('static'), first trial; AFG SnO_2; Al b.c.	0.50	15.5	65	5.0
R310	CC-seeding, shorter, thin a-SiC p (more transparent)	0.48	16.3	56	4.4
R224	CC-seeding; Asahi 'U' SnO_2; ZnO/Al back contact	0.48	17.3	64	5.3
R352	CC-seeding; Asahi 'U' SnO_2; ZnO/Al back contact	0.49	17.8	61	5.3
R175	Quasi-Static seeding, very low H_2 flow rate; SnO_2; Al	0.50	16.0	65	5.2
R246	Standard p-seeding; AFG SnO_2; Al back contact	0.47	14.9	67	4.7
R407	Improved p-seeding; Asahi SnO_2; ZnO/Al	0.49	17.9	64	5.6
R417	p-seeding on thinner a-SiC p (Asahi SnO_2; ZnO/Al)	0.50	17.8	68	6.1

Table 2 Comparison of nc-Si solar cells produced by CC-seeding and p-seeding.

It was hoped that, after some sufficient period of CC-seeding, the gas phase SiH_x concentration would eventually be high enough to completely counter etching of Si:H film by the powerful hydrogen plasma. If this balance were reached, there would no longer be any change in Si film

thickness, and the atoms on the surface (top layers) would simply be repeatedly re-configured towards more crystalline structure (nucleation). In reality, the etching-redeposition equilibrium is never completely reached (although it is much closer than dynamic seeding), because, among other things, the internal reactor-box has an open bottom to allow some SiH_x species to escape and condense outside of the plasma zones. Instead, CC-seeding always entails etching (Si film getting thinner with time), even if there is a relatively high initial SiH_4 in the H_2 mixture (before the chamber is 'closed' off for plasma ignition). Thus, in our system, the CC-seeding does not work like the ideal case when the SiH_x species can be prevented from escaping from the plasma zones. True steady-states are not reached in the gas phase and on the film surfaces. Visual inspections confirm that CC-seeding is indeed superior to dynamic seeding in terms of seed-layer uniformity, particularly at high RF power. Non-uniformity of nc-Si i-layer (sec. 3) has prevented us from directly verifying CC-seeding uniformity by examining spatial variation of nc-Si cells.

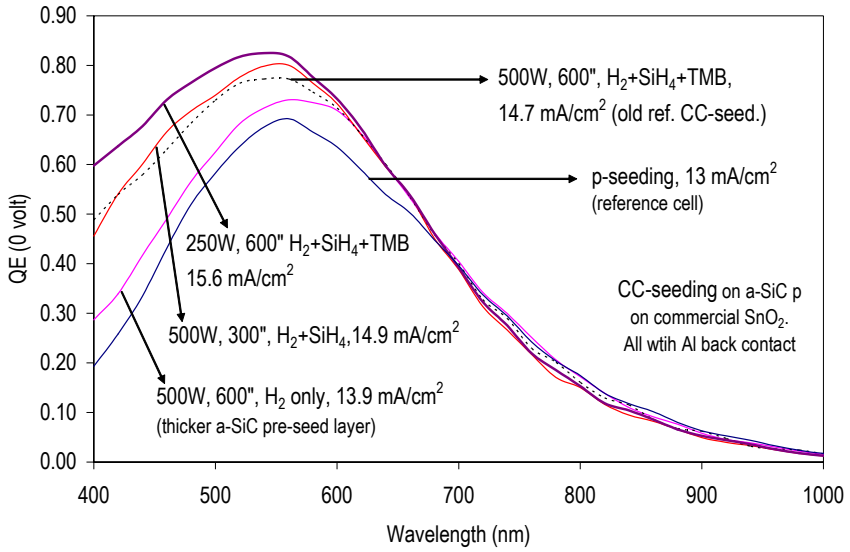

Figure 4 Examples of QE of nc-Si cells prepared by various CC-seeding recipes.

Figure 4 presents the QE spectra of four nc-Si solar cells made by CC-seeding compared to a cell made by p-seeding (dynamic seeding) which always led to depressed QE response in the visible spectrum for cells made on plain SnO_2. The main advantage of CC-seeding is the higher J_{sc} of nc-Si cells attributable to the reduced optical loss in the p-layer (markedly higher blue and peak responses). Note that all these cells suffer from mild boron cross-contamination in nc-Si i-layers due to lack of post-seeding 'flushing'. The absence of boron (TMB) in the supply gas mixture correlates well with improving spectral response, often at the expense of lower FF. Boron contamination seemed less problematic in CC-seeding cells when little TMB was used in the initial gas mixture filling up the chamber, compared to p-seeding with constant TMB supply. With brief Ar flushing after seeding, nc-Si cells look 'cleaner'. Rather high J_{sc} of ~16 mA/cm^2 was obtained by CC-seeding with ~60% QE at 400 nm and peak QE of 82% on low-quality AFG SnO_2. Examples are found in the following tables (e.g., R310 in table 7). Such cells were prepared by relatively short CC-seeding on thinner a-SiC p-layers. The cells with higher J_{sc}, however, tend to show lower FF (and efficiency), due to inadequate seeding and/or too thin a p-

layer (the a-SiC p-layer might have been weakened by the vigorous seeding plasma). Low FF would be obtained if CC-seeding time is too short (e.g., R222) or with too low a power (R317).

The principal challenge in optimizing the CC-seeding process has been poor reproducibility. The same recipe often did not produce adequately similar devices. It was rather coincidental that our very first attempt (R147) produced the best nc-Si cells on commercial SnO_2 superstrates (with Al back contact). Subsequent runs by CC-seeding were all inferior. Higher efficiencies by CC-seeding were only obtained using superior Asahi SnO_2 superstrates (usually in conjunction with ZnO/Al back contact), not due to improvement in CC-seeding recipe. The lack of process control had been incredibly frustrating for us over many months that delayed out progress in nc-Si cell improvement. At least two factors related to the history of the deposition system come into play. The first is the 'doping' history of the reactor. Depending on the type and doping level of the most recent layer from the last run (prior to the a-SiC p-layer in the present run), cell FF can be notably dissimilar. For instance, if the previous run was a relatively thick a-SiC p-layer film (or a-SiC p-film followed by H-plasma etching), the device prepared by CC-seeding would look better than that made after a normal n-layer. Thus, an earlier p-layer seems to 'cover up' some undesired surfaces of the reactor. We surmise that during CC-seeding, some of the internal surfaces in the reactor would be exposed to the plasma after the (locally-thin) a-SiC p-layer had been completely etched off, thus liberating dopants embedded in the under-layer. Under intense plasma, phosphorus cross-contamination is suspected to be more likely when the total thickness of p-layer (including p-seeding layer) falls below some minimum value. If phosphorus (in n-layer) is released, the CC-seeding layer is adversely impacted (more on this later). In contrast, plasma release of boron would not do much harm to the seed layer.

Cell #	Pre-run Reactor History (all cells on AFG SnO_2, Al b.c.)	V_{oc}	J_{sc}	FF	Effi
R147-3	Standard, made after reactor was coated with a p-layer	0.50	15.5	65	5.0
R221-2	Exact re-run of above, including p-layer coating of reactor	0.47	15.5	64	4.7
R210-2	Exact re-run of R147, but with 99.999% H_2 (vs. 99.9999%)	0.47	15.5	64	4.7
R155-2	As R147, except reactor was pre-coated with n-layer (not p)	0.46	14.4	60	4.0

Table 3 'History' and gas-purity dependence of nc-Si solar cells by CC-seeding.

Another factor affecting the consistency of CC-seeding is the reactor hardware itself. The inter-electrode spacings of the reactor could be slightly altered after cleaning and re-assembly. This problem was manifested when two nc-Si solar cell runs were made using identical recipes before and after reactor cleaning, showing markedly different cell efficiencies from the same substrate location. The inter-electrode spacing could vary by 1/32" to 3/64", a change large enough to cause non-trivial deviations in high-power plasma processes, especially the seeding procedure where the balance between etching and deposition is delicate. Also note that, large substrates and/or substrate carriers (for holding small pieces of substrates) are rarely perfectly flat, causing additional variations in discharge spacing.

We have also found that the purity of the H_2 gas affects the efficacy of CC-seeding (in addition to and separate from its effect on nc-Si i-layer). More than once (see table 3), when we changed the H_2 cylinder from 99.9999% to 99.999% (without any purifier or oxygen getter), vastly different cells were produced using the same recipe (former nc-Si cells would become mixed-

phase cells). Apparently, minute impurities in the initial gas mixtures (filling up the chamber before going into the closed-chamber mode) could drastically modify the surface nucleation process. This again reflects the weakness of the CC-seeding method. In brief, we believe that the CC-seeding technique should work better and more consistently in multi-chamber PECVD systems (where seeding can be done in a dedicated p-type deposition chamber) with carefully executed procedures. Since late Phase I, when an H_2-gas purifier was installed, no differences have been seen between UHP or research grade H_2 (99.999% vs. 99.9999%), and the process has been better controlled.

At times we suspected an effect of carbon concentration in a-SiC p-layer on CC-seeding and nc-Si cell efficiency. Higher CH_4 flow during a-SiC p-layer deposition apparently could degrade the potency of the seeding process, as shown, in **Table 4**, by two nc-Si solar cells prepared with different CH_4 volume fractions in the gas mixtures for a-SiC p-layer depositions. It would seem that carbon species incorporated into the base-layer can either directly deter surface-layer phase transition, or indirectly in the gas phase (after they are released from the solid phase by etching). At other times, however, carbon content in the a-SiC p-layer showed no obvious correlation with device performance. In fact, the use of unalloyed a-Si p-layers without any carbon (versus a-SiC p-layers) did not produce, by CC-seeding, nc-Si solar cells of better FF or efficiency. One might have suspected that, since the presence of carbon hinders the Si nucleation process, higher C% in the p-layer (which would be partially etched off), and later in the gas phase, would have some profound impact on the CC-seeding process. The absence of any consistent effect is puzzling.

Device#	Pre-seeding a-SiC Dep. Conditions (all on AFG SnO_2, Al b.c.)	V_{oc}	J_{sc}	FF	Effi.
R210-2	Standard CC-seeding recipe; standard a-SiC p pre-layer.	0.47	15.5	64	4.7
R203-1	High CH_4% in gas mixture for a-SiC p-layer	0.46	14.3	59	3.9
R205-1	Low CH_4% in gas mixture for a-SiC p-layer	0.48	14.5	63	4.4
R296-2	*No* CH_4% in gas mixture in depositing pre-seed layer (a-Si p)	0.46	15.2	53	3.7
R163-2	Thicker a-SiC p (pre-seed layer), somewhat lower RF power	0.47	14.1	66	4.4
R164-3	Thinner a-SiC p (pre-seed layer), even lower RF power	0.48	13.7	63	4.1

Table 4 Dependence of nc-Si solar cell by CC-seeding on pre-seeding a-SiC p-layer.

We wondered if a thicker p-layer (of wider-bandgap) is more suited as the precursor for CC-seeding (and p-seeding). A more transparent a-SiC p-layer with lower boron and higher carbon contents was developed for this purpose. Such a p-layer has worked well in a-Si single junction cells. The wider-gap p-layer (the under-layer grown just prior to CC-seeding) did not in general bring out higher nc-Si cell efficiency or J_{sc}. Still, device reproducibility was notably improved when using a thicker p-layer on SnO_2, avoiding etching-caused collapse of p-layer.

Table 5 lists some nc-Si solar cells prepared by CC-seeding using various initial gas mixtures (gas composition prior to 'closing' of the chamber). These cells were made on AFG SnO_2 TCO, with Al back contact. Their FFs are lower than what would be on less-textured LOF SnO_2. The J_{sc} and QE responses (blue and peak) of the cells are a function of the thickness and band-gap of the a-SiC p-layers, seeding time (degree of etching-away of the p-layer), and the SiH_4% of the initial gas mixture. Data suggest that the initially moderately-thick a-SiC p-layers were etched to

a large extent by prolonged closed-chamber plasma. In the extreme case, the a-SiC p-layer could be completely etched away (and SnO_2 reduced), resulting in cells of terribly low FF and J_{sc}. The very low FF of cell R308 in the table is believed to be caused by excessive CC-etching. Pure H_2 tended to cells of lower FF than those made from gas mixtures containing SiH_4 (and TMB which is delivered in SiH_4). Presumably, the existence of some SiH_4 in the initial gas mixture would retard the etching of the pre-existing a-SiC p-layer and allow the near-equilibrium between etching and re-growth of SiH_x species to be reached earlier. Another possibility is the dopant-burial effect by the initial deposition of a thin Si film (instead of etching from the start).

Run #	Initial Gas Mixture (filling up the chamber before seeding)	V_{oc}	J_{sc}	FF	Effi.
R308	Pure H_2 (no SiH_4 or TMB before Closed-chamber plasma)	0.49	15.6	45	3.4
R161	Pure H_2 (no SiH_4 or no TMB); flush > 10 min. after seeding	0.46	15.6	57	4.1
R307	H_2 + small amount of SiH_4 (no TMB); thinner a-SiC p	0.48	16.0	60	4.6
R342	H_2 + larger amount of SiH_4 (no TMB); wider-gap a-SiC p	0.49	14.7	63	4.5
R313	H_2 + small amounts of SiH_4 + TMB, thick a-SiC p	0.47	15.9	59	4.4
R333	H_2 + larger amounts of SiH_4 + TMB	0.47	14.0	63	4.1
R339	H_2 + largest amounts of SiH_4 + TMB	0.47	13.5	65	4.1
R342	H_2 + larger amounts of SiH_4 + TMB; wider-gap a-SiC p	0.49	14.7	63	4.5

Table 5 Dependence of nc-Si solar cells on initial gas composition prior to CC-seeding.

CC-seeding has been found to be sensitive to the degree of haze or texture of the TCO. The recipe works best on the smoother LOF SnO_2, versus the slightly rougher AFG SnO_2, and especially the more-granular Asahi SnO_2. Cells made on Asahi SnO_2, using recipes developed on the less-hazy LOF SnO_2, did not work much better (unlike the case for p-seeding) despite the far superior optical attributes of Asahi SnO_2. We suspect that CC-seeding is not quite as robust as p-seeding. A marginal seed 'template' on smoother SnO_2 would become less effective on the rougher substrates. CC-seeding has proved to be ill-suited for higher-textured TCOs.

More complicated multi-step CC-seeding schemes were only cursorily explored, including two-level RF power (high to low or low to high) and combination of CC-seeding with i-seeding or with p-seeding (see the next sub-section). These more sophisticated procedures did not lead to superior devices compared to the simple, one-step CC-seeding recipes. Since mid-Phase II, we focused on the simpler, more expedient p-seeding technique, and merely applied CC-seeding to some a-Si/nc-Si tandem cells without further fine-tuning. It remains to be seen if CC-seeding can be performed on ZnO-coated SnO_2, without first depositing a pre-seeding a-SiC p-layer.

We compared CC-seeding with 'quasi-CC-seeding (i.e., with constant flow of pure H_2 at a very low rate during seeding, versus the completely-static mode). Under relatively high power and chamber pressure (when low H_2 flow does not lead to rapid removal of Si_x species etched off from the film surfaces), the nc-Si solar cells made by quasi-CC-seeding were rather similar to the case of CC-seeding (using the same RF power, pressure, and seeding time). Quasi-CC-seeding can alleviate vapor-phase impurity buildup in the closed chamber which may impede seeding. There was little evidence of reduced cross contamination or improved seeding action in the solar cells, as shown in **Table 6**. The seeding uniformity is only slightly worse than true CC-seeding

(but would have been much worse had high H_2 flow been used). The best devices from either method have similar efficiencies of ~5% (commercial SnO_2 and Al for front and back contacts). Also, quasi-CC-seeding method worked notably better than low-pressure H-etching (using high H_2 flow and high RF power for high-rate etch without any deposition of film). Quasi-CC-seeding recipes share the same difficulties as those encountered by CC-seeding outlined above.

Run #	Seeding Type: closed chamber or quasi-static @ low H_2 flow	V_{oc}	J_{sc}	FF	Effi.
R161	True CC-seeding, pure H_2 (no SiH_4 or TMB)	0.46	15.6	57	4.1
R159	True CC-seeding, pure H_2; Ar flush before i-layer	0.47	15.5	59	4.3
R309	True CC-seeding, pure H_2; wider-gap a-SiC pre-seed layer	0.48	16.1	58	4.5
R175	Quasi CC-seeding, LOF SnO_2; reactor pre-coated with a-Si p	0.49	15.5	65	4.9
R178	Quasi CC-seeding per R175; i-layer SiH_4 flow higher by 13%	0.48	14.5	63	4.4
R221	Quasi CC-seeding, exact re-run of R175 incl. reactor history	0.47	15.5	64	4.7

Table 6 Comparison between CC-seeding and quasi-CC-seeding (low H_2 flow rate).

In an effort to retard the etching effect of strong hydrogen-rich plasma needed for fast seeding, we introduced argon (Ar) to the gas mixtures used in CC-seeding. A number of interesting nc-Si single junction cells was made using different H_2:Ar ratios (1:2 to 4:1). Apparently, the presence of substantial amount of Ar in the seeding gas mixture did indeed slow down the rate of etching (removal of Si species from the film surface), and did not greatly compromise seeding efficacy, provided that the dominant constituent of the initial gas mixture is H_2 and not Ar. In **Table 7**, examples are given of nc-Si single junction solar cells fabricated by CC-seeding with H_2+Ar (and small amounts of SiH_4 and TMB), in comparison with some cells created by H_2 'dilution' only. Both methods seem to work equally well. It is inconclusive as to whether the presence of Ar is advantageous for higher device performance, although we are inclined to think that in a single-reactor system, the suppression of etching-induced release of dopants (embedded in reactor interior walls) is highly desired for subsequent growth of 'intrinsic' nc-Si absorber.

Device #	Closed Chamber (CC) Seeding, Initial Gas Mixture	V_{oc}	J_{sc}	FF	Effi.
	(Mostly on commercial SnO_2, with Al back contact)	(V)	(mA /cm^2)	(%)	(%)
R310-2	H_2 dilution only; thin total p-layer (incl. p-seed layer)	0.49	17.0	56	4.7
R332-2	H_2 + Ar dilution; thicker pre-seeding a-SiC p-layer	0.46	14.8	65	4.4
R338-3	H_2 + Ar dilution; moderate pre-seeding a-SiC p-layer	0.48	15.7	63	4.7
R342-2	H_2 dilution only; wider-gap p-layer (higher C%)	0.50	16.5	59	4.9
R352-3*	H_2 only. *On Asahi SnO_2, with ZnO/Al back contact	0.49	17.7	61	5.3

Table 7 PV parameters of some nc-Si devices prepared by H_2 or H_2+Ar in CC-seeding.

To summarize, CC-seeding is an intriguing, under-explored method capable of producing more transparent, uniform, and effective seed layers with low latent contamination. CC-seeding is best

performed at high chamber pressures, with an initial H_2-dominated gas-mixture that contains some SiH_4 and a bit of TMB. Addition of Ar in the seeding gas has little effect. The drawbacks of CC-seeding include relatively poor device reproducibility sensitive to reactor history and substrate type. Quasi-CC-seeding produces similar devices as by true CC-seeding, which has been found to be compatible with conventional SnO_2 front contact (and a-SiC p-layer), and to be particularly suited for EPV's PECVD system (single-reactor with side-to-side gas flow pattern).

2.5 Conventional p-seeding and improvement of nc-Si single junction solar cells

As evident from earlier discussions on i-seeding and CC-seeding (closed chamber plasma), the nc-Si devices show common symptoms of low FF, resulting from weak seeding efficacy and, in the case of i-seeding, high defect density near the p/i interface. From the inception of this project, we intended to keep an open mind and search broadly for the high-performance seeding technique most compatible with our particular PECVD system. Thus, the conventional p-seeding technique was being developed during this program (more intensely in some periods than others), initially as a reference against which all other seeding methods were judged, and later as the optimal seeding method for high efficiency nc-Si solar cells (once it became clear that alternative means did not work as well), especially during Phase II. Eventually, we fruitfully applied the p-seeding method to ZnO-coated SnO_2 and obtained high-efficiency nc-Si solar cells.

Simply, p-seeding is the incubation process through the deposition of a boron-doped Si:H p-layer under energetic, highly H-etching plasma that promotes nucleation (and is resistant to amorphous film formation). The resulting p-layer (the seed layer) is probably not exactly nanocrystalline (which would require more time and greater film thickness than what is most favorable for solar cells), but it should be sufficiently 'mixed-phase' with dense nuclei to serve as a 'template' to induce immediate nc-Si growth. Generally, the boron-doped p-type Si:H seed layers behave like thick, narrow-bandgap films. The tricky part is the thickness of the seed layer which, optically, is rather opaque, and which must be sufficiently thick to achieve the desired seeding efficacy. As shown below, we have not been able to avoid excessive optical loss to the p-seed layer when plain SnO_2 was used as the front contact, unlike the case when SnO_2 was covered by a very thin ZnO over-coating (see section 2.5.3).

2.5.1 p-seeding on SnO_2/glass superstrates for p-i-n single junction nc-Si solar cells

Finding an optimal trade-off between optical loss (J_{sc}) and FF has been the central aim in our p-seeding experiments. Commercial SnO_2 on soda-line glass (versus costly, custom ZnO favored by other groups) had been our standard superstrate until late in Phase II when ZnO-coated SnO_2 was often used for nc-Si single junction cells (but not for a-Si/nc-Si tandem cells). To avoid SnO_2 'darkening' by hydrogen plasma, we normally grew a wide-bandgap a-SiC p-layer (30-300 Å) as a protective layer on SnO_2. This protective layer could be much thinner than that used for CC-seeding (where the a-SiC p-layer would be partially etched off, without any actual film being grown during seeding). Then a p-type seed-layer would be grown by intense H-rich glow-discharge. The nc-Si cells were much worse (low FF and J_{sc}) when p-seeding was performed directly on bare (un-protected) SnO_2. Note that the optical losses (QE at 400-600 nm) of the nc-Si cells (not amorphous or mixed-phase cells) were relatively insensitive to the thickness of the wide-bandgap p-type a-SiC underlayer. Rather, optical losses were, for p-seeding, dominated by the initially amorphous seed layer (low-bandgap incubation layer). Device data were often difficult to decipher, since low QE could be caused by optical and/or transport (collection)

problems. While it was far easier to obtain good FF (> 64%) and decent V_{oc} (0.46-0.5 range) with a single-step p-seeding (very simple recipe), at the same time it proved far harder to avoid hefty optical loss and obtain good J_{sc} for high solar cell efficiency, as indicated by the devices in the previous tables (other, much worse cells are not shown here). Note that truly nanocrystalline Si would be far more transparent (wider bandgap), compared to the largely amorphous p-seeding Si film with high absorption coefficient (enhanced by boron doping or narrowing bandgap).

Strong H-plasma 'etching' alone (using pure H_2 gas, vs. H_2+SiH_4+TMB in p-seeding) on a-SiC p-layer appeared to be capable of inducing nc-Si absorber growth (e.g., R130 in table 1), but the effectiveness seems inferior to CC-seeding or quasi-CC-seeding reported earlier. Similarly, when SiH_4 concentration in the p-seeding gas mixture is too low, seeding effect often becomes diminished (as net etching occurs during seeding). That is, if the seeding plasma is truly etching (causing a thickness reduction of the underlying a-SiC p-layer) without eventual growth of Si:H film, poor nc-Si cells are frequently seen. After a number of runs, we concluded that dynamic H-etching (using high H_2 flow, high power, at lower vapor pressures than CC-seeding) does not afford adequate seeding action when the nc-Si i-layer is grown from relatively 'soft' plasma at low growth rates. Stronger plasma for i-layer likely can relax the requirements for seeding (when H-etch seeding may work satisfactorily). Etching *alone* does not work well (especially on more textured TCOs), but it can be useful as the first step in multi-step seeding processes.

The deposition of a p-seed-layer (probably not truly nanocrystalline) on top of the a-SiC p-layer has worked more reproducibly. The seeding p-layer can be grown either directly on the a-SiC:H p-layer, or deposited after an H-plasma etching step with similar results. The 'nc-Si p' seeding technique has produced superior FF of nc-Si cells, good seeding uniformity, and improved reproducibility. The major problem that we have been working on, with quite limited success, is the low J_{sc} brought about by significant optical loss to the optically-opaque p-seed layer. Some examples of p-seeding produced solar cells are given in tables 1 and table 2 earlier. Conversion efficiencies of ~5% have been obtained on commercial SnO_2 with Al back contact for several runs, an example of which is seen in **Figure 5**.

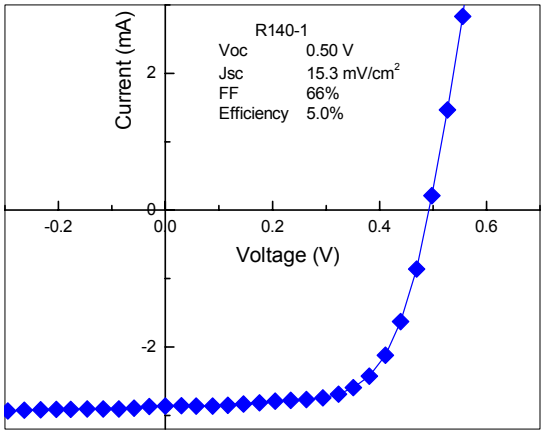

Figure 5 I-V of an earlier nc-Si single junction cell made by p-seeding (thick seed layer).

The process window is much wider for p-seeding since there is no need to guard against defect creation or contamination of p-layer (as the dirty process is entirely confined to the p-side of the

p-i interface). For instance, more energetic plasmas can be used for faster incubation. Recipe reproducibility and insensitivity to substrates were much improved when the thickness of p-seed layer was kept above some threshold value. The more robust p-seeding recipes (thicker p-seed layers), however, invariably lead to lower J_{sc} when bare SnO_2 is used (versus ZnO-coated SnO_2). In addition to p-seed layer absorption, the low J_{sc} values of the solar cells are attributable to optical losses to the front TCO contact and glass, low TCO texture, thick a-SiC:H p-layer (protective layer for SnO_2), and the lack of good rear reflector (Al). In many cases, poor carrier collection is suspected to further compromise the spectral response (particularly in the blue to green light region). In Phase I, only a few nc-Si devices made by p-seeding show reasonably good J_{sc} (from both light I-V and QE tests), prompting us to aggressively pursue CC-seeding capable of higher J_{sc} but also sensitive to reactor operating history as described earlier. We have been unable to lessen the optical loss of the boron-doped 'nc-Si' seed layer by simply reducing its thickness (by, e.g., decreasing the SiH_4/H_2 ratio of the supply gas during seeding for a fixed seeding time). It seems that some substantial seed-layer thickness (a threshold value) has to be reached before 'nucleation' can occur [14], as judged by nc-Si device parameters, suggesting certain inevitable optical loss due to the narrow bandgap of the initially amorphous or mixed-phase boron-doped Si:H seed layer. Thinner p-seed layer is less robust, poorly reproduced, and overly sensitive to substrate variations. J_{sc} can go down sharply with too higher a TMB content in the supply-gas mixture (> 1%) during p-seeding, due to narrowing of the bandgap of the seed layer, contamination of the nc-Si i-layer, or perhaps boron-induced hindrance of Si nucleation.

The time required for adequate seeding obviously depends on the intensity of the plasma (among other things) that dictates the interaction and exchange between atomic hydrogen and Si species. Stronger plasma induces faster nucleation, often at the cost of worse seed-layer uniformity. The symptoms of insufficient seeding may include poor FF and high V_{oc}. However, FF and V_{oc} do not necessarily vary, beyond a certain threshold, with increasing length of seeding. That is, longer (or further developed) seeding does not ensure a better FF or a markedly different V_{oc}, while the J_{sc} tends to decrease with increasing duration of p-seeding. As an example, **Figure 6** displays the variations of FF and efficiency (a), and J_{sc} and V_{oc} (b), of a series of solar cells fabricated with increasing seeding time, under a fixed set of p-seeding conditions from a gas mixture of H_2+SiH_4+TBM. All the other processing steps were kept the same for the series.

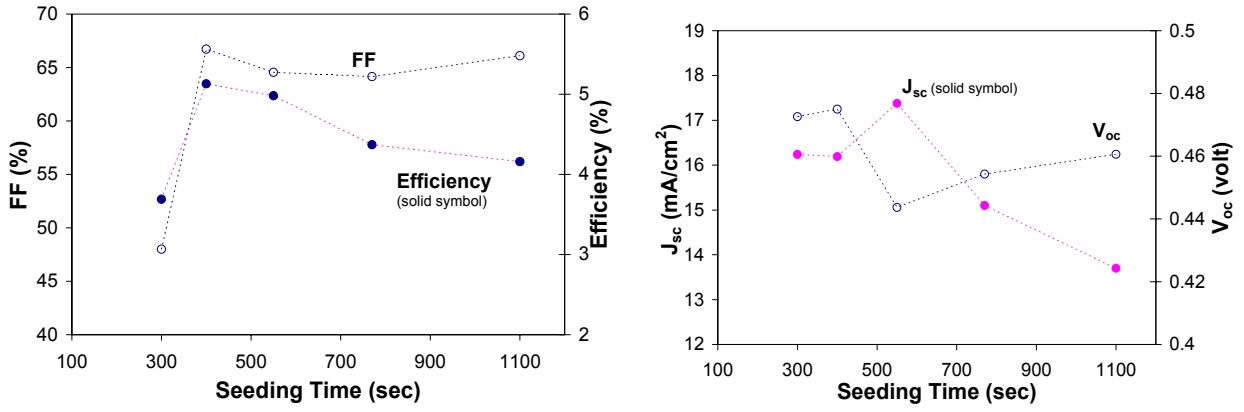

Figure 6 Variations of FF & efficiency (a), and J_{sc} & V_{oc} (b), with p-seeding time.

When the seeding time is too short, the under-seeded nc-Si solar cells show low FF and low efficiency as we have seen time and again. Seeding time much longer than some critical point (~400-450 seconds in this case) leads to reduced J_{sc} and efficiency compared to some 'optimal' seeding time. The crucial question remains: Does the p-seed layer have to reach some *minimum thickness* before it can be 'crystallized' enough to act as an effective template for nc-Si absorber? If certain thickness has to be reached for p-seed layer, significant optical loss will be inevitable.

A cleaner p/i interface could be obtained by limiting the TMB concentration during p-seeding and conducting post-seeding flush of the system. We have found that, for nc-Si *single* junction solar cells deposited in the p-i-n sequence, undue boron exposure to the reactor (prior to i-layer deposition) poses a bigger threat to device efficiency than phosphorus contamination (unlike the case for tandem cells reported later). Through a number of experiments on doping levels, seeding duration, pumping sequences, Ar gas purging time, etc., before nc-Si i-layer deposition, we have excluded cross-contamination as the main cause for low J_{sc} in well controlled runs. Still, for single-reactor PECVD, contamination from dopants and other impurities need to be constantly monitored. Interestingly, the concentration of boron (TMB) in the seeding gas mixture does not have a major impact on the J_{sc} when TMB concentration is below 1% of SiH_4 in the seeding gas mixture. Sample #R391 showing good efficiency (see table 8) had TMB concentration (TMB/SiH_4 ratio) of less than 0.1% in the seeding gas mixture of H_2+SiH_4+TMB. This finding is in contrast with a-SiC:H p-layers whose short-wavelength transparency is highly responsive to the boron content (TMB% in the gas mixture).

I.D. #	nc-Si Seeding Descriptions, Notable Features	V_{oc}	J_{sc}	FF	Eff.
	(All on commercial LOF or AFG SnO_2, with Al back contacts)	(V)	mA /cm^2	(%)	(%)
R374	*i*-seeding on a-SiC p-layer (seeding without TMB)	0.48	14.3	61	4.2
R383	i-seeding only on a-SiC p-layer. Higher J_{sc} but lower FF	0.47	16.0	55	4.1
R377	CC-seeding; nc-Si i-layer: SiH_4 flow grading ~ 25%	0.46	13.6	64	4.0
R391	p-seeding, very low TMB/SiH_4 ratio in gas mixture (< 0.1%)	0.48	14.1	67	4.5
R140	p-seeding, long seed time, over thick a-SiC p (pre-seed layer)	0.50	13.8	70	4.8
R145	p-seeding; some carbon added in seed layer, very low CH_4 flow	0.49	13.2	68	4.4
R393	p-seeding, small amount of CH_4 added to gas ($CH_4/SiH_4 < 0.1$)	0.47	12.9	64	3.9
R398	Strong p-seeding; nc-Si i-layer: SiH_4 flow grading ~ 25%	0.50	14.1	65	4.6
R400	Very thin a-SiC p-layer between SnO_2 and p-seed layer	0.49	13.9	68	4.6
R406	Thick a-SiC p-layer between SnO_2 and p-seed layer; thicker i	0.46	14.2	64	4.2
R410	p-seeding, very high R, thinner seed-layer; on very thin a-SiC p	0.48	11.8	66	3.7
R426	p-seeding under high R (H_2/SiH_4 ratio), on ZnO-coated SnO_2	0.49	13.2	63	4.1

Table 8 Selected nc-Si single junction solar cells prepared by various p-seeding recipes. Also shown for comparison are a few cells prepared by alternative seeding methods.

Table 8 presents examples of various p-seeding formulations designed to ascertain a seeding scheme capable of higher J_{sc} and higher efficiency (better trade-off among J_{sc}, V_{oc}, and FF). For comparison, some cells made by the competing i-seeding and CC-seeding methods are listed. As indicated by runs #R410 and R426 in the above table, high R (H_2/SiH_4 ratio) for p-seeding (hence presumably thinner p-seed layer) did not produce higher J_{sc}, even though the seed-films would appear more transparent. Such results had been repeatedly seen, on both SnO_2 and ZnO-coated SnO_2. Either the thinner p-seed layers were equally opaque as the thicker ones (very unlikely), or thinner seed layers were accompanied by weaker collection (poor seeding efficacy).

A number of film runs (~ 30) were devoted specifically to p-seeding, etch-seeding, and closed-chamber (CC) seeding, on plain SnO_2 coated with a-SiC p-layer. The resulting films (seed layer plus a-SiC base-layer) typically look much more transparent from CC-seeding than p-seeding (as expected from net etching by CC-seeding). The p-seed layers always looked too opaque (even for quite thin films < 30-50 Å) to produce good J_{sc} in cells. Thinner a-SiC p-layers did not result in higher p-seeding transparency. The heavy optical loss in either devices or TCO/seed-layer films could not be blamed on plasma reduction of SnO_2, as verified by ZnO coating of SnO_2. In the few experiments when we applied the p-seeding recipe which produced relatively transparent seed layers, the solar cell V_{oc} and FF were unsatisfactory, indicating immaturity of incubation that resulted in i-layers being mixed-phase (at least initially) linked to poor carrier collection. Incidentally, as stated earlier, CC-seeding tends to be more uniform under diverse conditions, while p-seeding is more prone to non-uniformity at high power and moderate to high pressure.

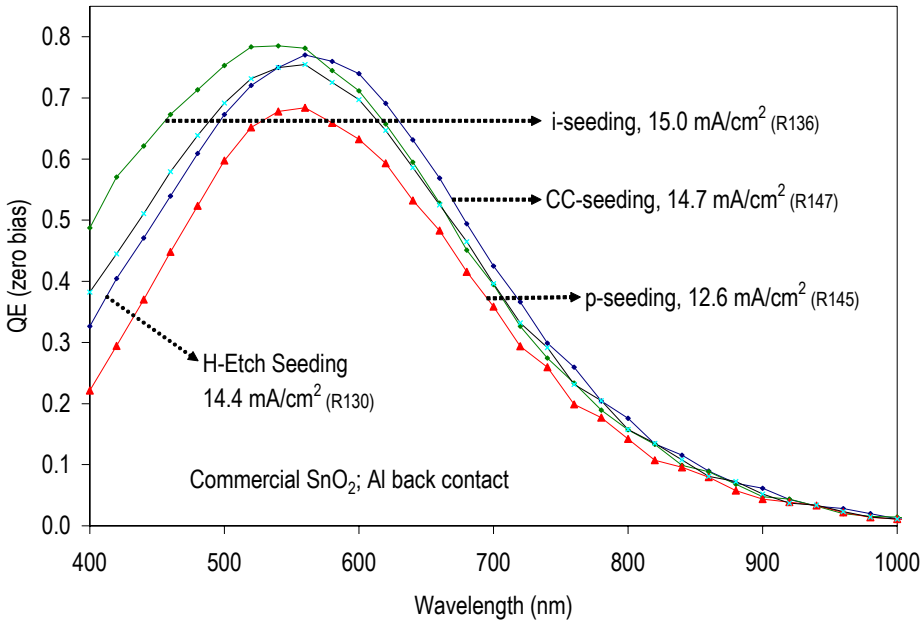

Figure 7 QE spectra of nc-Si solar cells produced by different seeding methods.

Examples of the impact of seeding procedure on QE of nc-Si solar cells are given in **Figure 7**. The i-seeding processes have often led to higher blue and peak QE but lower FF (poor photo-carrier extraction) compared to p-seeding. Good QE can also be obtained by the H-etch method,

which again is less thorough in seeding. Only a few p-seeding solar cells have shown reasonably good QE-derived J_{sc} and high efficiency of near 5% (with Al back contact), similar to the best values obtainable by the competing seeding methods using un-coated commercial SnO_2. All the nc-Si solar cells made with better-reproduced p-seeding recipes (using thick 'nc-Si' p-layer) have shown greatly suppressed QE at low short wavelengths and peak responses. For cells with the same i-layer thickness, good FF (> 65%) does not necessarily mean good efficiency. Many nc-Si solar cells of low J_{sc} were designed to contain thin 'total' p-layers (the sum of the a-SiC p-layer and p-type seed layer). It appears that when the total p-layer is too thin or too weak (and i-layer is too close to the SnO_2 interface), FF does not correlate well with carrier collection. The possibility of complex contamination (by both B and P?) cannot be ruled out, though.

A 'gentle' hydrogen plasma treatment (intended for defect passivation), performed after high-power intense seeding plasma, resulted in much worse nc-Si solar cells. Such a 'plasma cleaning' step likely damaged the 'seeds' on the seeding surface prior to nc-Si i-layer growth. Also, attempts at *direct* deposition of Si*C*:H seed-layer on SnO_2 (without an a-SiC:H under-layer) were unsuccessful. Amorphous silicon cells with high V_{oc} (near 950 mV) were obtained over areas where nc-Si was expected. In other areas, mixed-phase Si:H cells were obtained. Evidently, even moderately low amount of carbon can severely hinder the nucleation process.

2.5.2 Seeding efficacy versus substrate type, underlayer, and multi-step seeding

The robustness of seeding is vital not only for single junction nc-Si solar cells, but also for the bottom nc-Si cell in a-Si/nc-Si tandem devices that we have been aiming to fabricate. The following serves as a summary of our more recent lessons from p-seeding experiments:

- It is possible to fabricate good p-seeded p-i-n type devices on plain SnO_2 (in contrast to the commonly used ZnO). However, the use of SnO_2 as front contact, and the needed precaution against single-chamber cross contamination, seriously impair the optimization of seeding.
- Low J_{sc} remains the biggest issue with our present p-seeding techniques on uncoated SnO_2. So far, the more robust p-seeding recipes are accompanied by unacceptably high optical loss.
- Reproducibility of p-seeding (and other seeding schemes) depends on the reproducible operation of the reactor (in terms of contamination control and tight tolerances in electrode spacing variations upon reactor cleaning and reactor-box reassembly).
- The efficacy of seeding often depends on the properties of under-layers (C%, TCO texture).
- Interface i-layer grading may not be necessary when seeding is done 'right'.

An additional difficulty relates to the dependence of seeding on the surface roughness of the SnO_2 superstrates. Compared to the LOF-TEC7 SnO_2 of low haze (~5-7%), the AFG- PVTCO SnO_2 (which became our standard front contact in Phase II) has higher haze (~7-9%). Seeding has apparently been more difficult with higher texturing of the under-lying TCO by all the 'novel' seeding methods, as illustrated by examples in **Table 9**. The three pairs of nc-Si solar cells were co-deposited on LOF and AFG SnO_2 superstrates. Generally, p-seeding is insensitive to the type of substrates, compared to i-seeding, H-etch seeding, and more notably CC-seeding. As a result, we had to modify previously developed (for the LOF SnO_2) seeding recipes to make them suitable for the more textured AFG SnO_2. Longer term, higher textured TCO should

produce higher J_{sc}, particularly when better rear reflectors (ZnO/Al, ZnO/Ag) are used instead of Al. Note that the laboratory type, superior Asahi SnO_2 has higher haze (low teens) than either of the commercial SnO_2. Thus, deposition recipes developed on the low-cost LOF or AFG SnO_2 do not translate well to Asahi SnO_2 when making nc-Si cells using some of the seeding methods.

Cell I.D.	Type of SnO_2; Other Notes	V_{oc}	J_{sc}	FF	Effi.
	(All with Al back contact; i-layer thickness ~1.5μm)	(V)	mA/ cm^2	(%)	(%)
R266-1	LOF TEC7 SnO_2; i-seeding	0.46	15.3	63	4.4
R266-2	AFG new SnO_2; i-seeding (same as R266-1)	0.44	15.0	56	3.7
R292-1	LOF TEC7 SnO_2; CC-seeding at lower pressure	0.49	15.5	55	4.2
R292-2	AFG new SnO_2; CC-seeding, co-deposited with above	0.47	14.8	52	3.6
R273-1	LOF TEC7 SnO_2; p-seeding	0.47	14.9	66	4.6
R273-2	AFG new SnO_2; p-seeding (same as R273-1)	0.45	14.8	64	4.3

Table 9 Comparison of PV parameters of nc-Si devices prepared on two different SnO_2.

We made a few superficial attempts at creating wider-gap p-type seed-layers using Si:H alloys by introducing CH_4 or CO_2 (carbon or oxygen) to the H_2+SiH_4+TMB feed-gas mixtures during p-seeding. No alloying effect or efficiency gain were discernable in cells with SiC_x:H or SiO_x:H seed layers when CH_4 or CO_2 flow rates were low. The J_{sc} was still mostly low (< 14 mA/cm^2) using commercial SnO_2 front and Al back contacts. But at high CH_4 or CO_2 flow rate (leading to higher J_{sc} owing to more transparent p), the seeding action was destroyed (resulting in largely amorphous cells), suggesting excessive incorporation of carbon or oxygen in the seed layer. It is known that carbon and oxygen impede crystallization of Si:H films. Thus, even if the SiC_x:H or SiO_x:H seed films can be made p-type, a much thicker seed-layer (with higher optical absorption) probably would be needed to get the seeding job done, thus negating any gain from the bandgap widening of such seed layers. Alternative bandgap-broadening elements, such as Cl or F, may have a better chance of improving seed layer transparency without inhibiting nucleation compared to C or O. In view of the difficulties and limited resources, we focused on Si p-seeding for the vast majority of the runs.

Cell I.D.	Seeding Method (p-seeding), Comments	V_{oc}	J_{sc}	FF	Effi.
	(On Asahi SnO_2, with ZnO/Al back contact)	(V)	(mA /cm^2)	(%)	(%)
R352-2	Previous best cell by CC-seeding (sent to NREL)	0.49	17.6	62	5.3
R407-4	Improved p-seeding, relatively thin seed layer	0.49	17.8	64	5.6
R415-4	Improved p-seeding on very thin a-SiC p-layer	0.48	15.6	67	5.0
R417-3	Improved p-seeding, before light-soaking (annealed)	0.47	17.0	66	5.3
R417-3	Same cell as above, light-soaked (one-sun, 3 days)	0.50	16.9	69	5.8

Table 10 Selected nc-Si single junction solar cells on bare SnO_2 with ZnO/Al back contacts.

We made some headway in obtaining higher single junction nc-Si cell efficiency, on Asahi SnO_2 superstrates with ZnO/Al rear contacts, by using improved p-seeding, compared with previously produced best cells by CC-seeding, as shown in **Table 10**. The efficiency gain was mainly due to higher FF, owing to reduced sensitivity of p-seeding to the surface texture (roughness). The Asahi SnO_2 has much higher texture than commercial SnO_2 (AFG and LOF) used for most samples (see earlier tables). The stronger p-seeding recipes work better and more reproducibly on the higher-textured SnO_2 than the weaker CC-seeding method (which produces more transparent seed layers). As a result, we were able to produce nc-Si single junction solar cells, using ZnO/Al back contacts, with efficiencies over 5.5% or higher (close to 6%) on bare SnO_2. The good nc-Si solar cells listed in the table contain i-layers grown with mild grading of hydrogen dilution ratio (with increasing SiH_4 flow rate for a fixed H_2 flow rate) that helps with FF *and* uniformity of the nc-Si devices.

We also tried to combine the various seeding methods discussed above in order to reach a better compromise between FF and J_{sc}. For instance, it is tempting to take advantage of the high J_{sc} from H-etch seeding and good FF from p-seeding by performing a short p-seeding after H-etch. Other obvious ideas are to combine either i-seeding or CC-seeding, with a short p-seeding. A shorter p-seeding (thinner p-seed layer) was expected to reduce optical losses compared to the full-fledged version. **Table 11** provides a few examples of cells made by some 'hybrid' seeding techniques. Higher FFs (e.g., 61% vs. 65%) indeed have been obtained by the addition of a short p-seeding step at the end of CC-seeding (or H-etch), but, unfortunately, the J_{sc} invariably took a bigger hit than what would be anticipated from the addition of an ultra-thin Si:H p-layer (e.g., < 20 Å). It is unclear what causes large losses in QE response (from blue to green). Perhaps, the very early stage of p-seeding is vastly different from the later, more steady-state process (by which growth rate is inferred), and short p-seeding cycle should be regarded as a different beast.

Cell #	Seeding Methods Used (all cells on AFG SnO_2, Al b.c.)	V_{oc}	J_{sc}	FF	Effi
R221-2	Standard CC-seeding (static mode). Reference cell	0.47	15.5	64	4.7
R142-1	H-etch (long) on thick a-SiC p, then long p-seeding	0.48	12.9	66	4.1
R212-1	CC-seeding as R221, followed by fairly short p-seeding	0.47	13.2	65	4.0
R320-2	CC-seeding, followed by moderately long p-seeding	0.46	13.1	64	3.9
R378-3	CC-seeding, followed by i-seeding	0.45	14.0	59	3.7
R386-3	First i-seeding on a-SiC p, then a very short p-seeding step	0.46	13.8	65	4.1

Table 11 Examples of nc-Si cells made by hybrid seeding techniques.

Attempts to reduce p-seed layer thickness by first incorporating a thin, less-absorbing i-seeding layer as part of an overall p-seeding formula have also produced negative results. The device symptoms are low FF and low V_{oc}, likely resulting from dense defects at the p/i interface. We also suspect some boron contamination, or the two seeding methods are not entirely compatible. Also, the initial p-seeding plasma (the first 20 to 60 seconds) likely is different from that at longer time, such that there may be far more film deposited initially than extrapolated from the average film growth rate over longer period of time. We have combined a thinner p-seed layer with a subsequent i-seeding in order to reduce optical loss associated with p-seeding only. Again, when the i-seeding step is long enough to make a difference, a highly defective p/i

interface would apparently be formed to degrade the FF of the solar cell. The serious collection problem may indicate that the different seeding methods involved are incompatible.

In summary of our extensive p-seeding experiments on SnO_2 front contact (*without* ZnO coating, but with an a-SiC pre-seed protective layer), the p-seeding technique is very robust (insensitive to the deposition history of reactor, type of underlayer, or degree of texture of the superstrate). It is comparatively straightforward to produce nc-Si cells with good V_{oc} and excellent FF (when boron cross contamination is under control). However, the more robust p-seeding recipe (with little mixed-phase i-layer in the cell) is invariably accompanied by excessive optical loss. The central difficulty in p-seeding remains the lack of a good trade-off between high FF and high J_{sc}.

2.5.3 Optimal nc-Si single junction solar cells by p-seeding on ZnO-coated SnO_2

During the 2nd half of Phase II, when large-area ZnO sputtering became available at EPV, we evaluated ZnO films as both stand-alone front contact (see Sec.5), and especially as a thin coating over the existing SnO_2/glass substrates for improved seeding process for nc-Si single junction cells. Note that all the published high efficiency, p-i-n type nc-Si cells had been grown on custom ZnO, produced by wet-etching [9] of thick sputtered film to create high texturing. A key attribute of ZnO as front contact for nc-Si cell fabrication is its excellent resistance to hydrogen-rich plasma. Unlike SnO_2, the optical, electrical, and surface properties of ZnO do not change with exposure to H-species. We have not emphasized the use of 'bulk' ZnO as front contact partly due to resource limitations. Further, it is our belief that large-area ZnO/glass plates would not be commercially viable due to their high costs (especially using expensive, lower-absorption glasses). Also, we have not developed a sputtering recipe (and process control) capable of growing highly transparent ZnO with good conductivity. Another key reason to focus on native SnO_2 early on was the belief that SnO_2 would be adequate and more practical for the ultimate device of our efforts, a-Si/nc-Si *tandem* cells (which do not involve seeding on the front contact). It was false to assume that seeding on a-SiC p-layers (over SnO_2) would be at least as effective as ZnO (which is not a Si-based substance). As it turned out, it is far easier (faster or with thinner seed layer) to obtain good seeding on ZnO surface than on a-SiC (or a-Si) films.

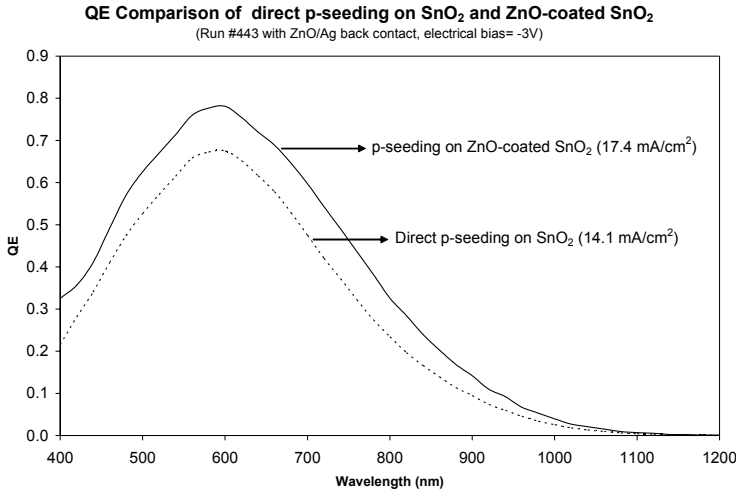

Figure 8 Comparison of QE Spectra of nc-Si solar cells prepared by p-seeding *directly* on bare SnO_2 and on ZnO-coated SnO_2 superstrates.

We concentrated on thin ZnO coatings (100-400 Å) over the existing SnO_2 as the front contact. This is a simpler answer (than bulk ZnO that needs long deposition time and texturing) to the colossal challenge of seeding on plain SnO_2. Only the surface of SnO_2 is modified, with little loss in optical transparency and little increase in series resistance in the device (due to thinness of ZnO). The ZnO/SnO_2 bilayers proved to be an immediate and immense success for p-seeding technique to produce efficient nc-Si cells of higher J_{sc} without sacrificing V_{oc} or FF, and without need for any pre-seed protective layer. In fact, p-seeding *directly* on ZnO is more expedient than that on ZnO coated by a-SiC! In contrast, as stated earlier, SnO_2 is ill suited for direct seeding. **Figure 8** shows the QE spectra (-3V bias) of two co-deposited nc-Si cells on SnO_2 and ZnO/SnO_2, respectively, demonstrating markedly depressed response in the case of SnO_2.

Device	TCO Type and Coating Before Seeding; Other Features	V_{oc}	J_{sc}	FF	Eff.
I.D. #	(SnO_2 is the AFG commercial type; all with Al back contacts)	(V)	mA/cm^2	(%)	(%)
R436-2	Plain SnO_2; shorter p-seeding; standard i-layer	0.47	11.7	55	3.0
R436-4	Same as above (R439), but on ZnO-coated SnO_2	0.48	13.8	64	4.3
R439-2	Plain SnO_2; short p-seeding; higher-power i-layer	0.49	12.4	33	2.0
R439-3	Same as above (R439), but on ZnO-coated SnO_2	0.46	14.9	64	4.4
R440-3	Plain SnO_2; shorter p-seeding; standard i-layer	0.50	11.8	50	3.0
R440-4	Same as above (R440), but on ZnO-coated SnO_2 (thin ZnO)	0.51	14.6	67	5.0
R443-2	Plain SnO_2; short p-seeding; high-power i-layer. Amorphous	0.79	8.9	34	2.4
R443-2	Same as above (R443), but with ZnO/SnO_2 (thin ZnO coating)	0.49	15.1	57	4.2
R444-2	Plain SnO_2; CO_2 was added to p-seeding feed-gas mixture	0.79	9.1	26	1.9
R444-3	Same as above (R444), on ZnO/SnO_2 (high-power i-layer)	0.49	15.8	53	4.1

Table 12 Comparisons of bare SnO_2 and ZnO-coated SnO_2 (AFG) for p-i-n nc-Si cells: p-seeding *directly* on the TCOs without other protective layer (co-deposited cells).

In addition to optical losses (SnO_2 reduction and more opaque seed film?), the inferior QE of SnO_2 suggests poorer seeding quality (collection problem). Some examples are given in **Table 12** of the enormous differences in performance of nc-Si cells co-deposited by direct p-seeding on SnO_2 and on ZnO/SnO_2. The seeding time needed for good FF (> 65%) is substantially shorter for ZnO/SnO_2 than SnO_2. It is worth repeating that p-seeding on the a-SiC surface is *not* any easier than p-seeding directly on SnO_2 (as judged by V_{oc} and FF of the cells). Clearly, there is a tremendous difference between ZnO and SnO_2 in not only their resistance to hydrogen plasma, but also in their 'affinity' or receptiveness to the initial formation of Si:H films under a highly etching plasma environment. It would take much longer for Si:H film to 'coalescence' on SnO_2 than on ZnO. In one test, we exposed both plain (bare) SnO_2 and ZnO-coated SnO_2 glass plates to standard p-seeding plasma for a few minutes. While there was clearly Si-looking film on the ZnO-coated SnO_2, none was observable on the 'native' SnO_2 plate which appeared to be somewhat 'darkened' by the plasma. It is evident that ZnO is much friendlier to seed layer

formation than SnO_2. It would take a much thicker p-seed layer (much more time, more optical loss) to get the same seeding action on SnO_2 compared to ZnO. No wonder ZnO has been the standard front TCO for nc-Si p-i-n single junction solar cells around the world.

Based on our experiences with seeding and i-layer growth (see later), we have obtained 'optimal' nc-Si single junction solar cells using p-seeding on SnO_2/glass superstrates that are coated with thin layers of sputtered ZnO (100-400 Å, conductive or somewhat insulating). Some of our high efficiency nc-Si cells are documented in **Table 13**. By ZnO coating of the front contact, we have obtained **6.5%** and 5.7% efficiencies for nc-Si cells, respectively, on Asahi SnO_2 and AFG SnO_2. **Figure 9** displays the I-V curves of two nc-Si solar cells prepared on ZnO-coated SnO_2.

Cell I.D.	Description and Comment	V_{oc}	J_{sc}	FF	Effi.
	(type of base-layer or TCO; type of back contact)	(V)	mA/cm^2	(%)	(%)
R246-1	Standard, on bare SnO_2 (AFG); Al back contact	0.47	14.9	67	4.7
R407-4	On a-SiC p/bare Asahi SnO_2; ZnO/Al back contact	0.49	17.9	64	5.6
R415-2	Bare SnO_2 (Asahi), thinner a-SiC p; ZnO/Al b.c.	0.48	15.1	66	4.8
R417-2	p-seeding on thinner a-SiC p; Asahi SnO_2; ZnO/Al b.c.	0.50	16.1	68	5.5
R440-4	p-seeding on ZnO/SnO_2 (AFG), no a-SiC p; Al b.c.	0.51	14.8	66.5	5.0
R456-3	Shorter seeding on ZnO/SnO_2 (Asahi); ZnO/Al b.c.	0.52	16.8	71.0	6.2
R461-1	p-seeding on ZnO/SnO_2 (AFG); thick nc-Si i; ZnO/Al b	0.50	16.2	70.0	5.7
R461-2	Co-dep as above, but ZnO on Asahi SnO_2; ZnO/Al	0.51	17.2	68.3	6.0
R462-4a	p-seeding, thicker i, on ZnO/SnO_2 (Asahi); ZnO/Al b.c.	0.50	19.0	66.6	6.3
R462-4a	Same as above, contact is closer to cell (all-around)	0.50	18.7	69.5	6.5
R462-4a	Same cell, NREL's measurement (X25 IV System)	0.52	18.2	68.5	6.47

Table 13 Higher efficiency p-i-n nc-Si single junction solar cells prepared by p-seeding on bare SnO_2 and on ZnO-coated SnO_2 front contacts ('optimal' cells).

Even though ZnO coating greatly facilitates p-seeding (than uncoated SnO_2), some minimal thickness for the seed-layer is still required to obtain good FF and V_{oc}. Higher optical loss to the p-layer (in the short-wavelengths) seems inevitable for p-i-n nc-Si solar cells compared to a-Si cells (using wide-bandgap a-SiC p-layer). For a-Si/nc-Si devices, seed-layer loss is much lower.

The 6.5% efficiency on a cell with thicker nc-Si i-layer (> 2 μm) has been confirmed by NREL. For this 'champion' cell, R462-4a (with ZnO-coated Asahi SnO_2 front contact and ZnO/Al back contact), the NREL measurement showed V_{oc}=0.521V, J_{sc}=18.2 mA/cm^2, FF=68.5%, and efficiency=6.47%. The difference in J_{sc} values between EPV and NREL tests was mainly due to uncertainty in the cell-area (which is somewhat fuzzy around the edges due to 'gaps' in masking during ZnO and Al sputtering). The higher V_{oc} value from NREL I-V test is a result of cooler measurement temperature at ~ 25 °C, versus the un-cooled cell I-V measurement at EPV.

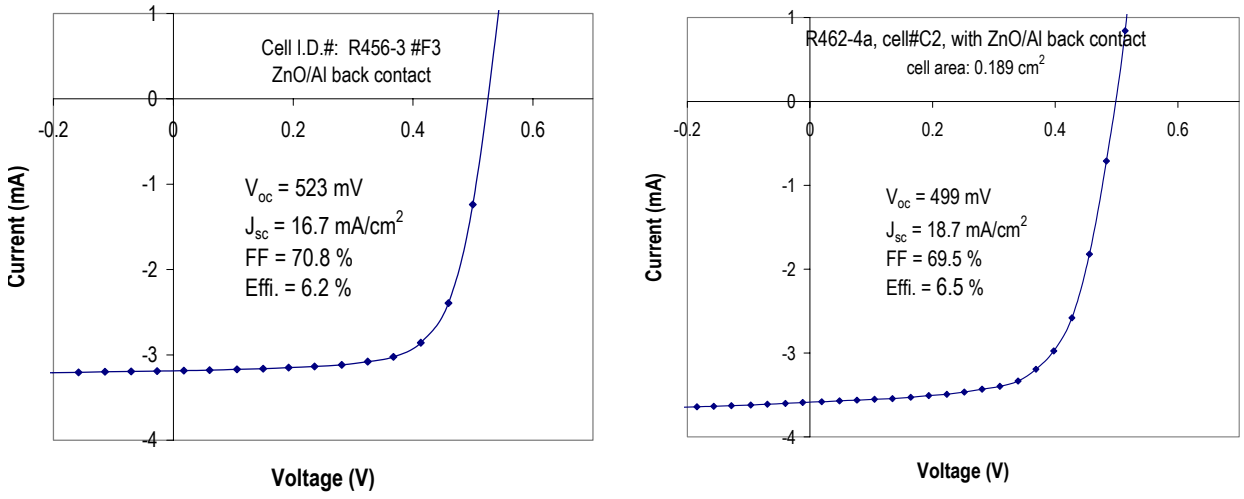

(a) (b)

Figure 9 I-V curves of two single junction nc-Si solar cells on ZnO-coated SnO_2/glass using ZnO/Al back contacts, with normal (**a**) and thicker (**b**) nc-Si i-layers.

2.6 Summary and conclusion of seeding experiments for nc-Si solar cells

After an extensive (if not exhaustive) study of various seeding techniques for p-i-n nc-Si single junction solar cells on *SnO_2* superstrates in the last two years, we have developed a more robust p-seeding recipe, insensitive to the degree of texture of the TCO superstrates, that delivers more consistent device performance (good FF and V_{oc}). This compares with our earlier seeding techniques that did not work satisfactorily on more-textured TCO. The J_{sc} obtained with such a recipe depends on the detailed balance during seeding between growth and etching (and the resulting optical loss to the seed layer), duration of seeding, and seed layer thickness. It seems that we have approached the 'optimized' nc-Si single junction cell performance on SnO_2 of near 6% with ZnO/Al back contacts. Further increase in efficiency (J_{sc}) of nc-Si single junction cells *on SnO_2* superstrates will be enormously difficult as the J_{sc} is principally limited by the incompatibility between SnO_2 and the seeding process. Further optimization of our nc-Si *single* junction deposition process (not necessarily a-Si/nc-Si tandems) needs to be conducted on TCOs which are resistant to H-plasma reduction (such as ZnO), as we shall discuss in Section 5.

We now summarize the key findings on seeding and related experiments during this project:

- Seeding has a bigger impact on nc-Si device performance than i-layer deposition conditions. The properties of Si:H i-layer (especially the initial portion) depends critically on seeding.
- The unconventional i-seeding, H-etch seeding, and the closed-chamber (CC) seeding methods are capable of producing good p-i-n nc-Si solar cells of high J_{sc} on plain SnO_2 superstrates.
- On *un*coated SnO_2 superstrates (not covered by, e.g., ZnO), all the various seeding methods (including p-seeding) have produced nc-Si cells of *comparable efficiencies* of ~5% and 5.5%, on commercial SnO_2 with Al and ZnO/Al back contacts, respectively (nc-Si i-layer ~ 1.5 μm thick). On the superior Asahi SnO_2 with ZnO/Al back contact, the efficiencies approach 6%.

- Still, the customary p-seeding is preferred for its robustness and reproducibility compared to all other seeding techniques, due partly to the single-reactor constraints in our case.
- ZnO-coated SnO_2 can withstand aggressive hydrogen plasma and is far more conducive to initial nucleation and coalescence of Si film *directly* on a foreign surface, compared to cases of bare SnO_2 or even a-SiC (a-Si) films used as the pre-seeding coating over SnO_2.
- The performance edge of p-seeding is evident when using *ZnO-coated* SnO_2 compared to uncoated SnO_2. Efficiencies of 6.5% and 5.7% have been obtained on ZnO/SnO_2 (Asahi and AFG SnO_2, respectively), with mediocre ZnO/Al back contact, for p-i-n nc-Si solar cells.
- The combinations of various seeding methods (hybrid seeding techniques) do not work better than the individual, stand-alone seeding methods (as tested on un-coated SnO_2 superstrates).

3. Deposition, Process Control, and Properties of nc-Si i-layers

3.1 A survey of nc-Si i-layer growth conditions in solar cell configuration

Compared to the overwhelming emphasis we have placed on the critical seeding processes, nc-Si 'bulk' i-layer deposition conditions have not been scrutinized quite as closely or extensively. A reason for this relative 'neglect' of the i-layer is that, seed layer and i-layer must *both* work well to deposit a good solar cell. The study of 'undoped' nc-Si film in device configuration is feasible only after the establishment of a fairly robust, effective seeding technique. Since the 2nd half of Phase I, a fixed set of conditions were somewhat arbitrarily chosen for the deposition of 'standard' nc-Si i-layers in order for us to focus on other issues such as seeding, reproducibility (contamination control), and tunnel junction for tandem solar cells. Later in Phase II, we again explored growth conditions for nc-Si absorbers, under fixed p-seeding, for higher J_{sc}, higher growth rates, improved uniformity, higher V_{oc}, and higher efficiency. In the first half of Phase I, we cursorily surveyed the PECVD parameter space for conditions that are compatible with steady, sustainable plasma of H_2 + SiH_4 (+ Ar) gas mixtures which have been typically employed in the RF-PECVD of nc-Si as reported in the literature. Important plasma parameters under study included RF power (RF plasma current), H-dilution ratio R ($R=H_2/SiH_4$ ratio), total gas flow rate, and chamber pressure. Substrate temperatures were only varied slightly, in the range of 170-200 °C which is similar to that for deposition of a-Si solar cells. The impurity contents of i-layers have not been analyzed. Many of the earlier solar cells were likely to contain mostly mixed-phase i-layers due to both inadequate seeding and less-vigorous discharge for i-layer.

Glow-discharge plasma could not be ignited and/or sustained for H_2-rich mixtures of H_2 + SiH_4 (e.g., R=20) at low pressures (for instance, < 0.6 torr). This might be explained, in part, by the relatively narrow spacing between the electrodes (separated by the two substrates that are placed on the surfaces of the opposing electrodes). Adding significant amount of Ar to the supply-gas mixture helps attain and maintain RF plasma at lower pressure and/or lower RF power. For deposition rate purpose, we have been mainly interested in moderate to relatively high chamber pressures (> 1.5 torr), using the high H_2 dilution (high R) approach to nc-Si growth. The thickness (and solar cell performance) uniformity of the deposited a-Si and nc-Si films over the 12"x15" substrates were routinely measured at selected positions. A general finding is that, under the conditions of high R (ranging from 40 to 250 for bulk i-layer) and high RF power (>

150W using the home-made RF impedance matching network), the higher the chamber pressure, the worse the film and device non-uniformity, even in situations when SiH_4 depletion ratio is estimated to be < 50%. Such deposition inhomogeneity (more on this later) is believed to result from strong plasma excitation (production of SiH_x radicals) and relatively poor distribution (flow pattern over the surface areas of the substrates) of the source gas (SiH_4) molecules inside the RF-PECVD reactor. Improvements of nc-Si film deposition uniformity will be a vital undertaking for achieving the ambitious sub-module performance goal (> 9%) set in the original proposal for this subcontract. Due in part to the lack of material characterization capabilities at EPV, few stand-alone nc-Si films have been deposited on plain glass or other types of substrates. We are also biased against convoluted film studies that often prove of little value in device optimization.

Run #	Seeding Method; nc-Si i-layer Growth Conditions	V_{oc}	J_{sc}	FF	Effi
R210	CC-seeding; standard nc-Si i-layer dep. conditions; ref. cell	0.47	15.5	64	4.7
R379	CC-seeding (no TMB), SiH_4 grading ~28% (low to high) in i;	0.45	15.0	62	4.2
R175	Quasi CC-seeding, LOF SnO_2 (reactor pre-coated with a-Si p)	0.49	15.5	65	4.9
R178	Quasi CC-seeding per R175; i-layer SiH_4 flow higher by 13%	0.48	14.5	63	4.4
R144	H-etch then p-seeding; nc-Si i @ higher power & rate ~3Å/s	0.48	13.7	62	4.1
R130	Pure H-etch on a-SiC p; power high ~ 80% for nc-Si i-layer	0.50	15.1	57	4.3

Table 14 Some nc-Si cells by different i-layer growth conditions, various seeding methods.

Even though we made a good number of nc-Si absorbers using various combinations of R, RF power, and pressure (many of the devices were made with i-seeding, and often with an initial i-grading) earlier in this project, the qualities of the different nc-Si i-layers in p-i-n devices cannot be readily compared to each other due to the substantial variations in the seeding procedures. Good devices must have high quality nc-Si absorbers, while the reverse is not necessarily true. The earlier 'shooting in the dark' efforts were intended to crudely elucidate some key concepts or promising approaches for nc-Si device fabrication, not to explicitly assess i-layer properties. Examples of nc-Si cells, made under different i-layer conditions and seeding methods other than p-seeding, are found in **Table 14**. As seeding can be more influential than i-layer process over device performance, we did not find any 'optimal' i-layer recipe. The higher-growth recipes are of more practical interests, of course. A firm conclusion regarding i-layers relates to the importance of their phase transformation, not the 'bulk' properties in well-developed nc-phase.

Via more developed seeding methods, nc-Si solar cells with reasonable FF have been deposited at higher than normal growth rates, using higher RF power that presumably causes higher defects in nc-Si. Device #R144 in table 14 is such a case. Device uniformity became markedly worse at higher growth rates not simply due to the variations of i-layer *thickness*, but also its *'phase*'. We conclude (and concur with some published reports) that the best nc-Si absorbers are made under plasma conditions close to the '*edge*' of the amorphous-to-nanocrystalline transition (see data later). Very high degree of nanocrystallinity is, perhaps counter intuitively, detrimental to device performance (at least for all the nc-Si solar cells we have produced). The understanding of this phenomenon, in our opinion, is infinitely more vital than, say, the achievement of lower defect density in nc-Si i-layers. Some kind of i-layer plasma grading or modulation may be helpful for maintaining the 'near-the-edge' conditions over large areas and/or over long deposition periods.

Using p-seeding technique, a number of nc-Si single junction solar cells, as well as a small number of a-Si/nc-Si tandem cells, were deposited under different conditions for the nc-Si i-layers in order to gain J_{sc} (higher red-light response) without losing FF and/or V_{oc}. For thicker cells, in order to maintain 'near-the-edge' growth conditions, small grading (profiling) of SiH_4 flow rate was sometimes used (with SiH_4 flow rate increasing linearly with time by 4-13%, e.g., from 8 to 10 sccm throughout the entire i-layer), thus changing the temporal profile of H_2 to SiH_4 dilution ratio. This i-layer grading has been found to slightly improve the V_{oc} and FF of the nc-Si single junction cells, at a small expense of J_{sc} (lower red-light response), for the reason that the nc-Si i-layer is prevented from becoming 'more nanocrystalline' versus the case of constant i-layer conditions (when SiH_4–flow grading is absent). A clear benefit i-layer grading, important for module processing, is the improved *device* uniformity due to expanded coverage of 'near-the-edge' nc-Si absorber over the substrates. Too much grading (> 50%?), however, resulted in low efficiencies as the i-layers became too amorphous near the end (and perhaps too nanocrystalline near the beginning). Of course, seeding plays a critical role in determining the effect of i-layer grading, since poorly seeded i-layer would show a natural evolution of its 'phase' with increasing nc-Si film thickness under constant plasma conditions.

Table 15 presents device parameters of some nc-Si cells, all produced by p-seeding, with various i-layer growth conditions and thicknesses, mostly on ZnO-coated SnO_2. Except the last two cells (R461-1, R462-4a), the SnO_2 was AFG-PVTCO (soda-lime glass). Cell efficiency goes up with thicker i-layer as expected, but we have not made more than a few thick cells (>2 μm) whose loss in FF (and V_{oc}) would eventually offset the gain in J_{sc}. The J_{sc}s of our 'champion' nc-Si single junction cells of thicker i-layers are well below 20 mA/cm^2 even on the superior Asahi SnO_2 (coated with ZnO), not to mention the commercial SnO_2. The ZnO/Al back contact is not sufficiently reflective in the red-light region. Better rear reflectors (e.g., ZnO/Ag) and other optical refinements are needed to raise cell efficiencies for the given quality of nc-Si absorbers.

Cell I.D.	Description and Notes	V_{oc}	J_{sc}	FF	Effi.
	(type of base-layer or TCO; type of back contact)	(V)	mA/cm^2	(%)	(%)
R246-1	Ref. cell, SnO_2, with STD nc-Si i-layer (low-rate); Al	0.47	14.9	66.8	4.7
R439-3	Short seeding; higher RF, thicker i, ZnO/SnO_2; ZnO/Al	0.46	14.8	63.5	4.3
R443-3	Much higher RF, lower R, thicker i, ZnO/SnO_2; ZnO/Al	0.46	16.8	56.7	4.4
R445-4	High RF, higher R, short p-seeding (ZnO/SnO_2); Al	0.50	15.9	58.1	4.6
R446-4	Higher RF power (x2 of STD); more non-uniform; Al	0.45	15.2	60.2	4.1
R461-2	Thicker i, ZnO/SnO_2(Asahi); ZnO/Al b.c.	0.51	17.2	68.3	6.0
R462-4	Much thicker i, ZnO/SnO_2(Asahi); ZnO/Al b.c.	0.50	19.0	66.6	6.3

Table 15 Comparison of p-i-n nc-Si single junction solar cells prepared by p-seeding under various i-layer deposition conditions (Al or ZnO/Al back contacts).

The relatively low V_{oc} (< 0.48 V) of many nc-Si cells might have resulted from some 'mismatch' between the seed-layer and the i-layer. For a given type of seeding, lower V_{oc} is normally found

in cells with higher degree of i-layer nanocrystallinity. Thus, it would appear that higher V_{oc} can be obtained if the initial i-layer is *barely* nanocrystalline (almost mixed-phase), not highly nanocrystalline. V_{oc} can also be affected by boron contamination and light soaking (see later).

Higher RF power has been used to increase deposition rate and to enhance nanocrystallinity of the i-layer for stronger absorption of red light leading to higher J_{sc}. While the J_{sc}s of such cells are indeed somewhat higher (and significantly so under large reverse electrical bias), these cells all exhibit significantly lower FFs and notably lower V_{oc}s, indicating that the i-layers are no longer 'near-the-edge', the preferred type of absorber for high efficiency. Examples of such runs, listed in table 15, include R439 (250W), R443 (325W), R445 and R446 (325W, longer time for thicker cells), and R465 (250W, much thicker). Another problem is the marked deterioration of uniformity of cell efficiency across the substrates. Clearly, we have the work cut out for us in both higher deposition rates and higher J_{sc} without sacrificing nc-Si growth homogeneity.

We compared nc-Si *n*-layer with a-Si n-layer for nc-Si cells and found no discernable difference. The nc-Si n-layer would simply be deposited directly on the nc-Si i-layer (no need for seeding). It seems that the contact to the sputtered Al is good enough with a-Si n-layer. Also, wider-gap a-SiC n-layer was tried for nc-Si solar cells without any apparent effect on efficiency. Such fine adjustments of device fabrication clearly are of secondary importance compared to other issues.

3.2 Contamination, device reproducibility, and process control

Dopant cross-contamination and gas impurity have severely hindered our efforts to effectively conduct experiments on fundamental device processes. Reproducibility problem has raised serious doubts about the validity of some seeding formulas and limited our choice of processing parameters. Apart from 'extrinsic' effects, we need to consider possible 'inherent' causes for the unacceptable performance variations in many ostensibly 'reproduced' nc-Si devices. One is the overall robustness of the seeding process as discussed earlier (doping efficiency, substrate type, seed layer thickness, etc.). Again, in a single reactor system, seeding and i-layer growth may depend on the recent operating history of the reactor. Also relevant is the compatibility of the seed layer (seeding surface) with the subsequent nc-Si i-layer. There are indications that excessive defects (related to harsh plasma conditions) on the seeded surface may degrade nc-Si (and a-Si) solar cell performance by conceivably limiting both V_{oc} and FF (and blue response). For example, when an *a*-Si:H i-layer was grown on a 'seeding layer' (made with high power and long duration that would have resulted in immediate nc-Si growth if nc-Si i-layer conditions had been used), the resulting a-Si:H p-i-n single junction solar cells exhibited much lower V_{oc} and FF compared to control devices deposited on standard a-SiC:H p-layers. Since the PECVD seeding process involves energetic etching plasma, we postulate that one should avoid 'overkill' in seeding. An optimal balance may exist between densities of 'seeds' and defects near the seeding surface. The delicacy of this balance could cause difficulties in reproducibility. Earlier, we cursorily discussed boron cross contamination resulting from seeding operations conducted prior to i-layer deposition. This subsection deals with contamination by the more 'lethal' n-type impurities, phosphorus and oxygen.

3.2.1 Phosphorus contamination of i-layers

We cannot overemphasize the difficulties in dealing with residual dopant cross-contamination of nc-Si 'i'-layers brought about by successive, alternate depositions of doped and 'undoped' layers in the same reactor in a single-chamber deposition tool. Greater progress would have been made

in understanding the nc-Si solar cell fabrication processes and in device optimization had we not been frustrated repeatedly by the lack of clear differentiation between contamination effects and true responses of device performance to the designed changes in processing conditions. On the other hand, there really should be no great surprise that contamination control is essential in a single-reactor environment as nc-Si is much more sensitive to background doping species (and to all sources of impurities) due to the much higher doping efficiency in nc-Si compared to that of a-Si. Apparently, in a single-reactor PECVD apparatus, without the benefit of a load-lock chamber that would permit the reactor to be 'sanitized' or 'covered up' between the depositions of successive layers, the accumulated doped layers from earlier deposition runs (or even in the same device run) can, by strong plasma excitation during seeding process, result in dopant contamination of the reactor even if the feed-gas mixture for the seeding plasma does *not* nominally contain any dopants.

The robustness of any seeding recipe must be judged in the context of its compatibility with low contamination requirement imposed by the single-chamber condition. As noted earlier, some of the CC-seeding and p-seeding recipes have been poorly reproduced and are sensitive to the single-reactor history of doped-layer depositions. In fact, the best nc-Si solar cells thus far were fabricated by p-seeding recipes suitable only if the reactor was relatively 'clean' (without n-layer deposition immediately prior to the present device deposition). The release of phosphorus from previously-deposited n-layers inside the reactor (within the same reactor cleaning-cycle), during and after intense plasma actions, has been a leading suspect of poor reproducibility in some promising seeding recipes, particularly those involving etching-dominant plasma steps (when pre-existing Si:H layers are exposed to chemically active plasma) that can 'liberate' dopants embedded in the doped layers shallowly buried below the surfaces of Si-film coatings. This mechanism of contamination is an important consideration in our recent efforts to attain better device reproducibility by developing tighter control over the p-seeding process, where the *growth* of p-type seeding film is much preferred than 'etching' dominated processes (involving removal of 'old layers'). That is, for contamination prevention, there should be net film addition (growth is stronger than etching) over the plasma exposed surfaces during seeding processes. Of course, as described in the last section, the situation actually gets very tricky, because when there is too much p-seeding film deposited, optical loss becomes unacceptably high.

Tests indicate that boron contamination from p-layers (including p-seeding) is mild relative to that of phosphorus resulting from n-layer depositions using PH_3. The extent of nc-Si i-layer contamination seems to correlate with the amount of PH_3 used in the most recent n-layers, and the thickness and doping level of the p-layer immediately preceding the nc-Si i-layer. In the most severe cases of P-contamination of the reactor following excessive use of PH_3 in the formation of nc-Si n-layers (intended to form tunnel junctions in tandem solar cells), the nc-Si absorbers became so conductive that the dark I-V curves of the devices no longer resembled diode behavior. The level of residual phosphorus inside the vacuum chamber, however, was beyond the detection limit by the RGA even in the most acute cases. Some clues about P-contamination may be provided by the dependence of QE spectrum on *forward* electrical bias, normalized to the zero-bias QE (to obtain a QE ratio spectrum), as illustrated by **Figure 10**. Consistent with its low FF, the relative QE reduction of the phosphorus-contaminated solar cell from run #R193 is much more pronounced compared to the 'uncontaminated' reference cell from run #R175 in the figure, especially at the longer wavelengths (suggesting difficulty with photo-hole extraction), upon application of a moderate, forward electrical bias. As expected, the lightly boron-contaminated sample, R240, shows some weakness in its QE ratio spectrum in the short-

wavelength region, but looks OK elsewhere. To suppress phosphorus contamination, we have developed n-layer processes with reduced PH_3 usage including shorter exposure time of PH_3 to the chamber, and with better 'burial' procedure by the subsequent p-layer and/or p-seeding steps. As a precaution (and a good general practice), the PH_3 gas-line was completely separated from the main gas line (manifold) devoted to undoped layers and p-layers. We have explored the 'air-exposure' practice for neutralizing P-contaminants in making a-Si/nc-Si tandem cells (see later).

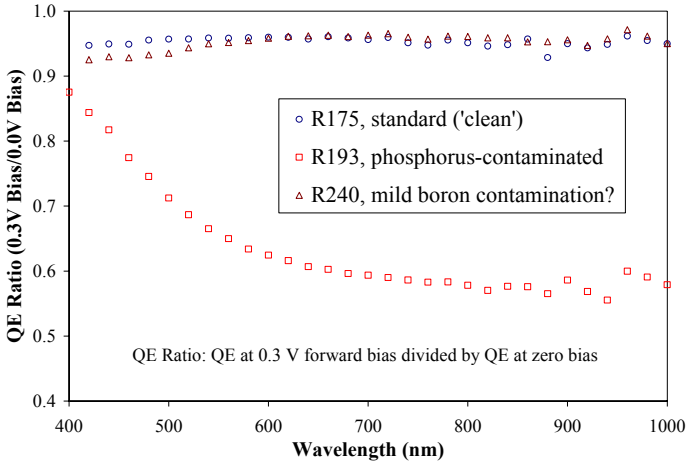

Figure 10 Effects of dopant contamination on QE-ratio spectra of three nc-Si solar cells.

3.2.2 Purity of process gases

The impurity levels of the process gases have also played a critical role in nc-Si device preparation. Due to the high R values needed for nc-Si i-layer deposition, the purity of H_2 gas has been found to be far more important than the base vacuum reading (typically below $3x10^{-6}$ torr) at the onset of nc-Si i-layer deposition. In Phase I, before we started to use oxygen getter (gas purifier) in the H_2 line, soon after the advent of some promising CC-seeding and p-seeding recipes for nc-Si single junction cells, we experienced a major drop in device efficiencies after the replacement of a nearly empty hydrogen gas cylinder (Cylinder I) with another cylinder (Cylinder II, from a different vendor). Even though the *nominal* purities of both cylinders were the same at six-nines (99.9999%), vastly different devices (especially FFs) were obtained using 'identical' deposition recipes and procedures. The device non-uniformity profile had also changed, such that some previous mixed-phase areas turned into amorphous-Si after the H_2 cylinder replacement. **Figure 11** depicts the effects of H_2 gas purity on the QE spectra of three nc-Si solar cells prepared under otherwise identical conditions by CC-seeding (within the same reactor-cleaning cycle and using the same commercial-grade LOF SnO_2 substrates). The highest QE and efficiency were obtained from the device made with the older, presumably cleaner H_2 from Cylinder I. The lowest QE came from a solar cell made with H_2 from Cylinder II. With the same 'bad' H_2 cylinder (II), a H_2-gas purifier was installed (before the mass-flow controller) to produce the solar cell with the intermediate QE in figure 11. The data interpretations for numerous nc-Si devices (showing poor reproducibility) were complicated by the use of H_2 gas of suspected lower purity. Some experiments indicate that even p-seeding (or CC-seeding) can be

sensitive to gas purity. This is rather surprising since p-seeding involves such heavy boron doping that low levels of impurities in H_2 are not supposed to matter. It is possible that when the seeding is not 'deep' (not well developed), gas impurities can compromise the seeds during or after seeding plasma. Note that good a-Si 'control' solar cells (FF > 73%) have been made with all the H_2 gas cylinders (without or with gas purifier). When a gas purifier is used on the H_2 gas line, no differences in nc-Si single junction devices were evident when the H_2 gas purity was lowered from 99.9999% (six-nines, far more expensive) to 99.999% (five-nines). Presently, the purities of our H_2 and SiH_4 are both five-nines (99.999%), as used in producing the good nc-Si and a-Si/nc-Si solar cells confirmed by NREL.

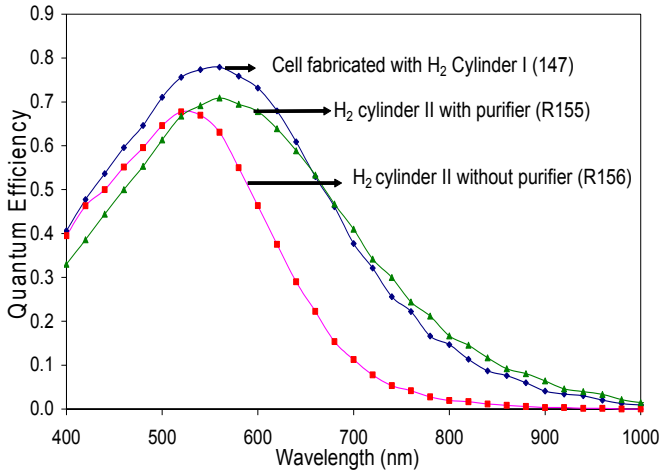

Figure 11 Effects H_2 gas purity on QE of nc-Si solar cells made by CC-seeding.

Table 16 presents the properties of representative solar cells made with or without dopant or gas-impurity contamination. We have made a number of repeat runs for R175, with widely varying results. Some of these runs had P-contaminated i-layers. But even in cases where phosphorus contamination was carefully prevented, the device reproducibility was still rather unsatisfactory.

Device I.D. #	Descriptions of Run (all cells on commercial SnO_2, with Al back contact)	V_{oc} (V)	J_{sc} (mA /cm^2)	FF (%)	Effi (%)
R175-1	Ref. cell, 99.999% H_2 plus purifier; Quasi-CC-seeding	0.49	15.5	65	4.9
R186-1	Same recipe as R175, but *contaminated* with phosphorus	0.51	~5.0	46	1.2
R221-1	'Exact' repeat of R175, including reactor 'history'	0.47	15.5	64	4.7
R196-2	Reduced phosph. contami. after *overnight* high-vacuum	0.47	15.0	61	4.3
R147-3	A 'clean' sample, CC-seeding, 99.9999% H_2	0.50	15.5	65	5.0
R210-1	Same recipe as R147, but 99.999% H_2 without purifier	0.45	14.3	63	4.1

Table 16 Comparison of nc-Si solar cells from 'clean' runs and contaminated runs.

In summary of section 3.2, cross-contamination by phosphorus can only be kept to acceptable levels for nc-Si devices by imposing rigorous operational care and severe limitations on the operating parameters for dopant-related processes. The minimum gas purity necessary for nc-Si solar cell fabrication (in our system) remains to be seen. This question must be answered in the context of another question raised later: Is the inferior performance of nc-Si solar cells of higher crystallinity caused by enhanced impurity (and/or residual dopant) contaminations?

3.3 Stability of nc-Si single junction solar cells

A number of nc-Si single junction solar cells have been light soaked under one-sun or 47-sun (accelerated light soaking) conditions. Some of the earlier devices made with inferior i-seeding recipes degraded severely (> 50%), as these cells appeared to have mixed-phase absorbers (high V_{oc} and low red response). This is not unexpected considering the thickness of the i-layers (near 1.5 μm). The later nc-Si single junction cells made by more advanced CC-seeding and p-seeding techniques, have shown relatively high initial efficiencies, higher red responses, high FFs, and excellent stability. As an illustration of the remarkable stability of properly grown nc-Si cells, **Figure 12** shows of the percentage change in efficiency with time of an nc-Si device under 47-sun illumination, along with that of an a-Si single junction solar cell (i-layer ~ 5500 Å). The 400-second exposure is equivalent to > 200 hours of one-sun soaking. No degradation is detectable for the nc-Si cell, as its change in efficiency is within the experimental uncertainty of the I-V tests. Such good device stability has been confirmed on many other (selected) nc-Si cells (with initial efficiencies > 4%), upon long-term exposure to one-sun illumination or under 47-suns. The largest degradation of any individual cells observed was only a few percent, which often contradicts data from co-deposited cells showing increases in efficiencies. Incidentally, we note that mixed-phase solar cells (Raman ratio $I_c/I_a < 1$) always show severe degradation upon light soaking (> 40%), in stark contrast to nc-Si cells of moderate to high nano-crystallinity.

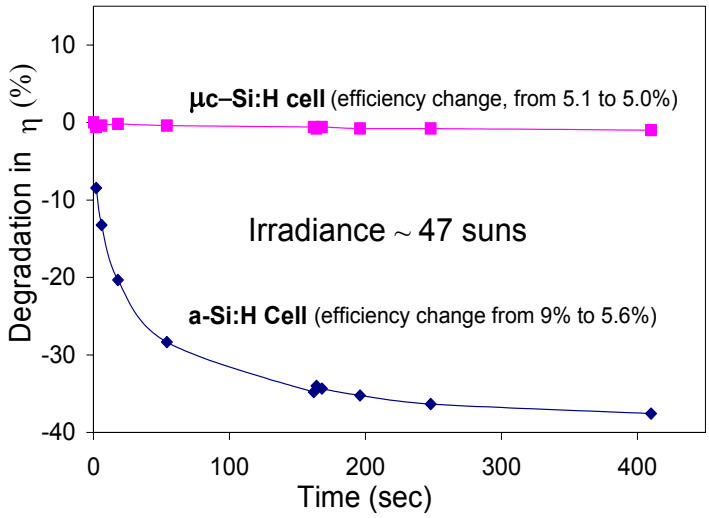

Figure 12 Efficiency changes of nc-Si and a-Si solar cells under 47-sun illumination.

Also encouraging is the fact that we have not observed any post-deposition, air-exposure induced instability among the nc-Si solar cells. If anything, the cell efficiency seems to increase slightly after weeks' of ambient storage. This fact is in sharp contrast with many reports from other laboratories on the post-deposition oxygen pickup in nc-Si cells (presumably due to porous microstructure), causing device instability and degradation that can overwhelm any light-induced degradation. Note that many of our earlier samples have been lost due to severe 'peeling' of the old AFG SnO_2 from glass. The problem has been resolved by the new version of AFG SnO_2.

The nc-Si single junction cells (with nc-Si i-layers deposited under conditions near the 'edge' to amorphous phase transition) consistently appeared stable (within 3-5% of the initial efficiencies) when studied using accelerated light soaking (ALS). In Phase II, we compared ASL with normal one-sun light soaking for a large number of devices, and found that nc-Si single junction cells did not degrade under one-sun. In fact, many of the nc-Si solar cells actually showed increases in efficiencies under one-sun (without correcting for possible losses in QE-derived J_{sc}s of the cells), as shown by the representative light-soaking histories of some cells in **Figure 13** (left) obtained from one-sun and 47-sun illuminations. The apparent increases in efficiencies under one-sun exposure came mostly from increases in the FFs of these cells under one-sun as shown in **Figure 13** (right). The V_{oc}s of these cells also often showed small to moderate increases upon one-sun exposure. This behavior is not quite the same as that observed under ALS (also shown in figure 13), perhaps because the changes occurred too quickly for ALS to capture. Also, the local cell temperatures would have been much higher under 47-sun exposure even with strong air-cooling. The light spectra of the 47-sun apparatus and the one-sun station are also different (tungsten-halogen versus metal halide lamps). For many nc-Si cells, the increases in FF and V_{oc} were not monotonic, and would be the largest (reaching peak values) in the first few days of one-sun exposure. Then they would decrease somewhat over longer time. But the final 'stabilized' values of FF and V_{oc} (after a few hundred hours) would, generally, still be unmistakably higher than their initial values. Overall, it is safe to conclude that our nc-Si *single* junction solar cells made with 'near-the-edge' type nc-Si absorbers are highly stable, staying within a few percent of their initial efficiencies under any light exposure or in room storage.

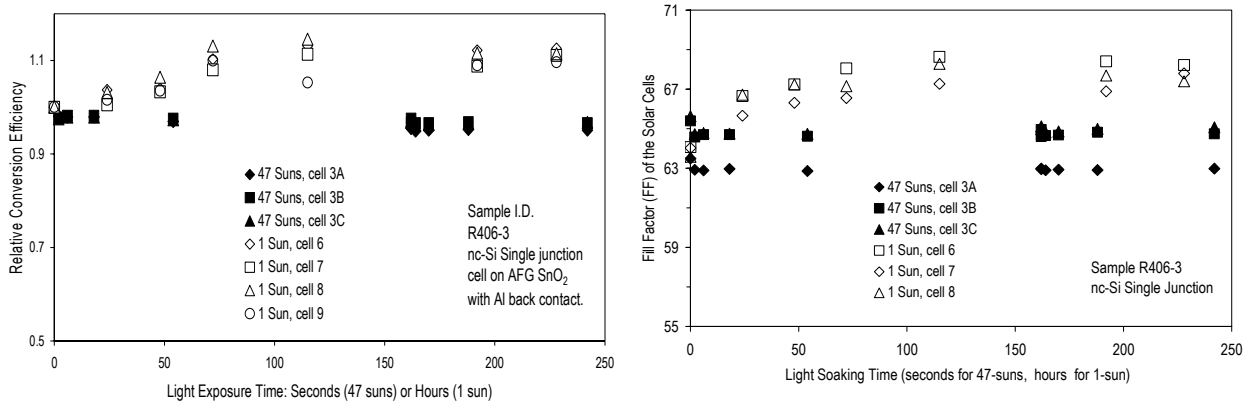

Figure 13 Variations of efficiency (left) and FF (right) with time of co-deposited nc-Si single junction solar cells upon 47-sun and one-sun light soaking.

The causes for the increases of FF and V_{oc} are unclear. All of the nc-Si single junction cells in this study had been previously annealed thermally at ~160 °C in air for 1-2 hours (in order to avoid the complication of possible thermal annealing effect under light) before they were subject to light soaking tests. Still, the combination of light and heat (sample temperatures might reach ~60-70 °C on the rotating one-sun light soaking station) may, speculatively, induce changes in the cell (e.g., at the TCO/p interface, or the p/i interface). There is no obvious rationale for the bulk of the nc-Si i-layer to 'improve' under light exposure. At first, frankly, we were rather skeptical about any kind of light-induced increases in cell performance, as the ALS data merely indicated the absence of significant degradation. There have been some nc-Si cells that show slightly losses in efficiencies, while co-deposited cells would show increases. To dampen the noises in one-sun light soaking data, we show in **Figure 14** the evolutions of averaged FF and V_{oc} of several adjacent nc-Si cells (co-deposited on the same piece of substrate) with light soaking time for four different runs. The corresponding efficiency data are shown in Figure **15**. Again, there are upward biases in these cell parameters with one-sun light soaking time. After more than 2000 hours, the average cell efficiencies are all slightly higher than the initial values.

To see if slight boron cross-contamination of the i-layer is responsible for light-induced increases of FF, we made a run (R435) of SnO_2/n-p-i-n/Al type nc-Si solar cells (with an n-layer against the TCO), in which the p-layer (including p-seed layer) does not make contact to the SnO_2. The cells from this run, on average, showed similar light-soaking behavior as the other nc-Si cells deposited directly on the SnO_2. Some individual cells from R435 showed improving FF, from 63-65% to ~ 67% after a number of days under one-sun, while others showed declining FF. The average FF stayed fairly constant over the 3-months light soaking period. Note that the i-layers of R435 cells probably are slightly n-type (not boron-contaminated p-type) due to the specific deposition sequence in the single-reactor. Hence, boron cross-contamination is unlikely to be linked with the observed light soaking behavior. Other more recent cells deposited directly on ZnO-coated SnO_2 superstrates also show no light or dark degradation. Hence, SnO_2 is unlikely to be a strong contributor to the observed light-induced changes. We conclude that the mild changes (slightly improvements) or fluctuations of nc-Si solar cells are not accounted for by some TCO-p interface process. Changes must occur inside the nc-Si cells regardless of contacts.

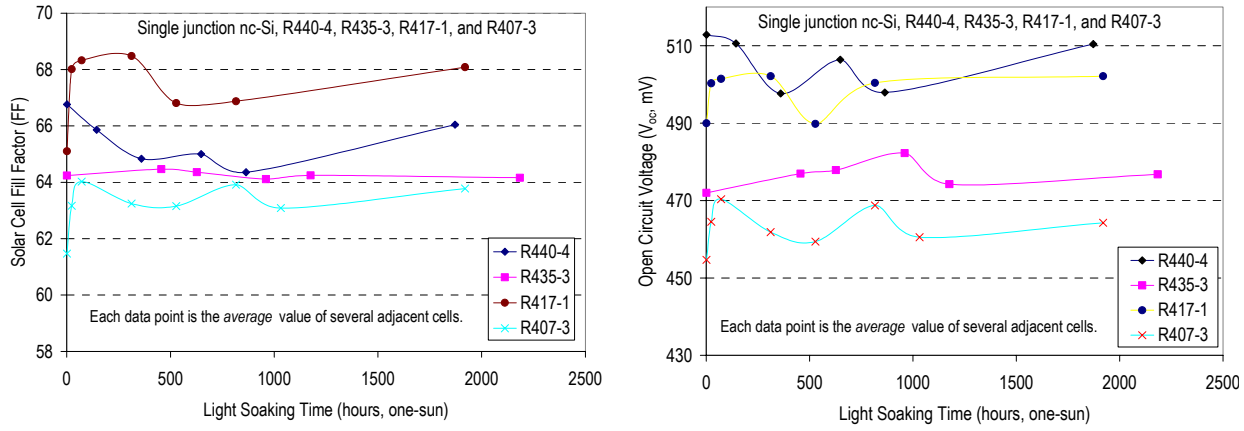

Figure 14 Average changes of FF (left) and V_{oc} (right) of nc-Si single junction solar cells from several runs with illumination time under one-sun.

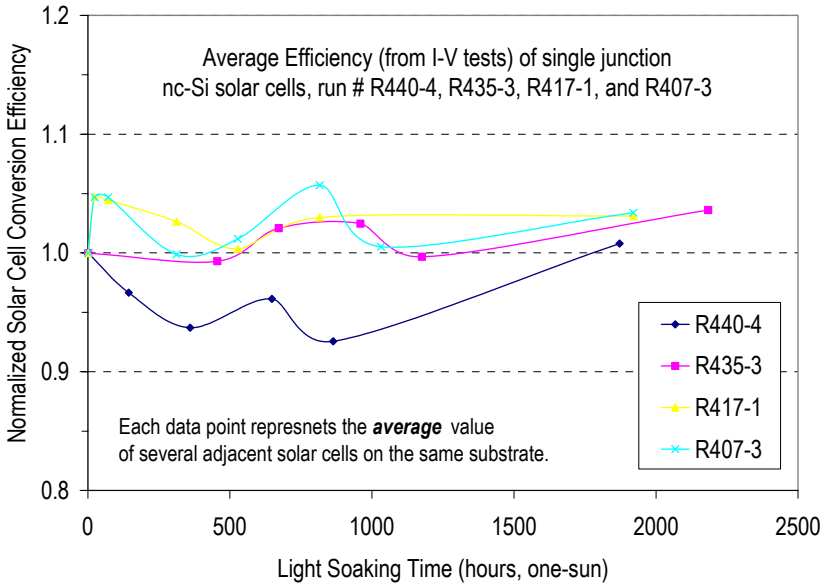

Figure 15 Variations with light-soaking time of *averaged* conversion efficiencies of nc-Si single junction cells, for four different runs, under one-sun exposure.

3.4 nc-Si absorbers deposited from Ar + SiH_4 gas mixtures (argon dilution)

A number of attempts have been made to find out if Ar dilution alone, instead of hydrogen, of silane is a viable method for growing nc-Si i-layers for solar cell purposes. Note that previously we had prepared a-Si:H solar cells, using substantial argon dilution of SiH_4 (with an Ar:SiH_4 dilution ratio up to 25:1), with superb initial performance. (Higher Ar dilution for a-Si is not advisable due to high defect density that leads to low solar cell efficiency.) The *stability* of Ar-dilution prepared a-Si solar cells upon light soaking showed no improvement compared to that of solar cells prepared by the traditional hydrogen dilution method, as we reported at this year's MRS Spring Meeting [11]. One of the original motivations for studying Ar dilution for nc-Si was to find an substitute, non-etching plasma for p-seeding directly on SnO_2 substrate (without plasma reduction or chemical alteration of SnO_2 associated with hydrogen plasma). An argon-rich, non-etching plasma also helps to keep the single-reactor system clean by avoiding etching-induced release of contaminants often encountered with strong H-plasmas.

When Ar was used for both i-seeding and bulk i-layer growth, with high Ar dilution > 40:1 and moderate RF power, no signature of nanocrystallinity was detected by device QE or Raman scattering measurements. Evidently, Ar-dominating plasma is not nearly as effective for *seeding* purposes as hydrogen-rich plasma. Later on, to facilitate nucleation and promote crystallization, we grew the Si:H absorbers, by Ar-dilution, on top of p-seeding layers which had been prepared by the more familiar hydrogen-dilution methods (e.g., i-seeding or p-seeding). The hydrogen dilution seeding recipes were the same as used for making good nc-Si absorbers from H_2+SiH_4 gas mixtures (pure hydrogen dilution) described earlier. That is, the initial seeding was done by hydrogen dilution, and the subsequent bulk Si:H absorber growth was carried out entirely with Ar dilution in a hybrid approach. No purifier was used for the Ar gas, which had a nominal purity of 99.9995%. When higher RF power was applied to the Ar + SiH_4 mixtures, nc-Si

absorbers were indeed obtained on hydrogen seeded surfaces. Selected samples from runs #R165 and R166, in device configuration without the Al back contact, were examined by Raman scattering spectroscopy at New Jersey Institute of Technology. The Raman spectra indicate substantial degrees of nano-crystallization in the absorbers (i-layers) made entirely by Ar dilution without hydrogen, as depicted in **Figure 16** for some samples from run R165 (from various positions over the 12"x15" plate).

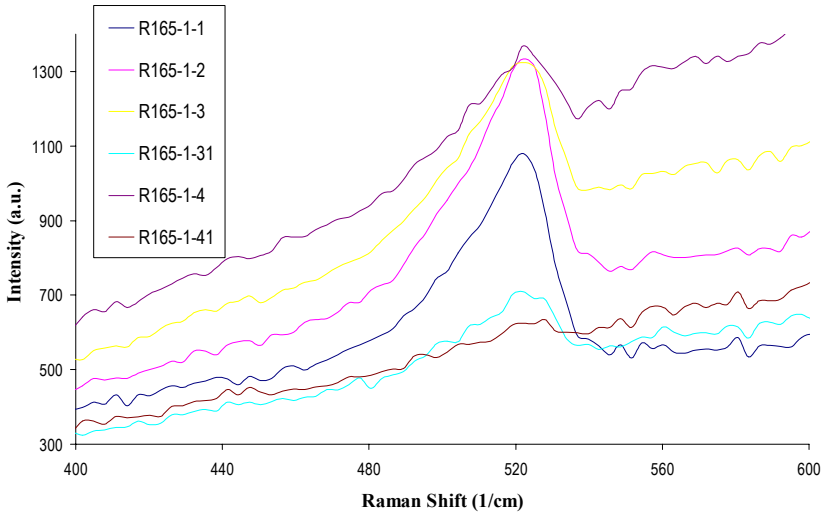

Figure 16 Raman spectra of nc-Si cells made from Ar+SiH_4 mixtures by H-dilution seeding.

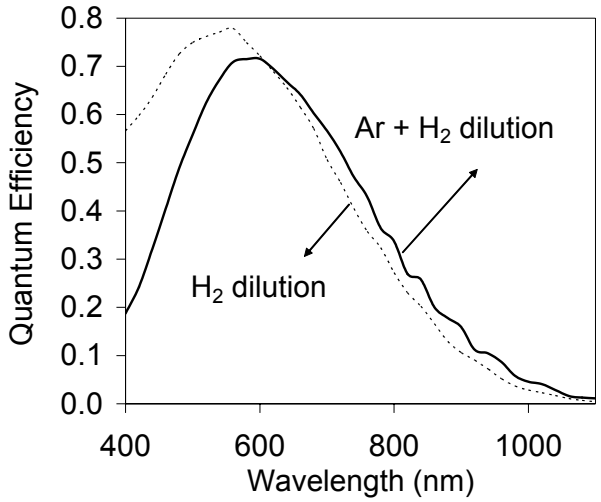

Figure 17 Examples of QE spectra of nc-Si solar cells (with Al back contact) whose nc-Si absorbers have been deposited by H_2 or Ar+H_2 dilution.

The Ar-dilution produced nc-Si solar cells have shown exceedingly low efficiencies (< 0.3%), with very low V_{oc} (< 0.3 V), J_{sc} (< 4 mA/cm^2), and FF (< 30%). Apparently, nc-Si i-layers derived from heavily Ar-diluted plasma are awfully defective, showing strong bias-dependence

of photo-carrier collection efficiency. (Similarly, a-Si:H cells made from Ar + SiH_4 mixtures with very high Ar dilution and/or at high RF power are also highly inefficient in PV performance.) Another serious issue with Ar dilution is the excessive non-uniformity in both film thickness and cell efficiency when high Ar dilution ratio and high excitation power are applied (considerably worse than that of hydrogen dilution under similar dilution ratios, total gas flow rate, and RF power). The nc-Si devices made with highly energetic Ar-rich plasma are stable against air and light exposures. In view of the low efficiencies of Ar-dilution produced nc-Si solar cells in the preliminary tests, we did not pursue this avenue. Instead, we have focused on the hydrogen dilution processes (perhaps aided by supplementary Ar dilution).

We have also made p-i-n cells with nc-Si i-layers deposited from mixtures of $Ar+H_2+SiH_4$ using high RF power and high dilution ratio. **Figure 17** compares the QE spectra of a nc-Si device deposited with $Ar+H_2$ dilution and another standard nc-Si device made with H_2 dilution only. These devices have the same i-layer thickness. The solar cell made with $Ar+H_2$ dilution shows enhanced long-wavelength spectral response, but depressed short-wavelength signal. The stronger red-light response may be partly due to increased internal structure (e.g., void, columns, and roughness) in the i-layer that can lead to increased scattering and absorption of light. The substantial loss of QE in the short-wavelength region for the $Ar+H_2$ diluted sample is partially attributed to the presence of a thick seeding p-layer (deposited by H_2-dilution method). There is a slight increase in efficiency for cells made with $Ar+H_2$ dilution (resulting mainly from higher FF) upon light exposure, similar to the conventional cells made with H-dilution alone. Films of nc-Si produced by $Ar+H_2$ dilution show strong non-uniformity in thickness and crystallinity. The performance of such nc-Si devices (by joint H_2 and Ar dilution) remains to be optimized.

In summary, RF-PECVD of Si:H thin films from SiH_4 highly diluted in Ar have been evaluated for solar cell applications. Both a-Si and nc-Si solar cells have been made with pure Ar dilution, but the concurrent presence of hydrogen is greatly beneficial for nc-Si i-layer quality (solar cell efficiency) and uniformity. Ar dilution of silane has found to be *ineffective* in seeding or nucleation for nc-Si film. For seeding purposes, hydrogen dilution is far superior (faster and more effective). Solar cells of nc-Si absorbers can be grown by diluting silane with Ar or $Ar+H_2$ mixtures. The nc-Si:H devices made with $Ar+H_2$ dilution show enhanced red-response but much lower efficiency compared with devices made with H_2 dilution only.

3.5 Structural and optical characterization of nc-Si absorbers

In this section, we report on the microstructural characterization and optical absorption spectra of the nc-Si i-layers, and correlate the 'film' properties with features of corresponding solar cells. Device (nc-Si absorber) non-uniformity will be described. High efficiency solar cells have only been made with 'near-the-edge' nc-Si absorbers (under plasma conditions rather close to the demarcation line of amorphous to nanocrystalline 'phase' transition). An optical technique has been developed at Syracuse University to probe nc-Si defect absorption in device configuration.

3.5.1 Non-uniformity, micro-structural characterization, and device correlation

We contend that *the* biggest stumbling block for high-rate, large-area nc-Si based PV *module* fabrication is the stringent '*near-the-edge*' deposition requirement for nc-Si. It is really hard to maintain 'near-the-edge' growth over large-area and/or over long periods of time using *simple* equipment. The narrow 'optimal' processing window for nc-Si is the root cause for poor uniformity of nc-Si *devices*. For device purpose, *thickness* uniformity is far less critical than

'phase' uniformity of nc-Si absorbers. In order to preserve the essential attributes of massively parallel processing of large number of plates in EPV's present PECVD system, reasonable nc-Si device uniformity must first be demonstrated in our R&D reactor. Otherwise, we cannot realize the promise, already proven for a-Si, of high throughput and low costs for nc-Si. We need to expand the process window for device reproducibility and uniformity without abandoning the basic features of the 'box-carrier' or introducing bulkier and elaborate gas distribution schemes.

In preparation of a-Si/nc-Si tandem module fabrication, some attempts at improving nc-Si device uniformity were made by depositing nc-Si absorbers in the non-depleting regime for the Si feedstock (SiH_4), typically at (relatively) lower vapor pressure with high gas flow rates. Even though much better film uniformity has been seen, the resulting nc-Si cells so far have had lower efficiencies (poor collection, and low V_{oc}), signifying that the nc-Si i-layers are either 'too nanocrystalline', or too electronically defective due to increases in ion-bombardments at lower pressures. Some solutions are to be contemplated for homogeneous yet fast growth of nc-Si.

The uniformities of i-layer microstructure and its correlation with device-performance were selectively investigated by Raman scattering. Strong spatial variations in i-layer microstructure *and* device properties frequently occur over the 12"x15" substrates, depending on i-layer growth conditions and the uniformity of the seeding layer. As an example, **Figure 18** (left) depicts the linear profile of the intensity ratio of Raman shifts, I_c/I_a (the ratio of signal at 520 cm^{-1} to that at 480 cm^{-1}), which can be considered a measure of degree of nano-crystallinity of the i-layer, of an arbitrarily chosen plate (from a deposition run with relatively high RF power). Figure 18 (right) is a schematic illustration of the distribution of Si 'phase' over the substrate. Under high pressure PECVD, a 'band' of visibly more-textured area is formed near the top of the plates (closer to gas-inlet) where the Si:H is thickest and the cells are mixed-phase type.

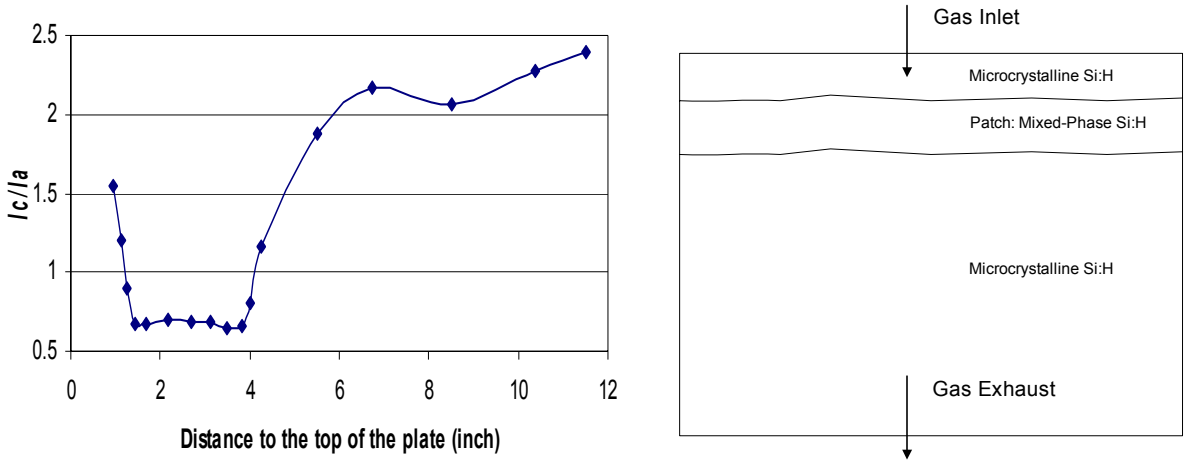

Figure 18 Raman scattering derived nano-crystallinity vs. sample position (left); illustration of 'phase' inhomogeneity of Si:H i-layer grown under gas-depletion conditions (right).

The substantial variation of I_c/I_a is unambiguously accompanied by strong variations in device parameters across the plate. The Si:H film becomes more nano-crystalline towards the bottom of the plate where the film is also thinner (lower deposition rate). The behavior is typical of plates

made with non-uniform i-layer thickness distribution that is accompanied by a substantial depletion of SiH_4. If the thickest-film areas were to be made nanocrystalline (rather than mixed-phase in nature or $I_c/I_a < 1$), then other areas would become overly nano-crystalline with severe degradation in device performance. In fact, the highest efficiency cells are consistently found near the borders between the mixed-phase region and that of nc-Si. We reiterate this critical fact: the highest solar cell efficiency is invariably found where the Si:H i-layer sits on the 'shoulder' of transition from mixed-phase to higher-nanocrystalline state (the so-called 'near-the-edge' type of nc-Si films), with I_c/I_a ratio between 1-1.5. Inferior device performance has been observed in areas that contain either mixed-phase Si:H or nc-Si of higher degrees of nanocrystallinity (compared to 'near-the-edge' materials). The nc-Si solar cells of high degree of nanocrystallinity consistently exhibit low FF and low V_{oc}. The red-light response is high only under strong reverse electrical bias, suggesting poor carrier collection (enhanced trapping and recombination). That is, the J_{sc} is actually lower in an nc-Si solar cell with an absorber of higher I_c/I_a ratio in spite of its superior optical absorption compared to the 'edge' type nc-Si i-layer. **Figure 19** presents the variation of V_{oc} (left) and QE-response at 800 nm (right) with Raman scattering derived I_c/I_a ratio for a collection of Si:H solar cells from different deposition runs (with Al back contacts). Among devices prepared by the same seeding technique (which has had overwhelming influence over device properties including V_{oc}), lower V_{oc} normally corresponds to higher nanocrystallinity of the absorber (with stronger red-light response under bias). Low FF and low V_{oc} also occur concurrently in solar cells with higher nanocrystallinity in contrast to devices with mixed-phase or 'near-the-edge' nc-Si absorbers (which tend to show high V_{oc} but low FF, or low V_{oc} but okay FF). Our findings are consistent with reports from other groups working on nc-Si solar cells.

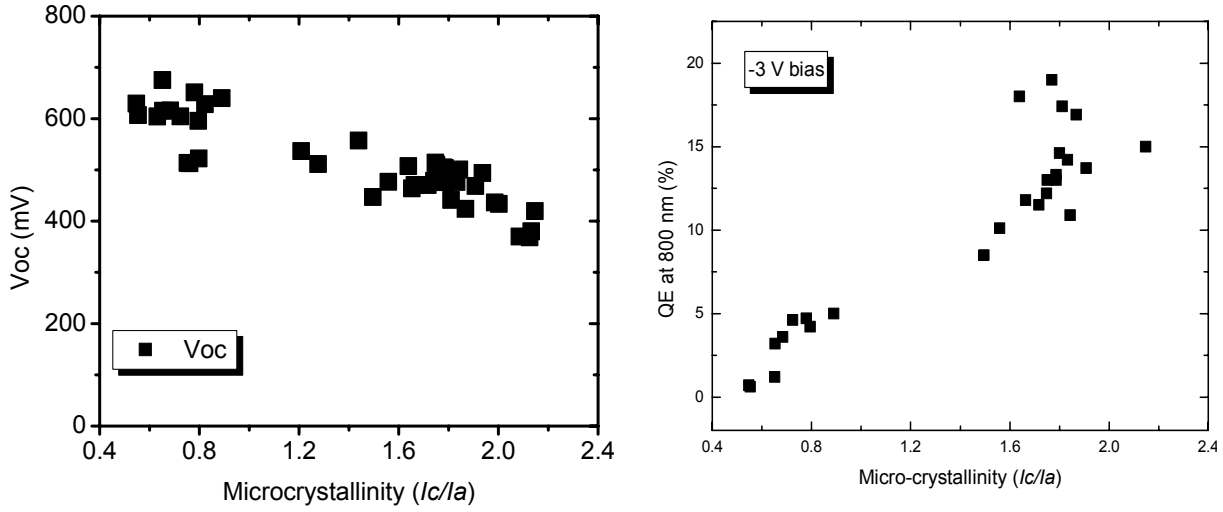

Figure 19 Variations of V_{oc} (left) and red-response (right) with I_c/I_a ratio of Si:H i-layer.

In addition to pronounced thickness variations, we frequently observe variations of surface 'texture' (the apparent haze or 'milkiness') over the deposited plates. Part of the changes in surface appearance may by caused by non-uniformity in seeding (as opposed to that of i-layer deposition), which has been noted under some conditions. Uniform deposition of nc-Si *films* certainly appears attainable, but we have yet to find ways to uniformly growing good nc-Si:H

devices. Device uniformity tends to get worse with increasing growth rate or higher SiH_4 depletion. A limitation of our reactor is the supply gas distribution that leads to non-uniform H_2 dilution profile (variation in the effective R) across the substrates under high plasma excitations. Since optimal nc-Si:H solar cells are obtained under conditions 'near the edge' or boundary of amorphous to nanocrystalline phase transition (a very narrow processing window indeed for large area deposition), spatial variations in SiH_x concentrations (among other things) naturally lead to vastly dissimilar degrees of i-layer nanocrystallinity over the substrate area.

A number of samples have been characterized by glancing angle x-ray diffraction (XRD) at NJIT. The XRD spectra of three solar cells with nanocrystalline or mixed-phase Si:H i-layers are shown in **Figure 20**. The XRD peaks at 2θ of 28.5° and 47.4° were taken as signatures of Si (111) and Si (220) planes, respectively. For the mixed-phase Si:H sample, no Si peaks were detected even though a weak signal at 520 cm^{-1} was seen in its Raman scattering spectrum. The sample with an I_c/I_a value of 1.88 ('near-the-edge' nc-Si) has the best PV performance among the three samples, and it shows strong Si (220) preference over Si (111). The sample with the highest nanocrystallinity (I_c/I_a=2.39), which is thinner than the 'edge' sample, displays a strong XRD signal at Si (111) and a comparatively weak signal at Si (220). The average 'grain sizes' of the two nc-Si:H samples have been crudely estimated to be 90 Å and 130 Å, respectively. Our data are consistent with other reports that the Si (220) planes orientation is favored by good nc-Si solar cells (presumably with the 'edge' type nc-Si absorbers). It is unclear if poor nc-Si absorber is always accompanied by a dominant Si (111) peak over Si (220) in its XRD spectrum.

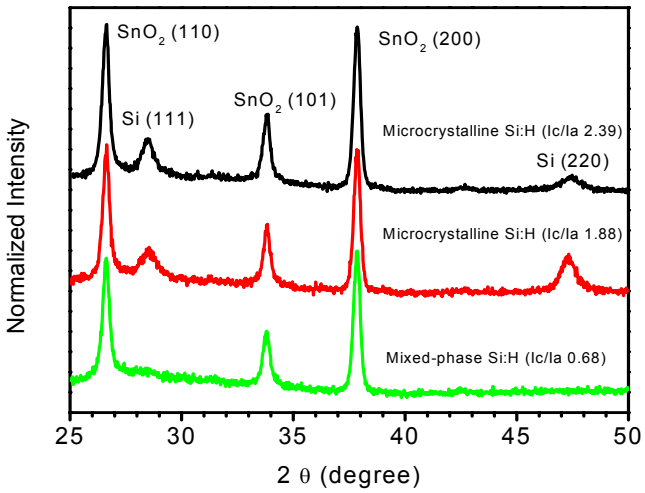

Figure 20 XRD data of mixed-phase and nc-Si solar cells.

Different surface morphologies have been observed by atomic force spectroscopy (AFM) for selected device samples. **Figure 21** depicts the AFM-derived surface profiles of two solar cells with nc-Si and mixed-phase Si absorbers, respectively. More irregular surface morphology and lower surface roughness were seen in solar cells with nc-Si i-layers compared to that observed in solar cells with mixed-phase Si:H i-layers. An increase of surface roughness (RMS, root mean square) value has been observed in the phase transition regions (the 'borderlines' between the mixed-phase and the nc-Si regions). Compared to areas with optimal I_c/I_a values ('near-the-

edge' films with good solar cell properties) which exhibit the lowest surface roughness, higher-nanocrystalline areas show slightly elevated surface roughness. More detailed structural data and graphic representations of our solar cells can be found in Liwei Li's Ph.D. thesis [15].

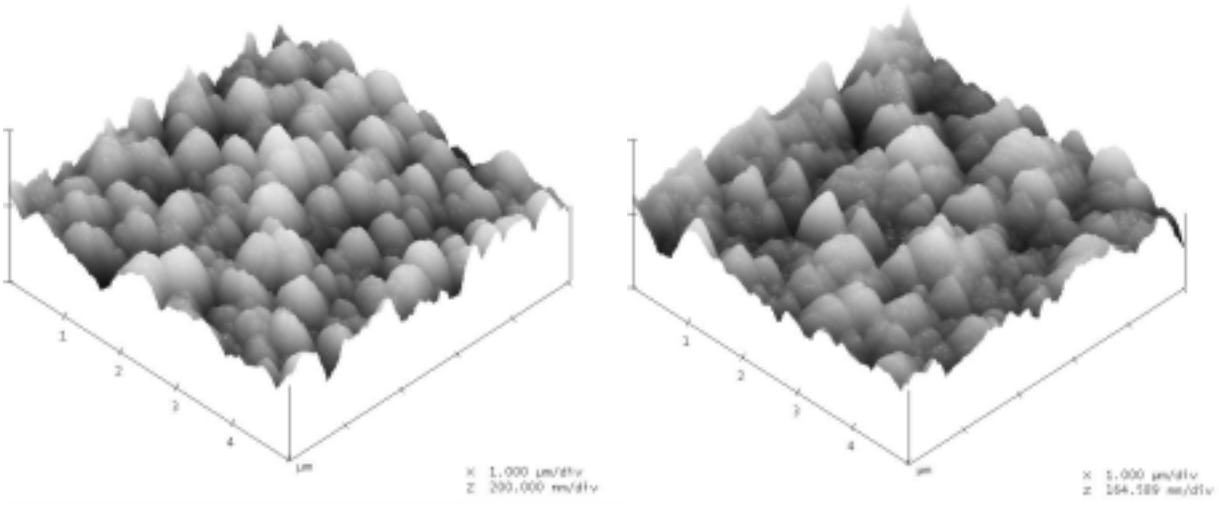

Mixed-phase Si:H nc-Si:H

Figure 21 AFM images of two solar cells with different i-layer properties.

In summary of this subsection, strong correlations among device performance, i-layer structural properties, and the related uniformity behavior of Si:H solar cells have been established by direct structural characterization using Raman scattering, XRD, and AFM techniques. Stable, high performance nc-Si solar cells contain nc-Si i-layers grown near the nanocrystalline-to-amorphous phase transition (or 'near-the-edge') where an optimal range of nanocrystallinity represented by moderate I_c/I_a values has been observed. Compared to solar cells containing i-layers of higher degrees of nanocrystallinity, the 'near-the-edge' absorbers (most favored by solar cells) having moderate nanocrystallinity exhibit preferential orientation corresponding to Si (220) planes, less-regular surface morphologies, and lower surface roughness.

3.5.2 Why 'near-the-edge' nc-Si makes better solar cell absorber?

Our device and structural data are consistent with the notion that the best (and stable) nc-Si solar cells comprise i-layers deposited near the border of nanocrystalline-to-amorphous (mixed-phase) transition. Such 'near-the-edge' type nc-Si films have moderate I_c/I_a ratio and smaller 'grain' size than the more crystalline films grown by, e.g., higher H_2 dilution. The extreme sensitivity of solar cell performance to the degree of nanocrystallinity of nc-Si i-layer is a major road block for device optimization, and for large area device uniformity (module fabrication). A great deal of variations in nc-Si absorber thickness can be tolerated in large-area nc-Si module preparation (since there is no penalty of light-induced instability proportional to absorber thickness), but not

the excessive spatial variations in efficiencies typically observed with our present processes. We must respond to the inescapable, overarching question in nc-Si PV technology: Is higher degree of nanocrystallinity *fundamentally* incompatible with good nc-Si device performance?

It is essential that some basic understanding (or conjecture) be established as to why higher nanocrystallinity results in inferior solar cells versus that of 'near-the-edge' nc-Si:H. We are of the opinion that, for nc-Si solar cell technology to be commercially viable (reproducible, uniform, high-throughput processes using relatively simple, low-cost manufacturing equipment), the PECVD processing window for nc-Si absorber needs to be drastically enlarged from its present, stringent requirement of producing '*near-the-edge*' material. What is wrong with nc-Si materials of higher degree of nanocrystallinity than the 'near-the-edge' variety? Is it easier contamination in the 'grains' (as opposed to the 'grain boundaries')? Insufficient hydrogen passivation of defects along 'grain boundaries' (loss of H coverage)? Unidentified deterioration of carrier transport in the film growth direction? Poor interface compatibility or higher density of p/i interface defects? Or something else? A more transport-friendly columnar structure has been speculated to exist in 'near-the-edge' type nc-Si. Perhaps, 'near-the-edge' nc-Si is required only near the p/i interface, not across the entire absorber thickness. We just do not know.

Some ideas can be tried to broaden the processing window for nc-Si films, including ways of independent control of atomic hydrogen for the *dual* roles of defect passivation and promotion of crystallite growth; the use of different gas/feedstock mixtures and/or diluents (e.g., adding some inert gas); variations in 'etching' chemistry (e.g., using halogens from SiF_4 or $SiCl_2H_2$) that does not rely solely on hydrogen; modulation of plasma conditions (e.g., gas flow and/or power level grading); lower substrate temperatures; very high TCO texture; alloying of nc-Si; and VHF PECVD at low pressure (low gas depletion) using specially designed electrodes (for uniformity). These tricks may help to prevent the nc-Si material from becoming 'too nanocrystalline'.

3.5.3 Optical absorption of nc-Si i-layer by infrared photocurrent spectroscopy

We sought characterization techniques for intrinsic nc-Si films and especially solar cells, which can be used as a guide for understanding and optimizing the fabrication process of nc-Si and their solar cells. This subsection (written by R.A. Middya) describes the efforts in establishing such a technique by A. Rafik Middya, Eric A. Schiff, and Jianjun Liang at Syracuse University.

Despite the tremendous progress in nc-Si solar cell technology in the last ten years, the electronic transport in devices and the critical factors controlling the performance of solar cells have not been properly understood. Conventionally, the constant photocurrent method (CPM) and solid state photocarrier grating (SSPG) techniques have been used, respectively, to estimate defect density and minority carrier transport in intrinsic nc-Si. However, both of these techniques provide information only about isolated films, but not actual devices. The carrier transport direction is different in the films (coplanar) than that of real-life solar cells (perpendicular to the substrate). Hence, we propose infrared photocurrent spectroscopy (IPS) as a more appropriate method to estimate the defect density in intrinsic nc-Si *directly* in p-i-n solar cell configuration.

In the IPS technique, an intensity-modulated (chopping frequency = 1 kHz) light beam from a monochromator is incident on the sample from the glass substrate side. Any light not absorbed by the various Si:H layers (p, seed, i, n) is partially reflected from the back Al contact. The modulated photocurrent, $J_{sc}(h\nu)$, of the solar cell is detected by a lock-in amplifier. The $J_{sc}(h\nu)$ spectrum is acquired by a computer. A thermopile was used to calibrate the photon flux $F(h\nu)$.

Two optical filters have been used to measure optical absorption over the wide range of photon energy (3.2 eV to 0.8 eV). One filter is used to cut off all the light below 780 nm, and another filter is used to block all the light below the wavelength 1000 nm. Assuming that J_{sc} is equal to the area density of photogeneration within the intrinsic layer of the solar cell, we can convert the photocurrent signal to optical absorption coefficient using the expression $J_{sc}(h\nu)/(\chi eF(h\nu)d)$, where e is the electronic charge, $F(h\nu)$ is the photon flux, d is the thickness of the intrinsic layer, and χ is a multiplication factor to take into account the reflection from the Al back contact. For simplicity, here we assume χ to be a constant, and we use a value $\chi = 1.4$ for later discussions.

We have measured by photocurrent spectroscopy three sets of nc-Si:H solar cells prepared at EPV using three different seeding methods. The samples have the standard device structure as described earlier: soda-lime glass/SnO_2/p/i/n/Al. The thicknesses of the nc-Si i-layers are in the range of 1.2-1.5 μm. The major solar cell parameters for the samples are given in **Table 17**.

The IPS derived optical absorption spectra of the absorber layers of four solar cells (two samples from each run of R130-1 and R140-3), are shown in **Figure 22**. The labels '130-1-e' and '130-1-f' refer to two adjacent, different 'dots' made on the same plate R130-1. Samples from R141-1 had peeled off during measurements. In the same plot, the optical absorption spectra of standard amorphous silicon (a-Si:H) and crystalline silicon (c-Si) are also shown for comparison.

Run I.D.	Seeding (nucleation) Method for i-layer	V_{oc}	J_{sc}	FF	Effi.
	(All cells on LOF SnO_2, with Al back contact)	(V)	(mA/cm^2)	(%)	(%)
R130-1	H-etch seeding on a-SiC p-layer	0.50	13.6	55	3.7
R141-1	i-seeding using high H_2 dilution to SiH_4	0.52	14.7	47	3.6
R140-3	p-seeding with thicker 'nc-Si' p-layer	0.48	13.2	65	4.1

Table 17 Properties of nc-Si solar cells studied by infrared photocurrent spectroscopy.

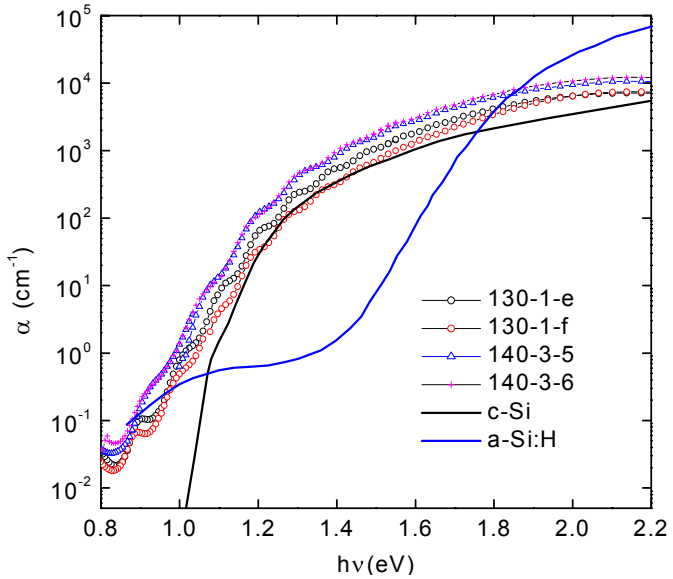

Figure 22 Optical absorption spectra of i-layers of selected nc-Si solar cells.

It can be seen from figure 22 that the spectral dependence of α of the nc-Si i-layers of all four solar cells resemble that of c-Si, and they are quite different from that of a-Si:H. In other words, we can state that, in these nc-Si solar cells, the photogeneration mainly occurs in the crystalline grains. The shape of the nc-Si absorption curves differs from that of c-Si for photon energies below 1.1 eV. The low-energy absorption of these samples appears to flatten near 0.8 eV, with a 'saturation' value of α at 0.8 eV around $5x10^{-2}$ cm^{-1}, which is in the same range as that of best nc-Si:H films reported in the literature (measured in co-planner configuration). It has been demonstrated that α at 0.8 eV reflects Si dangling-bond related defects in nc-Si films [17]. Therefore the defect densities of EPV's nc-Si samples, measured in solar cell configuration, are similar to that of best nc-Si:H films measured by CPM. However, optical absorption estimated in co-planner configuration always exhibits higher values than sandwich (CPM) configuration [18]. Thus, EPV's nc-Si devices may have slightly higher defect density than that of the best nc-Si films reported in the literature, *if* one does not correct for optical enhancement effect (which is stronger at longer wavelengths, not a constant) due to texturing and Al back contact in solar cells.

Slightly higher defect density (compared to the best reported in the literature) of EPV's sample R130-1 cannot account for the low FF of ~ 0.55. During the fabrication of solar cells, H-plasma seeding treatments on p-type a-SiC:H were performed before the growths of i-layers. Such seeding related process may induce lower extended defects ('twins and dislocations') within columnar grains than in i-layers without proper seeding procedure. The IPS data suggest that EPV's samples have low density of silicon dangling bonds (which are presumably concentrated at the 'grain boundaries', if the 'grain' and 'grain boundary' concepts are valid at all in nc-Si material). From earlier sections, the inferior performance of most of the nc-Si:H solar cells is attributable to inadequate seeding procedure (interface defects), rather than some 'bulk' defects.

A noteworthy feature of figure 22 is the variation of optical absorption (α), at a given photon energy ($h\nu$), among the nc-Si:H samples for $h\nu \approx 1.2 - 2.6$ eV. Moreover, interference fringes have been observed for all samples at $h\nu < 1.5$ eV. This type of variation in α (for the same $h\nu$) has not been widely reported, or at least the observed differences in the literature have not been so prominent for PECVD nc-Si:H films having varying crystalline fraction (X_c). However, there have been reports describing variation of α of HWCVD samples having different microstructures (i.e., different X_c) [19]. It is generally observed that the surface of nc-Si films prepared by hot-wire CVD is more textured than PECVD films, i.e. internal texturing (suitable for light trapping) of the two types of films can be quite different. Generally, α in the visible as well as in the infrared region may vary if i) crystalline fraction (X_c) varies or ii) internal texturing of the films varies with different H-dilution (or silane concentration). Thus, the large variations of α in the infrared region of EPV samples can be caused by i) variation in X_c (for samples from different runs, or of different film thickness), or ii) different internal texturing of the films which might be induced by small variations in the seeding surface prior to nc-Si i-layer deposition.

4. Tandem a-Si/nc-Si Solar Cells

This section describes device activities explicitly targeted at a-Si/nc-Si tandem solar cells. Because single junction nc-Si has too lower a V_{oc} and thus low efficiency, the true value of nc-Si solar cell can only be realized in spectral-splitting multijunction solar cells, such as a-Si/nc-Si

tandem devices, where nc-Si serves as the specialist for capturing long-wavelength light. A primary goal of this subcontract is to build efficient *and* stable a-Si/nc-Si tandem solar cells.

4.1 Some general observations

Broadly, there are two key obstacles to fabricating high performance a-Si/nc-Si cells. The first is the integration of the two separate p-i-n cells (top a-Si cell and bottom nc-Si cell) through a good contact-interface, known as the tunnel junction (TJ), between the n-layer of the top cell and the p-layer of the bottom cell. In the p1/i1/n1//p2/i2/n2 sequence, the n1//p2 intersection is the tunnel junction (TJ). This n-p junction is in reverse direction of the active cells. Here, electrons and holes must be able to efficiently recombine as if through a metallic contact in order to avert charge build-up and other complications. Effective TJ with low optical loss has long been a great challenge for the preparation of a-Si alloy (and nc-Si) based multi-junction solar cells. The second challenge, for *single* chamber PECVD where cross-contamination of nc-Si i-layer is detrimental, is the ensure minimal-contamination of the nc-Si bottom cell *after* the preceding deposition of at least three heavily doped layers in the same run, including particularly the n1-layer of the top cell. These two topics have taken the vast majority of our efforts in a-Si/nc-Si study, while the details of the many individual layers have not been adequately examined.

Since the top a-Si solar cell needs to be moderately thick (~2500 Å thick) in order to produce high enough current to match that of the bottom nc-Si cell (compared to the case of iso-bandgap a-Si/a-Si tandem solar cells), the stability of the a-Si top cell largely determines the light-induced degradation behavior of the tandem device (because the bottom nc-Si cell would not degrade much). Thus, we briefly explored deposition conditions for more stable a-Si i-layer by using higher H_2 dilution of SiH_4 at different power levels. Such conditions are believed to result in more 'protocrystalline silicon' compared to our earlier standard a-Si made at lower hydrogen dilution (H_2:SiH_4 = 6:1). Another incentive to change the a-Si growth conditions is the need for higher V_{oc}, as our single junction a-Si solar cell, on commercial SnO_2, have only ~ 820 mV at the deposition temperature of ~ 190 °C. The low V_{oc} partly limits the conversion efficiency of tandem cells. We have found that, depending on pressure, H_2/SiH_4 ratio, and RF power (when temperatures were kept about the same), the 'protocrystalline Si' solar cells can have V_{oc} of ~ 870 mV (on inexpensive AFG SnO_2), notably higher than the value of lower-dilution a-Si cells. Some 'protocrystalline Si' cells, however, actually showed lower V_{oc} (790-810 mV) when prepared under higher H_2 dilution, possibly due to the near-onset of 'phase transition' into the nanocrystalline state (at thickness > 4000 Å). We have yet to verify that the stability of the single junction 'protocrystalline Si' solar cells is truly superior to the reference a-Si cells. However, the light-soaking data of a-Si/nc-Si tandem cells incorporating such 'protocrystalline Si' top cell indicate that top cell stability should be quite decent (see later). This improved a-Si i-layer was incorporated into our 'champion' a-Si/nc-Si cell which showed 8.7% after 500 hours. More work remains to be done on improving the performance and stability of the a-Si top cell.

We compared a-SiO_x:H p-layers, made from a mixture of SiH_4+CO_2+TMB, for a-Si single junction solar cells with standard a-Si cells containing a-SiC p-layer from SiH_4+CH_4+TMB. The objective was to see if higher V_{oc} and/or transparency can be obtained without loss of FF by alloying with oxygen instead of carbon (which mostly gets incorporated in a-SiC:H as CH_3). Small gains in V_{oc} and J_{sc} (higher blue and peak QE) were observed, but these were offset by somewhat lower FF. Overall cell efficiencies were about the same for the a-Si single junction

cells. Due to resource limitations and demands from more urgent tasks, we did not pursue further the avenue of higher top cell efficiency by using an alternative wide-bandgap p-layer.

At present, we do not have a good standard (calibration) cell to accurately set the light intensity for I-V measurements of the a-Si/nc-Si tandem cells. The light from a single tungsten-halogen lamp (projector light bulb) serves as the 'solar simulator'. Thus, the J_{sc} values from I-V tests are likely subject to significant error. Wherever possible, we tried to use QE data to 'correct' our J_{sc} values in calculating cell efficiencies. But, quite often, reliable QE data are not available due to tunnel junction or other unknown reasons (when the QE currents would excessively vary with electrical bias, and 'collapse' under zero bias). To be self-consistent, we simply have been using an a-Si/a-Si standard cell to calibrate light intensity. From comparison of J_{sc} data obtained by some I-V tests at NREL and by QE at EPV, our J_{sc} values tends to be lower than NREL's by a few percent. On the other hand, our FF values are higher than NREL's measurements (for both nc-Si single junction and a-Si/nc-Si tandem cells), probably due to difference in spectral contents of the light sources. The most recent efficiency values of an nc-Si single junction cell measured at EPV and NREL are in agreements (~6.5%), although the J_{sc} and V_{oc} values are not identical.

The adhesion on SnO_2 superstrates by thick a-Si/nc-Si dual-junction solar cells (total thickness of Si:H layers $\geq$ 2 μm) was often found to be problematic on smaller pieces of SnO_2/glass attached to full-size, larger aluminum carrier plates (substrate holders). Post-deposition peeling of the Si:H films, upon exposure to air of the PECVD chamber, has 'ruined' the majority of our tandem cells with thick nc-Si bottom junction, even for carefully cleaned substrates. Tandem cells with thinner nc-Si absorbers ($\leq$ 1.5 μm) did not encounter trouble with adhesion. The film 'cracking' or steady flake-off event rarely occurred on larger (12"x15") commercial SnO_2/glass superstrates (which are less textured than the 3"x3" research grade SnO_2), or for single junction nc-Si cells of any thickness. We conclude that 1) a-SiC p-layers have weaker bonding than p-seeding layer on SnO_2; 2) Higher textured SnO_2, in this case, is no better than lower-textured SnO_2 for adhesion purposes; 3) Larger substrates suffer less film peeling apparently due to more effective relief of stress along the edges of the plates where Si:H films are thinner. Smaller substrates placed in the center of carriers do not get this kind of relief and, as a result, peeling would start from the edges and quickly propagate towards the interior areas. The adhesion of SnO_2 to glass has been excellent for any kind of plasma processing conditions or film thickness.

4.2 Tunnel junctions studied by the a-Si/a-Si test structure

In preparation of a-Si/nc-Si double-junction solar cell fabrication, we began to evaluate tunnel junction (TJ) processes using the simpler a-Si/a-Si test configuration in the 2nd half of Phase I. It made sense to side-step complications with nc-Si in the early going. Three types of Si-based TJ recipes were examined in a-Si/a-Si dual-junction cells: 1) nc-Si n-layer; 2) the combination of a-Si n^+ and nc-Si p-layer; 3) the combination of a-Si n^+ and a-Si p^+ (i.e., both n1 and p2 layers are heavily doped). **Table 18** presents the parameters of selected a-Si/a-Si tandem solar cells made with various TJs recipes, with Al back contacts, and on commercial SnO_2/glass superstrates. The efficiencies are before-light-soaking (initial) values. Good a-Si/a-Si cells can be made with nc-Si n-layer as TJ (the low V_{oc} observed is mainly due to insufficient thickness of the p2 layer), but the nc-Si n-layer approach has since been precluded from a-Si/nc-Si fabrication owing to the phosphorus cross-contamination issue. The n^+ method has worked OK. The n^+/p^+ formula has worked the best for a-Si/a-Si tandem cells, and proved to work OK for the more intriguing a-Si/nc-Si tandem devices. Most of the TJ experiments were initially devoted to fabricating nc-Si

n-layers (n1 layer for the top junction), using seeding and growths methods similar to those used for nc-Si i-layers described earlier, as nc-Si n-layer has enjoyed great success in forming TJ for a-Si alloy based multi-junction solar cells. Here, we must emphasize the fact that simply depositing a-SiC or a-Si p2-layer on top of a-Si n1-layer (to form an *amorphous* TJ) does not work well even for a-Si/a-Si tandem cells (FF in the 60% range with loss in V_{oc}), and is utterly unusable for the more demanding a-Si/nc-Si dual-junction cells. Note that, surprisingly and for some reason not yet understood, the TJ recipe being successfully used in our manufacturing of large-area a-Si/a-Si tandem PV modules could *not* be simply transferred to the smaller R&D system. This hurdle has caused unexpected delays in tandem cell fabrication and optimization.

To minimize optical loss in the n1 layer and eliminate a-Si n1, we tried direct seeding of nc-Si n-layer on a-Si i1-layer (at the i1/n1 interface) by H-rich plasma to form TJ. Direct seeding on i-layer damaged the a-Si solar cells (used as the top cell in a-Si/nc-Si tandem) as noted previously. The efficiency loss (lower FF) is notable even if the a-Si i-layer is only briefly exposed to an intense plasma of H_2+SiH_4+PH_3 mixtures (with net film growth, not etching). Thus, seeding is not advisable anywhere inside or on the a-Si i-layer (for TJ purpose or for nc-Si i-layer).

The seeding and growth of nc-Si n-layers involved relatively high concentration of PH_3 in the feed-gas mixtures. The nc-Si n-layer tunnel junction had worked well for a-Si/a-Si tandem cells, with FF of 74-75% in cells of well-balanced currents from top and bottom junctions. (It is worth noting that in a number of a-Si/a-Si tandem solar cells with presumably nanocrystalline Si n-layer TJs, the V_{oc} values were substantially lower than the 1.6 V obtained for reference a-Si/a-Si solar cells, all on commercial SnO_2. Our nanocrystalline Si n-layer TJ recipe remains to be fine-tuned for a-Si/a-Si cells). We found out, however, that a TJ process suitable for a-Si/a-Si tandems does not automatically work for a-Si/nc-Si 'micromorph' type devices due to the much stronger propensity of nc-Si to phosphorus cross-contamination, nc-Si 'i-layer' is markedly more susceptible to residual contaminants than a-Si i-layer. Furthermore, the TJ may influence the subsequent seeding process for the nc-Si i-layer. Prolonged use of PH_3, under high plasma power and especially high pressure for nc-Si n-layer seeding, had caused acute contamination even in subsequent nc-Si runs after extended periods of bake-out and high-vacuuming.

Cell I.D.	Type of Tunnel Junction (n1//p2 interface), Remarks	V_{oc}	J_{sc}	FF	Eff.
	(Al back contact; i2-layer a-Si thickness~0.45μm)	(V)	mA/cm^2	(%)	(%)
R283-2	a-Si n1//a-SiC p2 (low C%). Old reference recipe	1.57	6.1	66	6.3
R192-1	nc-Si n1//a-SiC p2 (thin). Bad contamination in nc-Si!	1.53	6.2	75	7.1
R215-2	a-Si n1 + thin nc-Si n1//a-SiC p2. Less contamination	1.56	6.0	72	6.7
R272-1	nc-Si n1 (fairly thin)//a-SiC p2 (lower TMB%)	1.52	6.1	71	6.6
R249-1	a-Si n^+//a-Si p^+ (thin) by conventional procedure	1.59	6.2	61	6.0
R294-2	a-Si n^+//a-Si p^+ (thin), new Ar dilution for p^+ layer. Clean	1.60	6.1	73	7.1
R295-1	a-Si n^+//a-Si p^+ (thin), thin p^+ layer deposited by Ar dilu.	1.55	6.2	73	7.0

Table 18 Different tunnel junctions tested in a-Si/a-Si tandem 'dummy' cells.

To minimize contamination of the bottom nc-Si i-layer, we have investigated tunnel junction recipes that entail less PH_3 exposure to the PECVD reactor compared to that needed for nc-Si n-

layer. Such techniques as relatively-heavily doped n^+/p^+ junctions have been explored, so has the use of an n^+ layer by itself (with short n^+ deposition time). The more-heavily doped amorphous Si based tunnel junctions have worked OK but not great, as the FF of the a-Si/a-Si tandem test devices were in the mid to high 60% range. We also observed that the presence of a thin, slightly n-type nc-Si layer (as an unintentional tunnel junction) sandwiched between n1 and p2 layers greatly reduced the V_{oc} and the FF of the tandem solar cells. We did notice that when the n1-layer thickness was greatly reduced (< 150-200 Å), cell performance fell dramatically.

From our study of a-Si:H i-layers produced from Ar-rich plasma [11], it is evident that *narrow-bandgap, highly defective* a-Si:H thin films (even *without* any doping) can be readily and quickly produced from Ar+SiH_4 gas mixtures of high Ar concentration, as judged by the very low V_{oc} of some of the solar cells. Such a low-bandgap material is an ideal candidate for TJ applications. We have succeeded in depositing thin p-type Si films (p^+ layer), from Ar+SiH_4+TMB mixtures, in a matter of 10-30 seconds, for TJ formation on a regular a-Si n1-layer. FF of ~ 0.74 has been obtained for a-Si/a-Si tandem cells with fairly balanced currents and (relatively) low optical loss. Cells from R294 and R295 in table 18 were fabricated by this Ar-dilution p^+ TJ. This novel, simple, fast, and effective TJ process, which does not rely heavily on the n1-layer, is far more compatible with the stringent low-contamination requirement for depositing tandem a-Si/nc-Si solar cells in a single chamber PECVD system. It has been applied to a-Si/nc-Si cells (see later).

4.3 Tunnel junction experiments in a-Si/nc-Si tandem solar cells

As a test for simple amorphous-Si TJ (a-Si n1-layer followed by a-SiC p2-layer), we produced an a-Si/nc-Si tandem solar cell, deposition #R253, using the CC-seeding method for the bottom nc-Si junction (seeding on thick a-SiC p2-layer). The device efficiency is low (see Table 19). The QE spectra indicated significant optical loss (in the TJ?) and low peak QE value. The FF and V_{oc} were both quite low. It was hard to tell if bad TJ or phosphorus contamination both contributed to the poor device showing. As we did not expect the a-Si TJ to work, and we had abandoned nc-Si n-layer for TJ, we have been more focused on n^+/p^+ type of TJ for a-Si/nc-Si tandem cells.

During Phase II, we took advantage of the newly developed Ar-dilution procedure for depositing p^+ layer (< 20 Å). Such a p^+ layer is believed to have a narrower electronic (mobility?) bandgap with very high density of defects which should greatly promote efficient carrier recombination than what is obtainable by conventional a-Si p^+ layers in the TJ (made by, e.g., straightforward glow discharge of SiH_4+TMB gas mixtures). The performance of the a-Si/a-Si trial cells using the n^+/p^+ type TJs with the new Ar-based p^+ recipe was satisfactory as shown earlier. The downside of the narrow-gap p^+ TJ approach is the added optical loss in the p^+ layer. An expected benefit of the Ar-dilution produced p^+ layer for TJ is its broader coverage of the reactor interior surfaces (due to the long-lifetime of Ar^*) contaminated by the prior n-layer deposition. The n^+/p^+ TJ (using strong Ar dilution for the thin p^+) proved to be somewhat successful in the fabrication of a-Si/nc-Si tandem cells, as shown by samples listed in **Table 19**. With this kind of TJ, using Asahi SnO_2 as front contact and ZnO/Al back contact, we obtained initial conversion efficiencies of ~8%. The closed-chamber (CC) seeding method was used for these cells, which contained thick a-SiC p2-layer deposited after the thin p^+ layer. CC-seeding was performed on the a-SiC p2 layer using recipes similar to those for single junction nc-Si cells described in section 2.

It is worth noting that the p^+ based tunnel junction produced with heavy Ar dilution (> 100:1) at relatively high power results in 'clean' bottom nc-Si cells without obvious signs of i-layer contamination, in contrast to some earlier attempts for p^+ layer (e.g., with H_2 dilution or without

dilution). Such tandem cells show very good total J_{sc} (with Ar produced tunnel junction), which can be in the range of 19-20 mA/cm^2 using mediocre ZnO/Al back contact and Asahi SnO_2 front contact, as shown in **Figure 23** and **Figure 24**. The relatively low FF values, though, indicate serious performance limitation of this recombination layer (TJ) in the context of a-Si/nc-Si tandem devices, versus the simpler a-Si/a-Si double-junction solar cells. We cannot rule out or ignore the likelihood of slight phosphorus contamination (not heavy contamination) which, as reported in Section 3, can actually boost the J_{sc} of the cells and 'kill' the FF at the same time. Possible phosphorus contamination of the nc-Si bottom cell produced by the n^+/p^+ TJ is harder to detect than, e.g., cells made with nc-Si n1-layer as TJ. The QE-derived total currents of the tandem cells (top cell plus bottom cell) often far exceed values obtained from single junction nc-Si cells. Even the red-light response was often notably higher than that observed in single junction nc-Si cells. Thus, the low FFs of the tandem cells could be due to the combined effects of CC-seeding (which does not work as well as p-seeding), poor TJ quality, and/or mild contamination of the nc-Si bottom cell. Because the current density is higher in a-Si/nc-Si cells than a-Si/a-Si, the required performance of TJ ought to be higher for the case of a-Si/nc-Si 'micromorph' cells. Still, the FFs for most of the cells are too low to be accounted for by the higher J_{sc}. Besides, the cell FFs did not change much under low-light I-V tests, indicating some deeper device flaws (which manifest themselves even at low currents). Further study is needed to identify the limiting factor(s) of performance.

Cell I.D.	TJ p^+ Method and Notes; Front Contact, Back Contact Type	V_{oc}	J_{sc}	FF	Eff.
	(All by CC-seeding. b.c.=back contact. nc-Si i2-layer ~1.5μm)	(V)	mA /cm^2	(%)	(%)
R294-2	Reference a-Si/a-Si cell; p^+ TJ; commercial AFG SnO_2, Al b.c.	1.60	6.1	73	7.1
R253-1	a-Si/nc-Si, a-Si p^+ (*not* by Ar dilution method); AFG SnO_2, Al	1.20	7.4	63	5.6
R298-1	p^+ by Ar-dilution recipe; AFG SnO_2, ZnO/Al	1.23	8.7	61	6.5
R341-2	p^+ by Ar-dilution recipe; AFG SnO_2, Al only back contact	1.21	7.4	66	5.9
R341-2	Same as above (co-deposited); AFG SnO_2, ZnO/Al (higher J_{sc})	1.25	8.6	63	6.8
R348-2	p^+ by Ar-dilution; Asahi SnO_2, Al back contact	1.26	8.1	63	6.5
R348-3	Same as above, but with ZnO/Al back contact (current balanced)	1.27	9.0	61	7.0
R350-2	p^+ by Ar-dilution; Asahi SnO_2, ZnO/Al (top cell limited)	1.28	9.6	65	8.0
R350-3	Same run as above, Asahi SnO_2, ZnO/Al. 7.4% @ NREL	1.29	9.4	62	7.5

Table 19 Some a-Si/nc-Si tandem solar cells prepared with n^+/p^+ tunnel junctions. The bottom nc-Si cells were prepared by (closed chamber) CC-seeding.

I-V and QE data from the a-Si/nc-Si dual-junction cells illustrate the utility of the CC-seeding technique (closed-chamber, static seeding) in combination with n^+/p^+ TJ. After the formation of n^+ and thin p^+ films (TJ), and the deposition of a moderately thick a-SiC p2 layer, CC-seeding was carried out before the deposition of nc-Si bottom cell absorber (just like the sequence for single junction nc-Si cells). For the cell in figure 23 (zero bias), the total QE current is 19.3 mA/cm^2, which is quite high even for the good Asahi SnO_2 and ZnO/Al back contact. Note that the total QE current (front cell plus back cell) from CC-seeding produced tandem cells are

usually much higher than that of cells produced by standard p-seeding (on a-SiC p2-layer) for the bottom cell, consistent with behaviors of single junction nc-Si cells (which show lower J_{sc} when p-seeding is performed directly on a-SiC p-layer). The FFs of a-Si/nc-Si tandems prepared by either CC-seeding or conventional p-seeding are as yet unsatisfactory due to the suspected reasons mentioned earlier.

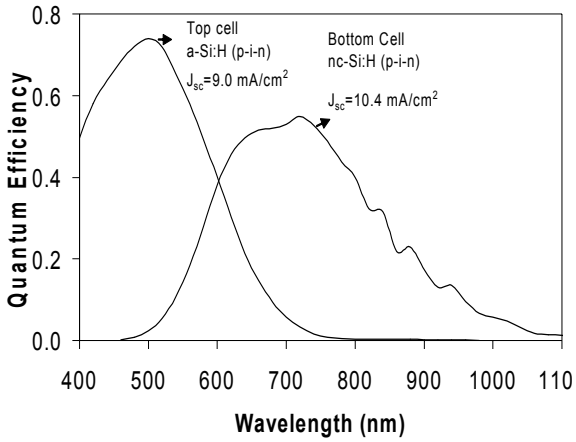

Figure 23 QE of an a-Si/nc-Si tandem cell produced by n^+/p^+ TJ and CC-seeding.

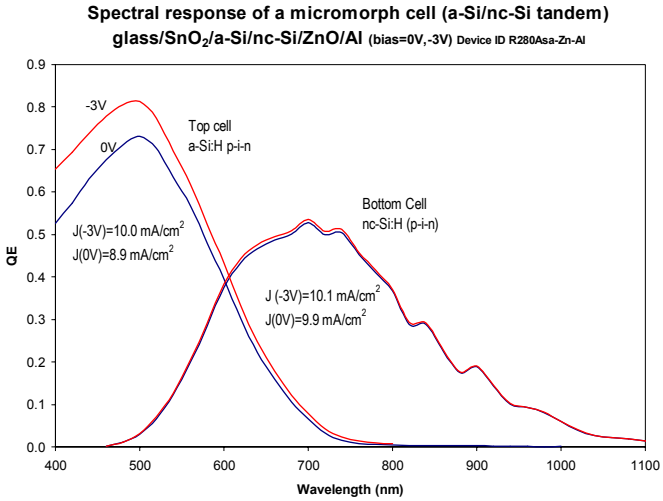

Figure 24 QE spectra of an a-Si/nc-Si cell under zero bias and -3V bias (with Asahi SnO_2 front contact and ZnO/Al back contact).

Overall, the performance of a-Si/nc-Si tandems cells made by any of the Si-based TJ has been disappointing, as the best FFs are only in the mid-60% range (see tables 19 and 20), well below what can be expected from the component cells. The V_{oc} has been low (1.24-1.3 V) as well. Only the J_{sc}s look rather good (with ZnO/Al back contacts), ranging from 9 mA/cm^2 from QE measurements to $\geq$ 10 mA/cm^2 from outdoor and indoor I-V tests (with total currents ~ 19-20

mA/cm^2). Mild phosphorus cross-contamination of the nc-Si bottom i-layers would not be unexpected in *single chamber* PECVD system. Many of the cells, however, do not show clear dependence of the bottom-cell QE on reverse bias, as can be seen from figure 24, which compared QE spectra under zero bias and -3V bias. However, some cells do exhibit the telltale sign of possible contamination by the strong bias-dependence of QE: a forward electrical bias (e.g., 0.8-0.9 V) makes the QE spectra 'collapse', particularly in the long wavelengths. In one of the tandem fabrication runs, we greatly extended the flow time of PH_3 in depositing the n1 layer. The resulting micromorph cell behaved like a bad single junction a-Si solar cell, as the bottom "i-layer" (nc-Si absorber) became too conductive. Thus, phosphorus cross-contamination of the bottom nc-Si i-layer remains a major source of concern. In brief, it appears that the requirement for cross-contamination control is more stringent when a good seeding method is used for the bottom nc-Si cell in 'micromorph', as the residual dopants are more 'lethal' right from the onset of nc-Si i-layer deposition (due to the absence of a mixed-phase or a-Si incubation layer).

Cell I.D.	Tunnel Junction Type; Seeding; Front Contact, Back Contact	V_{oc}	J_{sc}	FF	Eff.
	(b.c.=back contact. nc-Si i2-layer ~1.5μm)	(V)	mA /cm^2	(%)	(%)
R416-4	n^+/p^+ (Ar dilution method); p-seeding; Asahi SnO_2, ZnO/Al	1.26	9.8	59	7.3
R418-3	n^+/p^+ (Ar); thicker a-SiC p before p-seed.; Asahi SnO_2, ZnO/Al	1.25	10.1	61	7.7
R419-2	n^+ only; p-seeding directly on n^+ (without p^+!); AFG SnO_2, Al	1.05	6.9	44	3.2
R420-2	nc-Si n (n-seeding directly on a-Si i1)/nc-Si p2; AFG SnO_2, Al	0.72	7.5	50	2.7
R449-3	Air-vent after n^+, then H-etch & p^+ (Ar); p-seeding; AFG, Al	1.27	7.7	58	5.7
R450-4	n^+/p^+ (Ar), overnight high-vac. after p^+; p-seeding; AFG, Al	1.24	8.2	63	6.4
R451-3	n^+/p^+ (Ar), w/overnight high-vac. after n^+; p-seeding; AFG, Al	1.23	8.3	62	6.3
R452-3	a-Si n1, then nc-Si n1/a-SiC p2 (no p^+); p-seeding; AFG, Al	1.17	8.3	62	6.0
R453-3	nc-Si n1 (directly on a-Si i1)/a-SiC p2 (no p^+); p-seed.; AFG, Al	1.17	8.0	63	5.9

Table 20 Tandem a-Si/nc-Si solar cells obtained by different tunnel junction processes.

In **Table 20**, we show 'micromorph' a-Si/nc-Si solar cells made with various TJ procedures, some of which were targeted at contamination control. Two of the runs were conducted with *overnight* high-vacuuming to see if reduced P-contamination would result in better devices. The negative answer suggests that the TJ itself is a serious problem that causes low FF and low V_{oc}. The n^+/p^+ TJ may not be the best choice for a-Si/nc-Si. Potential cross-contamination arising from TJ (or seeding process) is unlikely to be the only concern as judged by QE measurements. Some of the tandem cells have rather large current mismatch (highly limited by the bottom cell). However the FFs of these tandem cells are not as sensitive to the large current mismatch as to the overall V_{oc} (or the V_{oc} of the bottom cell since the top a-Si has a fairly constant V_{oc}). This may be taken as an indication that the limiting factor for micromorph efficiency is very much the performance of the bottom nc-Si cell which can be sensitive to seeding (as in single junction nc-Si cells) as well as TJ. In brief, we recognize that, to improve the efficiency of the micromorph solar cells, we must improve the Si:H based (in-situ deposited) TJ process, the seeding process

for nc-Si bottom cell after TJ, and optical engineering (including an enhanced rear reflector). Despite the problems, our a-Si/nc-Si tandem cell data have demonstrated the potential feasibility of single chamber PECVD system for a-Si/nc-Si solar cell preparations.

4.4 ZnO interlayer for a-Si/nc-Si tandem solar cells

In view of the difficulties associated with Si:H based tunnel junctions (TJs), we explored the use of a thin ZnO film as TJ, deposited on a-Si n1 layer after the deposition of the top a-Si cell. It turned out the one can 'kill two birds with one stone' by using the ZnO-interlayer TJ. First, good Ohmic contacts can be made with both the top cell and with the bottom nc-Si cell, the seeding of which can be performed directly on the ZnO, just like the case of high-performance single junction nc-Si cells directly seeded on ZnO-coated SnO_2 superstrates (see section 2). In other words, the two component cells in the tandem can be separately processed as two un-connected individual p-i-n cells without worry about the TJ, in contrast to tandem cells requiring Si-based TJ. Secondly, the seeding is more effective on the ZnO surface than, say, a-SiC, as we have discussed in section 2, leading to a better performing and more stable bottom nc-Si cell. The a-Si/nc-Si tandem cell fabrication procedure, however, becomes much lengthier and more complicated when ZnO-interlayer is used as TJ in the a-Si//ZnO//nc-Si tandem cell structure. In order to deposit thin ZnO, the vacuum of the PECVD system must be broken, and the substrates removed from the reactor for loading into the sputtering apparatus. After the ZnO is done, the substrates are then re-loaded into the PECVD reactor for pump-down. The rest of the steps are the same as for the deposition of nc-Si single junction cells. The exposure of a-Si n-layer to air at elevated temperatures is not a problem. Obviously, the exposure of the vacuum chamber to air is extremely undesirable for nc-Si from the view point of oxygen impurities. Some extended vacuuming is needed to reach an acceptable base vacuum before nc-Si growth can commence.

A huge practical benefit of the ZnO-interlayer TJ procedure is the suppression of phosphorus remnants in the PECVD system (caused by n-layer deposition of the top cell) by air exposure when the chamber is hot. It seems that either water vapor (and O_2?) can scavenge and neutralize PH_3 residuals, or the oxidation of the surfaces by the 'hot' air helps prevent the release of dopant residuals. The end result is that the bottom nc-Si cells do not show P-contamination symptoms in a-Si//ZnO//nc-Si cells. **Table 21** compiles a number of a-Si/nc-Si tandem cells of the ZnO-interlayer design. All these cells have ZnO/Al back contacts. Except R457, the cells were grown on Asahi SnO_2 (with thicker a-Si i1-layer). Initial conversion efficiencies near 9% have been obtained. For an a-Si/nc-Si cell from run R462, post-light-soaking (500 hours at one-sun) efficiency of 8.7% has been measured at NREL. (EPV's value is ~8.1%).

Cell I.D.	Notes on ZnO-interlayer; Front Contact (SnO_2) Type	V_{oc}	J_{sc}	FF	Eff.
	(All by p-seeding directly on ZnO interlayer, with ZnO/Al b.c.)	(V)	mA/cm^2	(%)	(%)
R456-2	ZnO~400 Å, too conductive; Asahi SnO_2. Bottom-cell limited	1.29	7.5	78.5	7.6
R457-2	Thinner ZnO~100 Å ('insulating'); AFG SnO_2. Thinner top cell	1.30	7.9	70.6	7.3
R457-3	Thinnest ZnO <100 Å ('insulat.'); AFG SnO_2. Co-dep as above	1.29	8.3	70.3	7.5
R461-2	ZnO~100 Å (conductive); thicker nc-Si i2; Asahi SnO_2	1.34	9.7	68.4	8.9
R461-2	Same as above; Asahi SnO_2. Annealed at ~160 °C	1.33	9.9	68.3	9.0

R462-4	ZnO~200 Å (conduct.); thickest nc-Si i2; Asahi SnO_2. Peeling	1.35	9.5	68.7	8.8

Table 21 ZnO-interlayer tunnel junctions for a-Si/nc-Si tandem solar cells.

Figure 25 shows two I-V graphs of a-Si/nc-Si tandem cells with interlayer ZnO as TJ. The cell on the left has more balanced current or higher J_{sc} but lower FF, compared to the cell on the right which is more bottom-cell limited with high FF but lower J_{sc}. Presently, ZnO interlayer has outperformed Si-based tunnel junction (in-situ deposited, Si-based TJ with or without air-break) by a wide margin, and the ZnO recipe remains to be fine-tuned. We do not know the optimal thickness or conductivity of the ZnO interlayer. Conductive and relatively insulating ZnO of thickness between 50-400 Å, sputtered at room temperature, have been tried. Preliminary tests show that if the ZnO interlayer is too thin (<100 Å), tandem cell performance may take a big hit. Somewhat insulating ZnO is preferred to conductive ZnO, not mainly due to optical loss, but because of the lateral conduction that produces highly shunting behavior upon the making of contacts to the front TCO (when the interlayer ZnO would be 'touching' the metal or TCO).

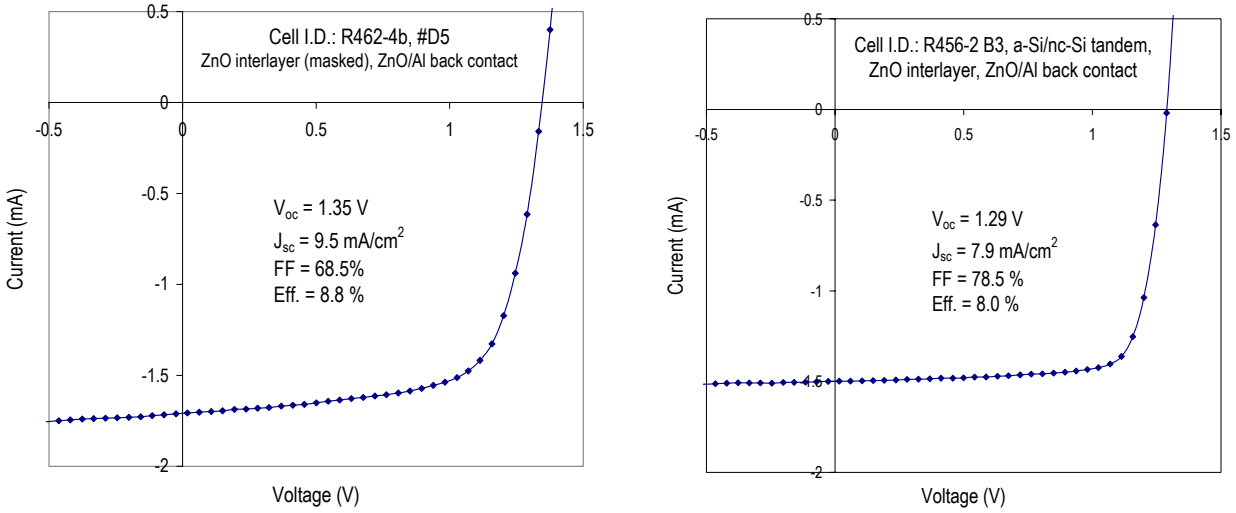

Figure 25 I-V graphs of two a-Si/nc-Si double-junction solar cells with thin ZnO interlayers. Left: a nearly-balanced tandem cell. Right: a tandem current-limited by bottom cell.

There was severe, spontaneous delamination of a-Si/nc-Si tandem cells containing thick nc-Si bottom cells (> 2 μm), made with ZnO interlayer, on Asahi SnO_2. The 'explosive' peeling of the stressed film would start at the corners and edges, upon the exposure of the deposited plates to atmosphere (venting of the vacuum), and move towards the interiors of the substrates. Peeling occurred regardless of the air-venting temperature (i.e., slowly cooling the substrates down to room temperature did not help). Often, delamination occurred over the entire substrates in a matter of hours, before cells could be measured. Careful cleaning of the substrates did not make

any difference. There was little difference between substrates placed on the powered electrode or the ground electrodes. Interestingly, *single* junction nc-Si cells of thick i-layer, made on ZnO-coated SnO_2 (AFG or Asahi), did not suffer delamination, possibly owing to stronger bonding of the p-seed layer to the TCO vs. the a-SiC p-layer in tandem cells. It is puzzling that, lower-textured AFG SnO_2 (with or without ZnO coating, alongside the Asahi SnO_2), exhibited little Si film peeling, contrary to the common observations that rougher surfaces provide better film adhesion (due, in part, to effectively larger interface contact areas). We note that the SnO_2 films did not delaminate from the glasses in any of the solar cells of various kinds.

4.5 Light-induced degradation of a-Si/nc-Si tandem solar cells

A number of small area dual-junction a-Si/nc-Si solar cells have been subjected to observations under light and/or in the dark (environmental storage). As in the case of nc-Si single junction solar cells, a-Si/nc-Si tandem cells have not exhibited any degradation upon extended room temperature storage (no degradation in the dark). The light-induced degradation behavior is more complicated. We have found that a-Si/nc-Si 'micromorph' solar cells *appear* far more stable under accelerated light soaking (ALS, ~ 47 suns light intensity), with efficiency reductions less than 10%, much lower compared to our standard a-Si/a-Si tandem solar cells and modules (on Al back contacts) which show efficiency degradations in the range of 15-20%. Most of the losses occur in the FF, with some reduction in J_{sc} for these dual junction a-Si/nc-Si devices. **Figure 26** below shows the efficiency and FF evolutions upon 47-sun ALS of an a-Si/nc-Si cell in comparison with an a-Si/a-Si tandem device. The efficiencies declined by about 20% and 5%, respectively, after 160 seconds at 47-suns (corresponding to ~ 100 hours of one-sun exposure). The moderate ~5% degradation, after 5 minutes under 47-sun irradiation (ALS), has been confirmed by a number of tests on different cells, consistent with the initial findings.

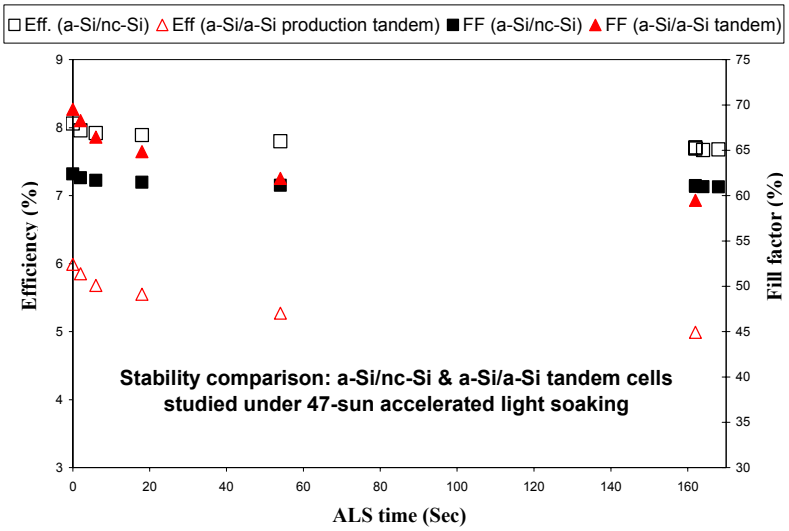

Figure 26 Stability comparison of a-Si/nc-Si and a-Si/a-Si cells by accelerated light soaking.

We have compared the degradations of 'micromorph' cells by accelerated light soaking (ALS) and by the slower, more realistic one-sun light soaking. Our earlier ALS data have been

tempered by the later one-sun tests. We realized that, while a-Si/a-Si tandem cells suffer similar efficiency losses under either one-sun or ALS, the a-Si/nc-Si micromorph cells experience far larger degradation under one-sun than ALS. The discrepancy between ASL and one-sun data, exemplified in **Figure 27** below, may be explained by actions of some sort of 'slower' defect creation mechanism which would be masked during the short ALS tests. Most of the 'extra' efficiency loss reflects larger decrease of FF under one-sun soaking. The typical 10-15% degradations in efficiency of a-Si/nc-Si tandem cells (with somewhat balanced top and bottom cells) are consistent with a stable bottom cell and a top cell that is expected to degrade slightly over ten percent (for a-Si i-layer thickness near or slightly over 2000 Å). For some reason, the a-Si top cell (which is far less stable than bottom nc-Si cell) does not respond as strongly to more intense light as it does to lower-level illumination. To improve the stability of micromorph cells, higher R (H_2/SiH_4 dilution ratio) has been used in depositing the a-Si i-layer in the top cell, such as in the case for run# R462 (with NREL-confirmed post-light-soaking efficiency of 8.7%).

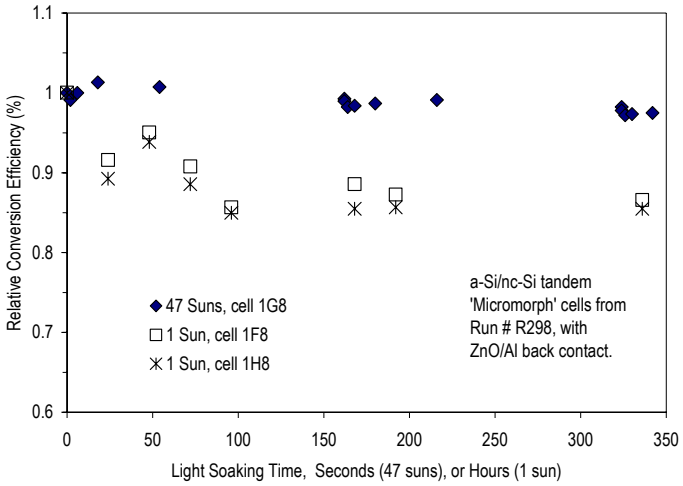

Figure 27 Efficiency variations of a-Si/nc-Si cells under 47-sun and one-sun illumination.

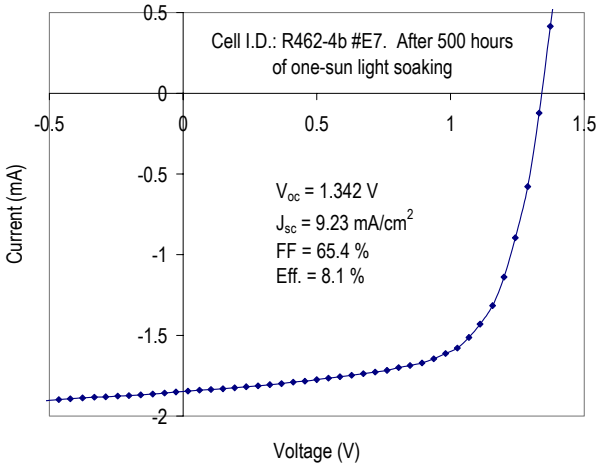

Figure 28 I-V curve of an a-Si/nc-Si tandem cell after 500 hours of one-sun light soaking.

The I-V curve in **Figure 28** was taken on a tandem a-Si/nc-Si solar cell (later sent to NREL as a deliverable at the end of Phase II) after 500 hours of continuous one-sun light-soaking. The initial cell efficiency was ~ 8.8% as measured at EPV. The 8.1% efficiency after light soaking represents a modest 8% degradation in conversion efficiency, mostly due a drop in FF (from ~ 69% to ~65%). Note that the cell efficiency would have been 8.5-8.6% if the light-intensity for I-V measurement had been calibrated by the J_{sc} values of tandem cells determined by NREL, instead of our own calibration cell (a-Si/a-Si tandem which does not have the same spectral response as a-Si/nc-Si micromorph). This light-soaked cell (R462-4b) has been measured at NREL for an efficiency of **8.7%**, with V_{oc}=1.38 V, J_{sc}=9.5 mA/cm^2, FF=66.6%. The J_{sc} of the dual-junction cell in the above figure is bottom-cell limited both before and after light exposure. In this case, the full impact of the degradation of the unstable a-Si top cell (compared to the rather stable bottom nc-Si cell) is partly masked by the tandem structure. That is, for such cells, a lower initial efficiency (due to current imbalance) also leads to lower *percentage* loss of efficiency after light soaking. The tandem cells with well-balanced current likely would show larger degradations (as seen in the earlier figures). Generally, the design of tandem devices should make the more stable component as the current-limiting cell.

Tandem a-Si/nc-Si module fabrication. We have made only superficial efforts in fabricating a-Si/nc-Si micromorph modules, as we felt that the key to good nc-Si related module performance is the yet-unresolved nc-Si i-layer uniformity problem. Module activities had been planned mainly for Phase III in the original 3-year plan. We did demonstrate that our well-established processing procedure for a-Si/a-Si double junction modules can be readily applied to a-Si/nc-Si tandem modules of 12”x15” size, since the three laser scribe steps need only slight adjustments (including cell width to account for higher current density in the case of a-Si/nc-Si structure). We show in **Figure 29** a photograph of our first 12”x15” a-Si/nc-Si tandem module (left), and its normalized V_{oc} variation across the 12” width in the direction of gas flow (right graph). The tandem module showed excellent interconnection of the individual cells. The low module efficiency (< 5% initial value) reflects poor tunnel junction and unsatisfactory nc-Si bottom cell which shows pronounced inhomogeneity.

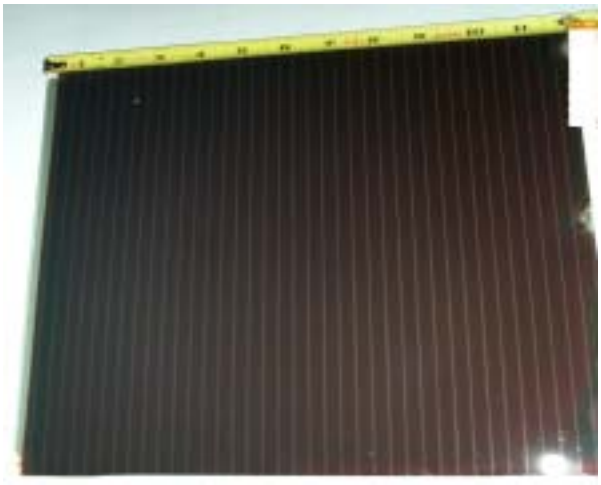

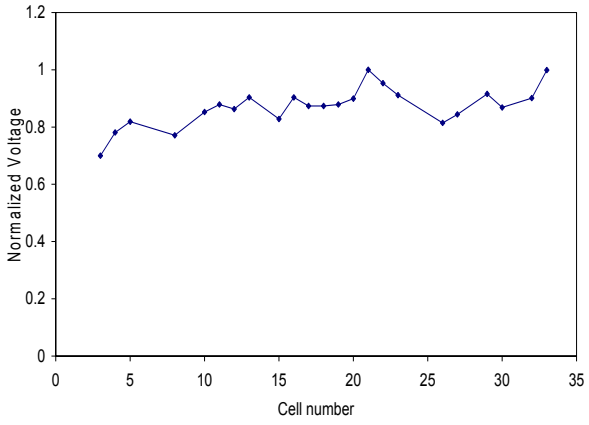

Figure 29 Photograph of a 12"x15" a-Si/nc-Si micromorph tandem module (left).

Figure 30 Variations of V_{oc} of individual segments across the width of the first a-Si/nc-Si tandem module prepared by EPV's single chamber RF-PECVD (right).

5. Front Contacts and Back Contacts of p-i-n Type Solar Cells

This section deals with some device topics not directly related to nc-Si PECVD processes.

We explored the applications of two new TCOs, Mo-doped indium-oxide (IMO), and Ti-doped indium oxide (ITiO), to nc-Si solar cells [16,20]. The IMO and ITiO were prepared at EPV by the novel hollow-cathode technique. The attraction of IMO and ITiO films is mainly their superior long-wavelength transparency and good conductivity, made possible by the high carrier mobility. The combination of textured, relatively resistive but highly transparent ZnO with highly conductive and highly transparent IMO or ITiO can form an efficient light trapping bilayer structure that has proved to outperform the conventional TCOs (SnO_2 and ZnO) for front contact of p-i-n type solar cells, especially nc-Si cells, we shall see section 5.2. These films also show promise as TCO/Al (or TCO/Ag) back contacts for reduced long-wavelength optical loss.

We repeatedly observed excessive texturing of nc-Si solar cells by selected seeding recipes. This *film-growth* induced 'roughness' apparently is effective in boosting light absorption (light trapping) in the cells. In fact, red-light transmission is visibly weaker through such rough films compared to normal nc-Si cells of the same i-layer thickness. Note that this texturing of nc-Si films is distinctive and separate from the normal, conformal texturing resulting from the roughness of the superstrate (in our case, SnO_2). There is a great deal of variation of this effect with deposition conditions and pre-existing substrate roughness. Generally, the effect is stronger when the substrate in less rough. Also, the effect is sensitive to the base-film (the history of deposition before the nc-Si i-layer). The gains in optical absorption of nc-Si solar cells with 'milky' surfaces were confirmed by QE measurements. The higher long-wavelength responses presumably came from increased scattering from the rear-contact interfaces and subsequent absorption of light. But, we also found that cells with the enhanced optical absorption (rough surface) show lower V_{oc} and lower FF compared to 'smooth' cells. It is possible that higher texturing/roughness correlates with 'crystallite collision' inside the nc-Si absorber, which is believed to degrade solar cell performance. It remains to be seen whether high V_{oc} & FF can be *simultaneously* obtained with higher J_{sc} caused by enhanced surface roughness. This will be a longer-term topic in our research of nc-Si, micromorph, and a-Si related thin film solar cells.

5.1 Comparison of different back contacts

For simplicity, reproducibility, uniformity, and fast device feedback, most of the solar cells prepared under this subcontract had been routinely finished with sputtered Al back contact without ZnO. The expected low J_{sc} does not hinder our interpretation of the various plasma effects (e.g., seeding) since we only need to see the relative changes in device performance. As stressed earlier, low J_{sc} has been the biggest weakness of our nc-Si (and a-Si) devices. A primary reason for the low J_{sc} is the use of weakly-reflecting Al back contact, which is inappropriate for higher efficiency demonstration. The other obvious reasons include high optical absorptions by the commercial SnO_2 and by the 3-mm thick soda-lime glass substrate, low-texturing of the SnO_2 front contact, i-layers that are neither highly nanocrystalline nor very thick, and the poor

transparency of the p-seed layers. We have compared the QE spectra of co-deposited nc-Si solar cells with Al and ZnO/Al back contacts made by magnetron sputtering. **Figure 31** shows the QE spectra of three nc-Si solar cells made with the same recipe. Two of the samples were grown on the same commercial LOF TEC7 SnO_2 front contact but they have different back contacts, Al or ZnO/Al. The third sample has the special Asahi type 'U' SnO_2 front contact, and ZnO/Al back contact. An increase in J_{sc} of ~ 2 mA/cm^2 has been seen with ZnO/Al back contact versus Al contact, mainly due to a boost in the long-wavelength response. As a reference, the increase in J_{sc} is about 7-8% for a-Si single junction solar cells when ZnO/Al is used instead of Al alone. This compares with a gain of ≥ 12% for nc-Si single junction cells when a ZnO layer is inserted between the a-Si n-layer and the Al film. The higher texture and better transmission of the Asahi SnO_2 (on a more transparent, thinner glass substrate) account for the higher red-light response in the third nc-Si solar cell in figure 31. The FF of the cell with Asahi SnO_2 front contact is actually quite low (~ 60%) due to lack of optimization of the CC-seeding recipe on the more textured substrate (compared to the low-haze LOF SnO_2) as we stated before.

To reap the benefit of ZnO/Al back contact, we tried to fine-tune the ZnO sputtering process for more repeatable, low-resistance contact to the a-Si n-layers. To this end, a shutter was installed in our R&D sputtering machine such that proper target conditioning (pre-sputtering after the system's exposure to air upon sample loading and unloading) could be performed prior to ZnO deposition on to the solar cells. Later on, we adopted the large-area ZnO process, in the R&D inline sputterer, originally developed for our CIGS solar cell and modules. The same sputtering procedure (for conductive or insulating ZnO) has been used for the thin ZnO interlayers as tunnel junctions for micromorph cells as described earlier.

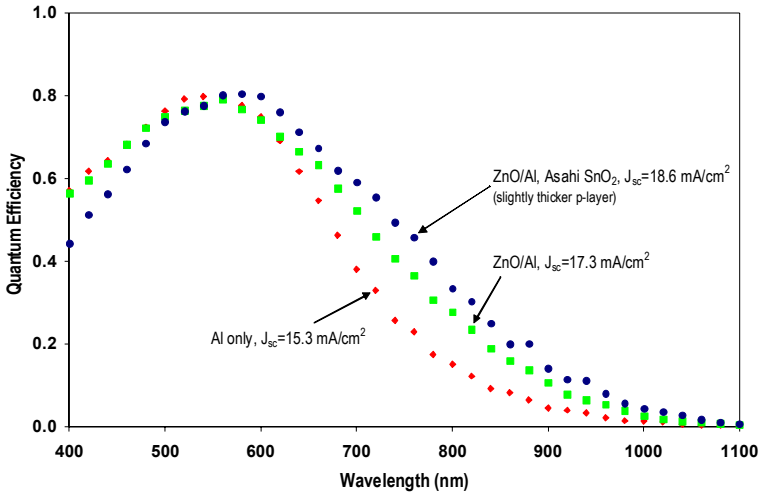

Figure 31 QE spectra of three solar cells with Al or ZnO/Al back contacts.

As a matter of curiosity and necessity (in order to establish some backup metallization capability other than Al), we sputtered Mo on some a-Si and nc-Si single junction devices to compare their performance with standard Al back contact (without ZnO). The Mo sputtering parameters were similar to those used for depositing thick Mo back contacts on glass substrates for CIGS device fabrication at EPV. Our data indicate that Mo can make good electrical contacts to a-Si n-layers

of p-i-n solar cells, and the FFs and V_{oc}s are comparable among co-deposited cells incorporating either Al or Mo back contacts. However, the J_{sc} (by I-V and QE measurements) of the cells prepared with Mo contacts were notably lower than that of Al (by ~1-1.4 mA/cm^2 for a-Si solar cells with ~4500 Å thick i-layer), presumably due to poorer reflectivity at the a-Si/Mo interface compared to that of Al. Thus, Mo should be used only as a 'last resort' contact.

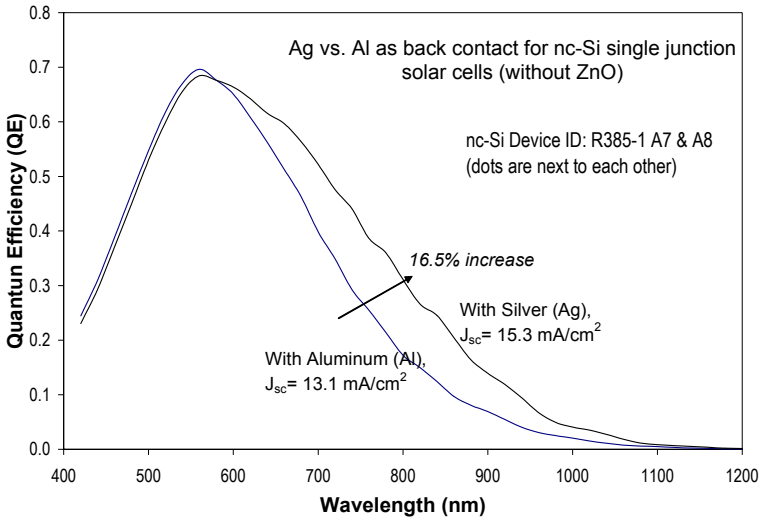

Figure 32 QE comparison of nc-Si cells with Ag or Al back contact (without ZnO).

Presently, EPV does not have silver (Ag) sputtering capability. We have evaluated Ag back contact, thermally evaporated in an old bell-jar system without shutter, for nc-Si solar cells. **Figure 32** compares the QE of two similar nc-Si single junction cells with respectively Ag or Al back contact (without ZnO before the metal film). A nice increase in long-wavelength response is clearly observed by the use of Ag as the back reflector versus Al, resulting in ~16% increase in J_{sc}. Unfortunately, evaporated Ag does not make good contact (poor adhesion) to the a-Si n-layer, thus the Ag-containing solar cell has markedly lower FF that compromises its efficiency.

For many years, ZnO/Ag has been the back contact of choice for thin film Si:H based solar cells. Our tests confirmed the superior response of ZnO/Ag compared to ZnO/Al for both single junction nc-Si solar cells and a-Si/nc-Si micromorph tandem devices, as shown respectively in **Figure 33** and **Figure 34**.

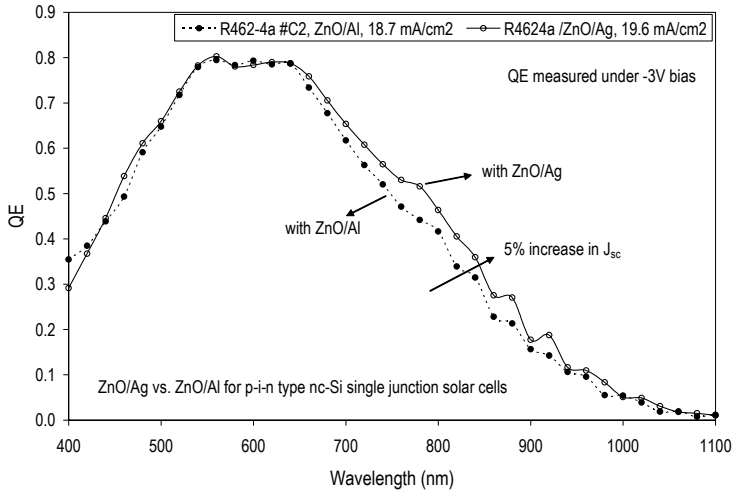

Figure 33 QE spectra of nc-Si single junction cells with ZnO/Ag or ZnO/Al back contact.

Again, due to poor interface quality of evaporated Ag, the higher J_{sc} (stronger red-light response) obtained from ZnO/Ag back contact over ZnO/Al has not translated into higher cell efficiency due to lower FF. In general, very poor Ag film adhesion was observed on ZnO as well as on a-Si. Ag layer would easily peel off upon contact during I-V or QE tests. Higher substrate temperatures greatly improved adhesion of evaporated Ag, but the reflectivity of the back contact would be somewhat tarnished. We either have to modify our evaporation procedure for Ag, or, more sensibly, use the proven sputtering techniques for Ag deposition.

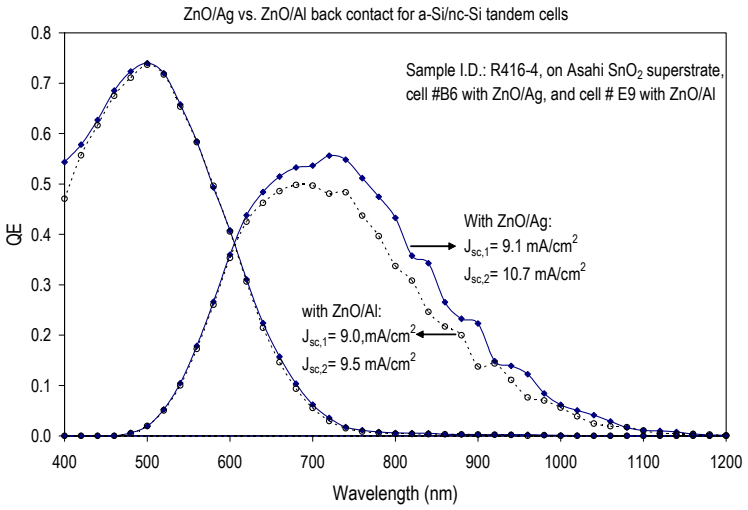

Figure 34 QE spectra of a-Si/nc-Si tandem cells with ZnO/Al or ZnO/Ag back contact.

Another metal film, sputtered copper (Cu), was appraised against Al for back contact, in the configuration of ZnO/Cu and ZnO/Al, for both nc-Si single junction and a-Si/nc-Si tandem cells. **Table 22** shows the parameters of some co-deposited single junction nc-Si cells, on ZnO-coated SnO_2 using optimized p-seeding, with ZnO/Al, ZnO/Ag, or ZnO/Cu as rear contact. ZnO/Cu and

ZnO/Al contacts produce similar FFs and V_{oc}s. The J_{sc} seems to be slightly lower for the ZnO/Cu cell versus ZnO/Al, as indicated by the QE spectra in **Figure 35**. I-V tests show similar J_{sc} for ZnO/Al and ZnO/Cu contacts. Thermal annealing would darken the Cu films, but there is no appreciable change in device performance. Nor is there any apparent Cu diffusion problem.

Back Contact (R457-4)	Comments (i-layer thickness ~ 2 µm, sputtered ZnO & Al)	V_{oc} (V)	J_{sc} (mA /cm^2)	FF (%)	Effi (%)
ZnO/Ag	ZnO/Ag, before thermal annealing	0.486	18.8	59.1	5.4
ZnO/Ag	ZnO/Ag, after thermal annealing	0.499	18.9	57.4	5.4
ZnO/Al	About the same before & after thermal anneal	0.502	17.5	66.2	5.8
ZnO/Cu	Sputtered ZnO/Cu, after thermal annealing	0.530	16.9	62.9	5.6

Table 22 ZnO/Al versus ZnO/Ag (evaporated) and ZnO/Cu back contacts for p-i-n type nc-Si single junction solar cells.

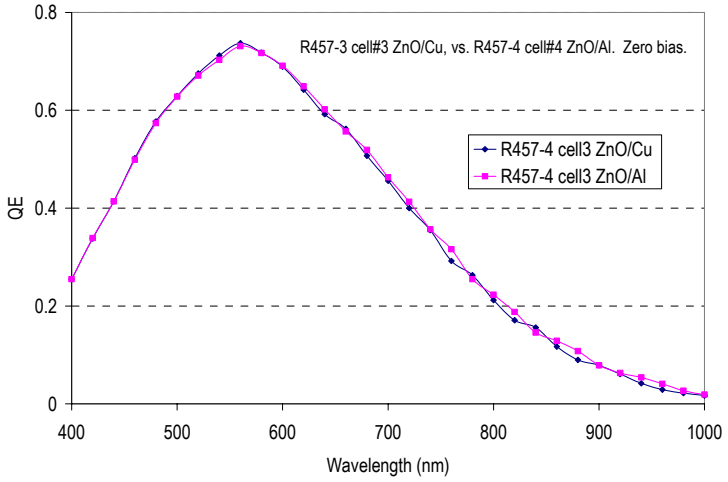

Figure 35 QE spectra of single junction nc-Si cells: ZnO/Al vs. ZnO/Cu back contact.

We conducted preliminary trials of using highly reflective Barium Sulfate ($BaSO_4$) coatings as part of the rear reflectors for nc-Si based solar cells. As $BaSO_4$ is an electrical insulator, an auxiliary conductive contact had to be used over part of the cell area. We did observe increases in J_{sc} (notably higher red-light response) from ZnO/$BaSO_4$ contacts, but the FF loss of the cells resulted in lower efficiencies vs. the standard ZnO/Al back contact. An attempt was made to mix $BaSO_4$ with conductive 'silver paste'. However, the resulting composite (paint) back contact was neither conductive nor reflective enough to be of any practical value.

5.2 Alternative front contacts (TCO superstrates)

As reported earlier, bare SnO_2 is a highly unsuitable TCO for high performance *single* junction nc-Si cell processing. We have encountered tremendous difficulties in avoiding SnO_2 plasma-reduction and in promoting speedy nucleation without incurring excessive optical loss when attempting to devise an effective yet robust p-seeding recipe. In Phase II, we started working on

alternative TCOs as front contacts that might offer superior performance to our standard SnO_2 superstrate for both single junction nc-Si and tandem a-Si/nc-Si solar cells. A TCO such as ZnO enjoys great advantage over SnO_2 in its resistance to hydrogen-rich seeding plasma sustained for a considerable period of time in the vicinity of the TCO surface. Another obvious incentive to study alternative TCOs is to reduce optical loss in the TCO itself. Further, more custom-engineered texturing of the TCO will allow for better light trapping in the cells. Novel TCOs can also be used in the TCO/metal back contact (vs. the standard ZnO/metal), where the TCO may consist of one or multiple layers. Note that the 3-mm thick soda-lime glass used for commercial SnO_2 (AFG and LOF) has at least 10% optical absorption in the long-wavelength region.

In order to achieve the highest short-circuit current density, advanced nc-Si based p-i-n type solar cells ideally demand the simultaneous possession of *four* important features in the front transparent conducting oxide (TCO): high visible transparency, low electrical resistivity ($\rho < 5 \times 10^{-4}$ ohm.cm), efficient light trapping surface texture, and *minimal* free carrier absorption in the infrared region (up to λ=1200 nm). So far, such an ideal TCO with *all* these attributes has been unavailable. Conventional TCOs, typically with charge carrier mobility around 25 cm^2/Vsec, exhibit significant free carrier absorption at long wavelengths (> 800 nm) which reduces short-circuit current density of nc-Si solar cells. Using a novel hollow cathode sputtering method, we have achieved a record free carrier mobility of 81 cm^2/Vsec for indium oxide films doped with group-IVA element titanium (ITiO). The highly transparent ITiO coatings show little free carrier absorption up to λ=1750 nm. Also, we have produced molybdenum doped indium oxide films (IMO) with similar electro-optical properties. One of the most successful light trapping structures can be obtained by anisotropic etching of fiber-texture oriented ZnO [9]. In order to achieve both high transparency and effective light trapping, we experimented with a bilayer TCO structure comprising surface textured, intrinsic ZnO and an overgrown high mobility TCO (IMO or ITiO). Such a ZnO/IMO (or ZnO/ITiO) bilayer has been found to exhibit no appreciable free carrier absorption at long wavelengths up to 1750 nm. Such a structure with all the above mentioned necessary features is called a Transparent Conducting Light Trapping Oxide (TCLO). We demonstrated for the very first time in nc-Si solar cells the incorporation of novel TCO top contacts: IMO, ITiO and bilayers of surface textured i-ZnO/IMO and i-ZnO/ITiO. QE data indicate that the use of flat IMO layers as the front contacts can increase the long wavelength response of nc-Si solar cells by 18% compared to *textured* commercial SnO_2 substrate. The incorporation of surface textured i-ZnO/IMO and i-ZnO/IMO layers as the top contacts enhance the spectral response by 14-34% for single junction nc-Si cell as well as the bottom nc-Si cell in a-Si/nc-Si 'micromorph' tandem solar cells.

Texturing of the EPV hollow-cathode sputtered IMO was provided by etching a lightly-doped (transparent), underlying ZnO film. Due to processing flaws such as poor seeding method (not tuned for the new TCO), the IMO/ZnO and ITiO/ZnO bi-layer front contacts had not produced good devices (poor V_{oc} and FF), despite its superior optical properties versus SnO_2 for generating higher J_{sc}. We have found that ITiO by itself has produced bad devices, unlike the ITiO/ZnO combination. We have yet to modify our seeding recipes developed for SnO_2 or ZnO-coated SnO_2 to work better with the newer TCOs. Note that there is no longer the need to deposit an a-SiC p-layer to protect the TCO. This is a big plus for nc-Si single junction cell preparation. **Figure 36** illustrates the device structure employed in our study of the new TCO films for front contact and back reflector of p-i-n nc-Si solar cells. In this sketch, the front contact is the bilayer of intrinsic ZnO (etched) and ITiO or ZnO and IMO. ITiO or IMO films have also been briefly explored as the TCO in TCO/Al back contact. **Figure 37** and **Figure 38** show the higher long-

wavelength transmissions of IMO and ITiO films versus, respectively, conventional ITO (indium tin-oxide) film and ZnO films (conductive and insulating ZnO).

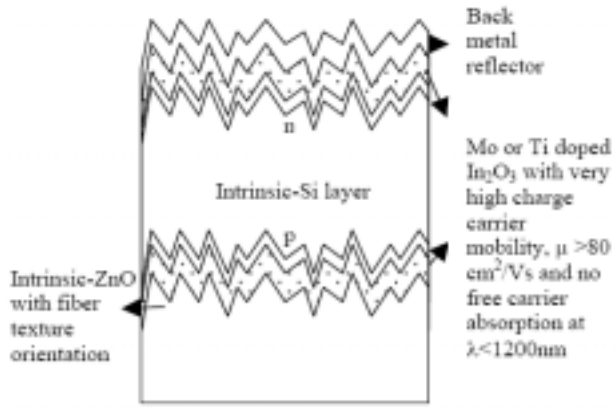

Figure 36 Schematic structure of p-i-n type nc-Si solar cells for testing the new TCOs.

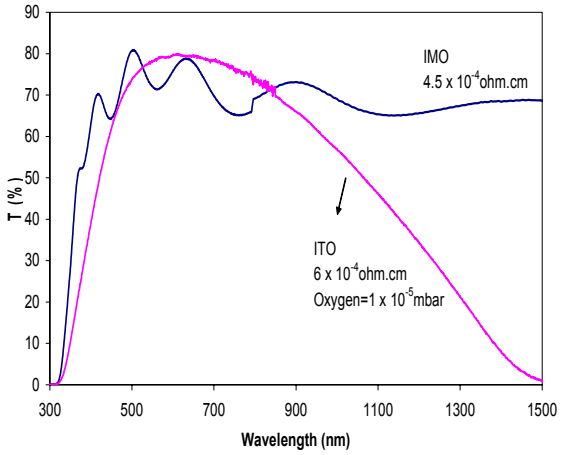

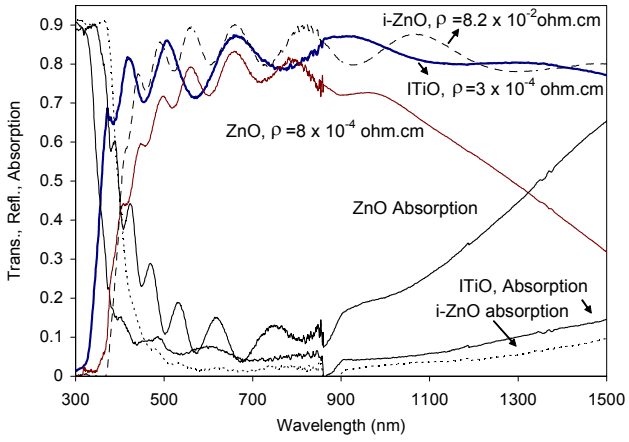

Figure 37 (left) Comparison of transmission spectra of an ITO film and an IMO film with comparable bulk electrical resistivity (sheet resistance).

Figure 38 (right) Comparison of transmission and absorption spectra of a high-mobility ITiO film with those of conducting and intrinsic ZnO films.

We have made single junction nc-Si solar cells on ZnO and on the experimental ZnO/IMO and ZnO/ITiO bi-layers, where the underlying ZnO provides texturing (created by wet etching). In **Table 23**, we show examples of nc-Si single junction solar cells deposited directly (without the protective a-SiC p-layer needed for SnO_2) on ZnO and ITiO/ZnO bi-layers. Judging from the good FFs of the nc-Si cells (which have fairly thin nc-Si i-layers of ~ 1 μm), there appears to be no serious contact barrier between the TCOs (ZnO, ITiO) and the p-seed layers. The relatively low J_{sc} is due in part to the use of Al back contact. Also note that the new TCOs were deposited on inexpensive, quite absorbing, 3-mm soda-lime glass. The p-seeding recipes (developed on SnO_2 with a-SiC p-underlayer) for these cells had not been re-engineered for the new TCOs for

higher efficiency. We have made nc-Si cells of more absorbing (thicker) i-layers on ITiO/ZnO bilayers, leading to high red-light response (at 800 nm) over 30% using TCO/Al back contacts.

TCO Type	Descriptions	V_{oc}	J_{sc}	FF	Effi.
	(i-layer thickness ~1.5μm, all with Al back contact)	(V)	(mA /cm^2)	(%)	(%)
SnO_2	AFG SnO_2, reference TCO (coated with a-SiC p)	0.48	13.2	66.3	4.2
ZnO/ZnO	ZnO/ZnO dual layer; top ZnO insulating, specular	0.48	12.8	67.1	4.1
ZnO/ZnO	ZnO/ZnO dual layer; top ZnO insulating, textured	0.49	13.5	65.2	4.3
ZnO/ITiO	Ti-doped InO on insulating, specular ZnO; bilayer	0.46	11.8	68.6	3.7
ZnO/ITiO	Ti-doped InO on insulating, textured ZnO; bilayer	0.47	12.8	66.2	4.0
ZnO/ITiO/ZnO	Text. i-ZnO/ITiO/conductive ZnO; triple-layer	0.46	15.5	60.0	4.3

Table 23 nc-Si p-i-n single junction cells made on various novel TCOs (front contacts) by p-seeding directly on the TCOs without a-SiC protective layer.

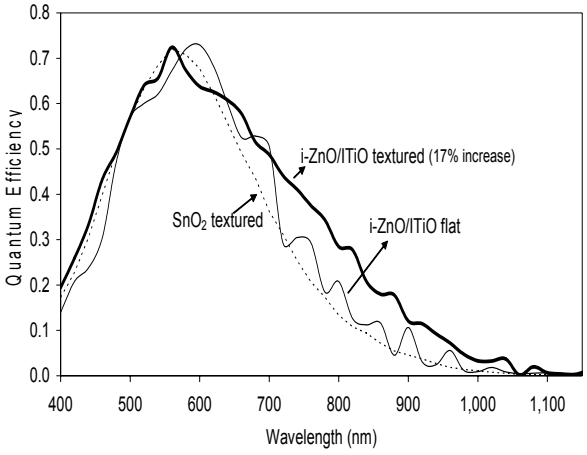

Figure 39 (left) Effect of texturing of i-ZnO/ITiO bilayer on the QE of an nc-Si solar cell vs. those on flat i-ZnO/ITiO bilayer and commercial SnO_2 (on soda-lime glass).

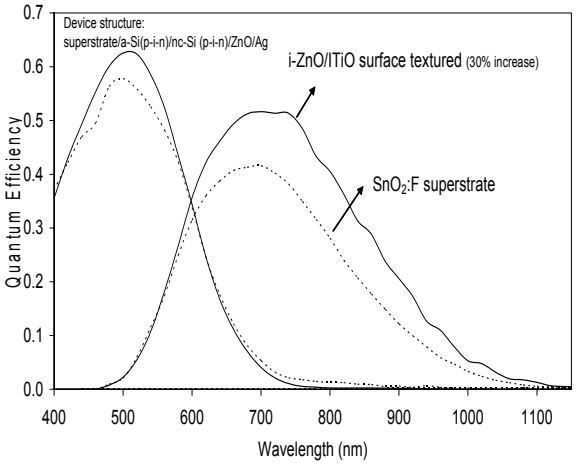

Figure 40 (right) QE spectrum of an a-Si/nc-Si tandem solar cell on a surface-textured i-ZnO/ITiO bilayer vs. that on a commercial SnO_2/glass superstrate.

The outstanding ability for capturing red-light of the i-ZnO/ITiO bilayer (as front contact) has been clearly established by QE data as shown, e.g., in **Figure 39** and **Figure 40**, which display the spectral responses of respectively single junction nc-Si and tandem a-Si/nc-Si solar cells. The current gain in the bottom nc-Si cell in a-Si/nc-Si micromorph is remarkable compared to the tandem cell deposited on SnO_2. A potential problem, however, is the compatibility of the new TCO with wide-bandgap a-SiC p-layer which is deposited on the TCO for the a-Si top cell. We still have to find out the causes of mediocre efficiencies (despite the high J_{sc} values) of micromorph and single junction nc-Si cells deposited on the new TCO.

Finally, we note again that, traditionally, the degree of texture in thin film solar cells (needed for more efficient light trapping) relies almost entirely on the roughness of the substrate (in our case, the superstrate TCO or SnO_2). We have observed that, in many of our nc-Si (and a few a-Si) depositions, 'milky' surfaces emerged because of deposition-enhanced surface roughness, which evidently produces light trapping effect when coated with a back reflector (e.g., ZnO/Al). This effect is more pronounced on low-textured SnO_2 (e.g., LOF TEC7), and is often absent in higher-haze SnO_2 (e.g., newer type AFG SnO_2), depending on film growth conditions. We believe that PECVD-enhanced texturing of the absorber layer is an important topic for future research, as it promises to substantially reduce the reliance on the front TCO for enhanced capture of light.

6. Thin Film Silicon grown by PECVD and HWCVD at Syracuse University

This section was prepared by A.R. Middya with only minor editorial and necessary formatting changes by YML for its integration with the main body of EPV's report. It is an account of the development of deposition methods for, and characterization of, nc-Si (and presumably some poly-crystalline silicon) thin films at EPV's lower-tier subcontractor, Syracuse University (SU). The responsible scientific personnel at SU for this project are: A. Rafik Middya (principal investigator), Eric .A. Schiff (Co-P.I.), and Jianjun Liang (graduate student).

The Personnel at EPV have provided A.R Middya with extensive comments and questions, many of which were (and still are) in disagreements with his views and interpretations. The opinions and conclusions expressed in this section do not necessarily represent those of EPV's.

Executive Summary:

The modification of an existing RF PECVD reactor (non-functional) into a combined plasma and hot-wire CVD system has been completed. An innovatively designed ceramics filament holder have been fabricated to minimize impurities in the silicon layers as well as to create confinement of thermal radiation from the filament to lower substrate temperature. Highly photoconductive a-Si:H films have been developed only by RF PECVD. A new type of polycrystalline silicon thin films with (111) preferential orientation and pentagonal and hexagonal rings on the surface morphology (AFM) have been developed for *the first time* on glass substrate at low temperature (250 ºC) by ceramics hot-wire CVD. The growth rate of these films is ~ 8 A/s. The existence of second phase of silicon in addition to conventional crystalline Si phase have been identified by Raman spectroscopy and X-ray diffraction. The growth of this type of noble poly-Si films may be attributed to the 'confinement effect of thermal radiation from the filament' on the reacting species. The impurity analysis by secondary ion mass spectroscopy (SIMS) exhibit tungsten (W) impurity in ploy-Si films is the below the detection limit for $T_f < 1650°C$, however, other metallic impurities (Ni, Cu, Fe, Cr & Al) have been observed. We found high concentration of carbon impurity in hot-wire CVD poly-Si films compared to the materials prepared by RF PECVD under similar condition. We performed infrared photocurrent measurement on μc-Si solar cells fabricated at EPV to estimate the defect density of the absorber layers and correlated with the solar cell performances. Syracuse University and EPV set an example of effective collaboration between university and industry.

Objective of the Project:

In this project, we proposed to develop an advanced thin-film fabrication technique, combined plasma and hot-wire CVD to prepare μc-Si and poly-Si thin films with high growth rate and at the same time maintaining low defect density. We also proposed to develop and/establish characterization techniques, which will be capable of identifying physical properties, that can be correlated with the solar cell parameters. The results accomplished in the entire period (Phase I & Phase II) of the project are described below.

6.1 Modification of an plasma reactor to a combined plasma and HWCVD system

6.1.1 RF PECVD

At Syracuse University in the group of Prof. Eric Schiff, we have a plasma-enhanced chemical vapor system supplied by Plasma Technology (Ltd), UK and it has the capability of both deposition and etching. The reactor was used routinely until 1994, after that, because of shift of priority, the deposition system was used as required basis. In 1997, some instrumental problem developed in the reactor, since then, the deposition system has not been used. The emphasis of research in the group of Prof. Schiff has been for past twenty years on electronic transport in amorphous silicon (a-Si:H) thin films and pin a-Si:H solar cells. Therefore, in order to develop deposition and characterization facilities of microcrystalline silicon (μc-Si) materials and solar cells, which is the main emphasis of present subcontract, in the initial period (three months) of the project, we mainly focused on developing infrastructural facilities.

The accomplishment of infrastructural facilities include, 1. RF PECVD system fully operational which comprises of hardware and process modification and finally, testing the equipment by depositing a-Si:H films, which exhibit electronic properties, similar to that of standard a-Si:H films, 2. Metal evaporation unit (Edwards) functional, 3. Setting up dark conductivity, photoconductivity and mobility-lifetime measurement accessories.

Before we describe the modification we made to develop the combined plasma and hot-wire CVD system, it is relevant to describe the RF PECVD system, we have, and its special features. It is a standard capacitively coupled radio frequency plasma-enhanced chemical vapor deposition (RF PECVD) system with planner electrode in diode configuration. There is a provision to convert it to triode configuration. The process is computer controlled. The specific feature of the RF PECVD reactor, which is different from standard PECVD reactor, is its Pyrex glass chamber wall instead of stainless steel, which makes chamber cleaning easy and minimizes the contamination from degassing from chamber wall during materials and device fabrication. The reactor has also the capability of depositing n- and p-type a-Si:H films and its alloys, thus it should be possible to produce pin a-Si:H or μc-Si:H solar cells in our existing deposition system.

6.1.2 Combined plasma and hot-wire CVD

From our previous experience [21,22], we observed that the major source of metallic contamination during film deposition and device fabrication by hot-wire CVD technique, is from the evaporation of filament holder and also from the electrical connections between the filament and electrical wire. The metallic impurities drastically affect the lifetime of the photogenerated carriers in silicon thin films. In order to minimize the impurity incorporation during process of silicon thin films, we have selected filament holder made of ceramics materials instead of conventional metallic one. The chemical composition of ceramics materials, we selected is

Zirconium phosphate, which has high melting point (2750 °C). We have found from the electrical power balance calculation at the filament that significant amount of electrical power is consumed by the filament holder to maintain a particular filament temperature. Based on this calculation, we designed an innovative filament holder. The design of the filament holder is shown in **Fig. 41**. The filament holder is made of two rectangular ceramics frames, mounted by four ceramics posts and spacer for height adjustment. The bottom one we call base and top one, we call filament support. The ceramics posts and spacers allow to adjust the distance between the filament and substrate. It is also possible to give a tilt of the plane of the filament w.r.t. incoming flux of the process gas. The reason for this shape of the filament holder is to mount the filament on top of an anode electrode of a parallel plate RF PECVD system and to vary the substrate-to-filament distance. The particular shape of the filament holder also took care of minimizing the mass of the filament holder, which will reduce the thermal budget, i.e. decrease the current required to obtained particular filament temperature. The specific design of the filament holder will allow to test an important concept, "confinement of thermal radiation from the filament to activate the reacting species to lower the substrate temperature during the growth of microcrystalline and polycrystalline silicon films". When the filament will be at elevated temperature, the box structure of the filament holder will create confinement of thermal radiation from the filament because the ceramics bars of the box will radiate heat and reduce the thermal convection from the box area. The confinement of thermal energy within the filament holder box can be visualized by comparing the similar situation when filament is mounted on a single metallic frame, where radiative heat continuously transported away from the filament zone by convection. Therefore, the particular design of the filament holder will create confinement of thermal radiation from the filament in the film processing zone surrounded by ceramics.

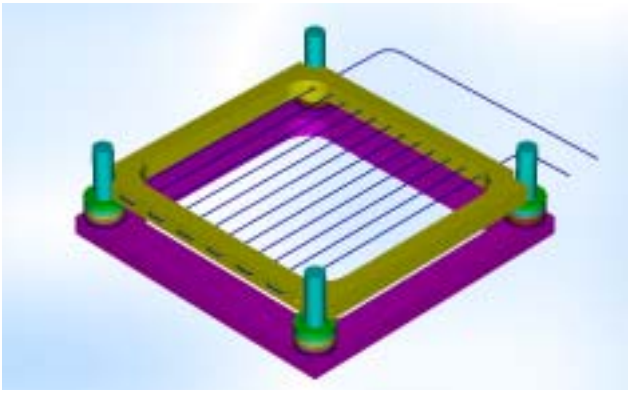

Figure 41 Design of the filament holder.

The area of the filament holder is 10x10 cm^2 and it can hold up to 12, 10 cm wires, i.e. total length of the wire is 1.2 meter. We selected tungsten wire with 0.5 mm diameter as the catalyzer. This particular filament design allows processing of 10x10 cm^2 silicon layer and solar cells. The filament holder has been fabricated in our machine-shop. It may be noted from Fig. 1 that the mechanical components, connecting the tungsten filament and electrical wire are away form the area (outside the ceramics frame), where Si layers will be processed, which further minimizes the incorporation of metallic impurities. The problem of thickness inhomogeneity during hot-wire CVD processing arises from the inhomogeneity in temperature distribution due to radiation from

the filament, i.e. due to the particular design of the filament holder. Because of this fact, we fabricated filament holder, which can hold 10x10 cm^2 filament area. We believe that some of the technical challenges of relatively new hot-wire CVD technology, like impurities and thickness inhomogeneity can be solved by the new design of the ceramics filament holder. The filament holder is put on top of grounded electrode (anode) in a RF PECVD system. In order to bring electrical power to the filament inside the reactor, we made a suitable mechanical design to put electrical feedthrough in the reaction chamber and also selected a special type of wire, which can sustain high temperature (200 $^{\circ}$C) and minimizes the current leakage from the wire in the plasma. The other end of the feedthrough is connected with a Variac to adjust the current through the wire. We use a optical pyrometer (Leedthrop, PA) to measure the filament temperature; the Pyrex glass chamber wall allow fair estimation of filament temperature by taking average of the filament temperature over entire length. The RF power supply is attached to the top electrode. The process gases are entered in the reactor through top electrode (shower head type), which are decomposed by the hot filament as well as RF power in combined plasma and hot-wire CVD system. Thin films are formed from the radicals arriving at the substrate surface, generated from the hot-filament as well as radio frequency power excitation. The system, we have developed, can operate in three different modes, 1. RF PECVD, 2. Hot-wire CVD and 3. Combined plasma and hot-wire CVD. Although, the emphasis of present project is to develop high quality μc-Si:H films and solar cells with high growth rate, however, the multi-mode deposition capability of our system, will provide us opportunity to explore different process technologies to prepare a-Si:H and μc-Si:H films as well as research scope for better understanding on correlation between growth process and electronic properties (carrier mobility and lifetime).

Interaction of hot-filament with SiH_4 and H_2 plasma in combined plasma and hot-wire CVD:

After completion of the modification of our existing RF PECVD system to a combined plasma and hot-wire CVD, our first attempt was to understand the technical problems, which may arises due to the heating the tungsten filament in the presence of plasma of reactive process gases. For this purpose, we generated silane and hydrogen plasma in the reactor and then heated the filament up to 1600°C temperature, we observed an interesting effect, the glow discharge process in combined plasma and hot-wire CVD. At high RF power (58 watt), silane and hydrogen plasma is turned off as soon as the filament is turned on and glow of the plasma is visible again as soon as filament is turned off however, at low RF power (41.7 watt) and same dilution (20:1), plasma is once again turned off with turning on the filament, however unlike previous case (RF power ≈ 58 watt) plasma did not turn on automatically with turning off of the filament. Interaction of the heated filament with plasma is also sensitive to H-dilution, although under high dilution (20:1) plasma is turned off as soon as filament starts to ignite, whereas at low dilution (3.5) and same RF power (58.5 Watt), glow discharge did not turned off with turning on power to the filament, although the brightness of the plasma decreases. This phenomenon indicates that there is a strong interaction between the heated filament and plasma, this may be because of the fact that the electron-impact dissociation process is strongly influenced by the hot-filament. We are at present in the process of understanding in more details the interaction of silane and hydrogen plasma with the heated filament, so that we can develop a qualitative model on primary dissociation process in combined plasma and hot-wire CVD. Simultaneously, we are also trying to solve the technical problems associated with having stable combined plasma and hot-wire CVD process with wider process window. Because of the complexity in understanding the combined plasma and hot-wire CVD process, we decided until the middle of Phase II of this

project that we will focus on investing the impact of process parameters on electronic and structural properties of films prepared by only by RF PECVD as well as by hot-wire CVD.

6.1.3 Development of ceramics hot-wire CVD

In the hot-wire CVD system, we are developing, Tungsten wire is used as catalyzer. We start with 3 wires of 10 cm length each, mounted in the filament holder. The diameter of the wire 0.5 mm and total resistance of the wire is 0.4 Ω. Based on our previous experience, we took special care in mounting the filament in the filament holder as well as followed a specific procedure to "form" the filament. We found filament does not break in normal circumstances and we do not have to change the filament ("edging effect") after certain number of depositions. Therefore, in our hot-wire CVD system, filament lifetime is not a problem. However, we did observe breakage of top part (frame) of the filament holder supporting the filament, the cracks or breakage is always found to appear at the specific portion of the filament, near the electrical connections, the reason for cracks at the specific location is not very clear, however, we also observed that ceramics become very brittle after many runs of deposition, which indicates ceramics undergoes structural rearrangement when the filament is hot. We do not know at present any other ceramics, which has higher melting point than one (Zirconium phosphate, melting point ≈ 2750°C) we are presently using. We investigated by increasing the lateral dimension of the top frame by 0.25 inches, however, that did not solve the cracking problem, suggesting that structural rearrangement due to over heating is the cause of breakage of the ceramics frame. We are still at the stage of optimizing the materials and geometry of the filament holder to improve the longevity of the filament holder as well as to achieve the greater effect of confining the radiative heat from the filament.

In our approach for materials development, we selected one deposition condition, based on our previous experience and first thing we did is to verify the reproducibility. The condition, we selected is 20:1 hydrogen to silane ratio, silane flow was 15 sccm, filament to substrate is 2. 5 cm, filament temperature ~ 1400°C, substrate temperature was set at 250°C. We prepared several samples under same condition, always, we got polycrystalline silicon on glass, having textured surface. The appearance of thick sample looks like single crystalline silicon. The structural properties and impurities in these samples have been described below. For some sample, substrate temperature were set to 0, in those cases non-uniformity even in small area 1'x1', have been observed, indicating actual substrate temperature, as a result of setting temperature and radiative heating from the filament is close to 250°C. We varied H-dilution as well as filament temperature, to investigate their effects on structural, electronic properties and impurities in the μc-Si and poly-Si films, which have been described in details below.

6.2 Development of amorphous and microcrystalline silicon films by RF PECVD

As mentioned earlier, we spent initial three months to bring the RF PECVD system at Syracuse University back to operational mode to verify that the reactor is capable of producing a-Si:H and μc-Si:H films with electronic properties comparable to the state-of-the-art amorphous and microcrystalline silicon films. The deposition conditions and the preliminary properties of the samples have been described in **Table 24**. It may be noted from the table that the sample 061002 is amorphous having dark conductivity (σ_d) and photoconductivity (σ_{ph}) 4.1×10^{-9} Scm^{-1} and 2.5×10^{-6} Scm^{-1} respectively. The photoconductivity has been measured with a monochromatic light from a ($\lambda \sim 670$ nm) laser having wavelength 670 nm and photon density ~ 10^{16} $cm^{-2}sec^{-1}$.

Sample No.	Type of Sample	Silane Flow (sccm)	H_2 Diln.	P_r (mT)	RF Power (Watt)	T_s (°C)	σ_d (Scm^{-1})	σ_{ph} (Scm^{-1})
061002	a-Si:H	26	0	160	9.0	150	$4.10x10^{-9}$	$2.50x10^{-6}$
073002	μc -Si:H	18	0	125	8.2	200	$2.58x10^{-8}$	$1.24x10^{-7}$
071602	μc-Si:H	25	20:1	477	32.3	250	$7.75x10^{-9}$	$3.20x10^{-8}$
073102	μc-Si:H	37	20:1	730	23.4	250	$3.61x10^{-7}$	$1.13x10^{-8}$

Table 24 Deposition conditions and opto-electronic properties of a-Si or μc-Si films.

The spectral response of pin a-Si:H solar cells with ZnO/Al back contact at 670 nm is only < 40%, i.e. most of the photon at this wavelength is transmitted through the sample. The value of σ_{ph} of the sample 061002 appears to be high for 670 nm illumination, which can be attributed to high carrier mobility or lifetime of the sample, high σ_{ph} and relatively higher dark conductivity (~ 10^{-9} Scm^{-1}) of the sample indicate that carrier mobility in this sample can be higher than standard a-Si:H films. When the silane flow rate is decreased to 0.8 sccm, the photosensitivity (σ_d/σ_{ph}) reduces to 20.8, indicating sample become microcrystalline (even high defect density a-Si:H films, the photosensitivity can not be 10). Under low silane flow condition, the residence time of SiH_4 is long which causes higher dissociation of SiH_4 into silicon related radicals and atomic hydrogen (H), in other words low flow of silane is equivalent to high hydrogen dilution condition. In case of sample #071602 and #073102, with increasing hydrogen dilution, photosensitivity decreases to 0.24 and 31.9 respectively indicating samples are μc-Si.

In order to identify the parameter space for amorphous-to-microcrystalline silicon transition under plasma CVD condition, we prepared series of samples with different hydrogen dilution, all other parameters were maintained constant. The silane flow for these series of samples was 24.6 sccm, substrate temperature was maintained 250°C and the rf power was fixed around 20 watt. The sample preparation condition and properties have been shown in Table 24. The photoconductivity of the sample has been measured both under white light with intensity ~ 50 mW/cm^2 as well as under monochromatic light (λ ~ 600 nm) with photon density ~10^{17} cm^2sec^{-1}. The mobility-lifetime (μτ) product has been derived from photoconductivity under monochromatic light. The thickness of the samples has been derived from the interference fringes from the transmission measurement. It may be noted from the **Table 25** that the dark conductivity remain nearly same around $5x10^{-8}$ S/cm with increasing H-dilution up to 8, for higher dilution, σ_d drastically increases to

Sample #	SiH_4 flow (sccm)	H_2 flow (sccm)	P_w (Watt)	T_s (ºC)	σ_d (S/cm)	σ_{ph} (S/cm)	μτ (cm^2/V)
090403	25	0	20.8	250	$4.29x10^{-8}$	$2.01x10^{-5}$	$4.67x10^{-9}$
090503	24	138	19.3	250	$5.0x10^{-8}$	$6.77x10^{-5}$	$2.67x10^{-8}$
082903	13	210	18.7	250	$4.8x10^{-8}$	$8.47x10^{-5}$	$1.01x10^{-8}$
083003	24	430	18.3	250	$4.91x10^{-5}$	$2.65x10^{-5}$	$2.49x10^{-8}$

Table 25 Preparation conditions and electronic properties of a-Si and μc-Si thin films.

$4.91x10^{-5}$ S/cm for H to SiH_4 ratio ≈ 17.6. The photoconductivity under white light increases by a factor of 4 as H-dilution increases from 0 to 8 and for higher dilution σ_{ph} decreases. The $\mu\tau$ product increases by a factor of 5 from $4.67x10^{-9}$ cm^2/V to $2.67x10^{-8}$ cm^2/V, as H-dilution increases from 0 to 5.6. *The large increase of dark conductivity form $4.8x10^{-8}$ S/cm to $4.91x10^{-5}$ S/cm as well as drastic drop of photosensitivity from 57 to 1.85 with the increase of H-dilution from 8 to 17.6, indicates phase transition from amorphous-to-microcrystalline silicon films*. At this point, it is not clear why the dark conductivity is high for samples prepared without H-dilution, is the phase of the sample also amorphous-to-microcrystalline transition zone or the films contains impurity? The large difference between $\mu\tau$ product and the σ_{ph} values indicates that the high dark conductivity is not related to the impurities in the bulk, rather thickness dependence structural change , i.e. structure near the surface is different from bulk of the materials since σ_{ph} under white light measurement sensitive to absorption across the thickness, whereas $\mu\tau$ product reflects the bulk properties of the sample. *The high σ_d ~ $5x10^{-8}$ S/cm for all the samples in Table II indicates that the samples could be in the in the phase boundary of amorphous-to-microcrystalline transition (a-Si:H-like materials) and have significant structural inhomogeneity across the thickness.* The results of Table 24 and Table 25 indicate that highly photoconductive a-Si:H to a-Si:H-like materials and μc-Si films can be easily prepared in the RF PECVD system in our group. One of the key feature of this reactor, which has immense technological advantage is the Pyrex glass chamber wall which is specially advantageous in preparing μc-Si films, since normally combination of high rf power and high hydrogen dilution, which is used to prepare μc-Si films, etches chamber wall of the reactor (which is generally stainless steel), consequently, carbon, oxygen and nitrogen incorporate into the films, which deteriorates the optoelectronic properties of the resulting films.

6.3 Development of μc-Si and polycrystalline Si thin films by ceramics HWCVD

Our approach to test the idea of introducing ceramics filament holder in hot-wire CVD reactor is to prepare μc-Si films under same condition, to find out there is any distinct reproducible feature present in the films, which otherwise is not expected to observe. In the first series of samples, we maintained constant silane and hydrogen flow of 15 sccm and 300 sccm respectively, filament temperature (T_f) ~ 1400°C, substrate-to-filament distance (d_f) ~ 2.5 cm, substrate temperature, we maintained by an external heater is around 250°C. The deposition rate has been calculated by mechanically measuring the thickness of the sample, we obtained maximum deposition rate ~7-8 A/s for samples prepared with 20:1 hydrogen dilution and 1800°C filament temperature. After sample preparation, we performed optical, morphological, structural characterization and impurity analysis of the sample.

6.3.1 Structural properties of μc-Si and polycrystalline silicon (poly-Si) thin films

The appearance of the most of the samples look like single-crystal silicon, indicting *formation of polycrystalline silicon thin films on glass at relatively low temperature (~250°C)*. This type of samples (color similar to that of c-Si) have been observed on glass substrate (poly-Si) prepared by hot-wire CVD at relatively high temperature (~ 450°C) [21,22]. The samples prepared by our

newly developed ceramics hot-wire CVD appears to be rough and surface roughness dependent on sample thickness, during optical transmission measurement in the infrared region no interference fringes are observed even for thin sample, rough surface of the film from early part of the film growth. The morphology of the films has been investigated by scanning electron microscopy (SEM) and atomic force microscopy (AFM). **Fig.42 (a)** show SEM micrograph of poly-Si films, prepared with the deposition condition, mentioned earlier. It may be noted from the micrograph that the small grains having size ranging from 0.1 μm to 0.5 μm distributed throughout the sample. It has been observed that when H-dilution is increased to 30:1 and 40:1 grains size increases and distribution of the grain changes particularly for 40:1 dilution. The morphology changes drastically, when the filament temperature increases to 1800ºC keeping H-dilution same as 20:1 as shown in **Fig. 42(b)**. The average grain size increases compared to films prepared with 1400°C and an ordered distribution of grains is visible from the SEM micrograph Fig. 42(b), i.e. parallel lines can be drawn through the grains. Thus, the grain size of poly-Si films can be controlled by H-dilution and filament temperature**. Fig. 43** (a) and Fig. 43 (b) show the AFM topography of poly-Si samples prepared with 20:1 and 30:1 dilution. Fig. 43(a) is the same sample corresponding to Fig.42(a). Several distinct features are visible on the AFM surface morphology of sample prepared with 20:1 dilution. Grains, precisely clusters of small grains having size 0.1μm to 0.5 μm distributed throughout the sample surface, these cluster of small grains appear as a grain in the SEM micrograph [Fig. 42(a)]. Instead of conventional AFM surface morphology of μc-Si and poly-Si films, a definite geometrical pattern, i.e. pentagonal and hexagonal rings are found to distribute throughout the sample surface, these features vary and disappear with the variation of process parameters, like H-dilution and filament temperature. Fig. 43(b) show the AFM surface morphology of sample prepared with 30:1 dilution, similar type of features are observed as in Fig. 43(a). Thus, the pentagonal and

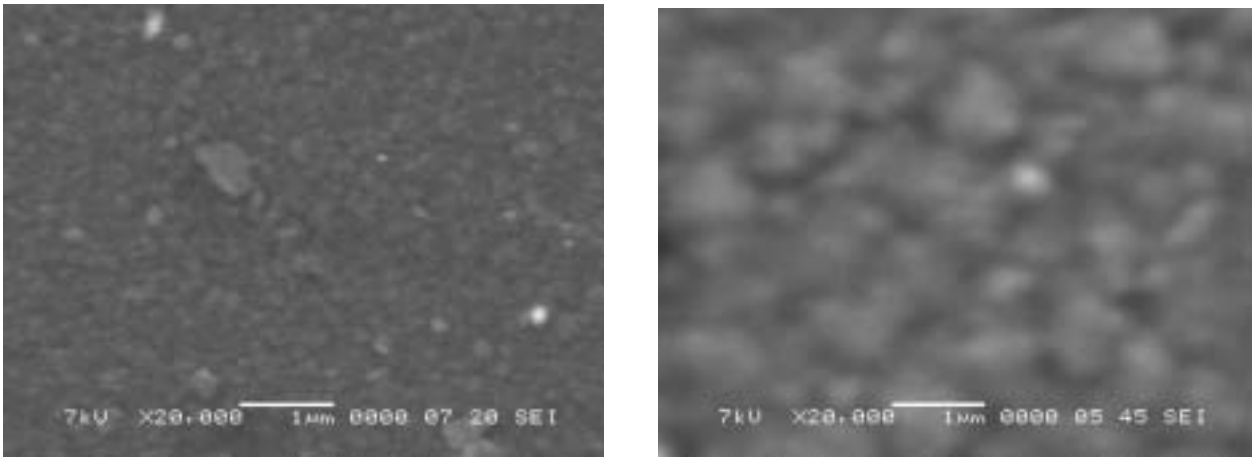

(a) (b)

Figure 42 (a) SEM micrograph of poly-Si film by H-dilution≈ 20:1 and $T_f \approx 1400$ºC.
(b) SEM micrograph of a poly-Si film by H-dilution≈ 20:1 and $T_f \approx 1800$ºC.

hexagonal block formation of solid indicate that the formation of specific type of atomic arrangement inside the materials. Our previous results on correlation between AFM and X-ray

diffraction on poly-Si films suggests that any ordered feature in the distribution of grains is correlated with atomic-scale structure of the materials [23]. **Figs. 44** (a) and 44(b) show the AFM phase of poly-Si films prepared with 20:1, 30:1 and 40:1 H-dilution respectively. The phase image [**Fig. 45**(a)] exhibit small grains 10 to 30 nm grows perpendicular to the substrates, extended throughout the thickness of the layer. The structure of the films appears to be like c-Si nanorods/columns immersed in the disorder silicon phase of the materials. The disordered silicon phase could be amorphous silicon. On comparison of Fig. 45(a), Fig. 45(b), and Fig. 45 (c), it is evident that with increasing H-dilution, density of c-Si nanorods/columns continuously increases from 20:1to 40:1 H-dilution and the diameter of the columns decreases, for samples prepared with 40:1 dilution, dense columnar grains are observed throughout the sample.

The pentagonal and hexagonal rings are distributed throughout the AFM surface morphology, these features vary and disappear with the variation process condition, like H-dilution and filament temperature. Thus, the pentagonal and hexagonal block formation of solid indicate that the formation of specific type of atomic arrangement inside the materials. Our previous experience suggests that any ordered feature in the distribution of grains is correlated with atomic-scale structure of the materials [23]. Figs. 44(a) & 44(b) show the AFM phase of poly-Si films prepared with 20:1 and 40:1 H-dilution respectively. The phase image [Fig. 44(a)] exhibit small grains 10 to 30 nm grows perpendicular to the substrates, extended throughout the thickness of the layer. The structure of the films appears to be like c-Si nanorods/columns immersed in the disorder silicon phase of the materials. The disordered silicon phase could be amorphous silicon. On comparison of Fig. 44(a) and Fig. 44(b), it is evident that with increasing H-dilution from 20:1to 40:1, density of c-Si nanorods/columns continuously increases for samples prepared with 40:1 dilution, dense columnar grains are observed throughout the sample.

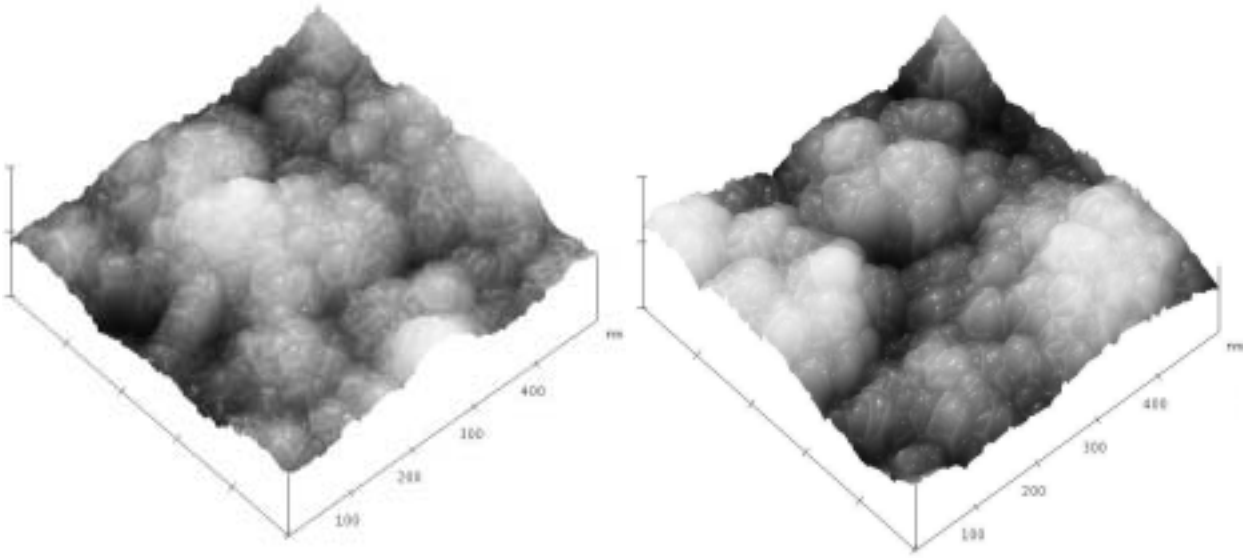

(a) (b)

Figure 43 (a) AFM topography of poly-Si films prepared with 20:1 dilution.
(b) AFM topography of poly-Si films prepared with 30:1 dilution.

This is a first time direct demonstration of influence of H-dilution on nucleation and growth of grains of poly-Si films on glass substrate. The crystallographic structure of the films has been analyzed by Raman spectroscopy and X-ray diffraction. **Fig. 45** (a) show the Raman spectra of three samples prepared with 20:1, and 30:1 H-dilution and 1400ºC and 20:1 and 1800ºC. It may be noted from figure 45(a) that for all three samples, peak around 520 cm^{-1} and 380 cm^{-1} have been observed. The peak at 520 cm^{-1} correspond to transverse optical (TO) mode of c-Si, 380 cm^{-1} peak is also TO mode, however, it is related to the different phase of c-Si, known as Si-XII (r8) [24]. Fig. 45(b) shows the enlarged view of 520 cm^{-1} peak, it is clear from the figure that there is no peak at 480 cm^{-1}, which corresponds to amorphous silicon (a-Si) component, however, peak around 507 cm^{-1} has been observed with nearly same intensity as 520 cm^{-1}, the 507cm^{-1} peak is generally assigned to grain boundary. The materials, we developed is polycrystalline silicon thin films, composed of c-Si grains and disordered grain boundaries, as observed by AFM phase image. When H-dilution or filament temperature is increased to 30:1 1800°C respectively, TA & TO peaks appear at the same position only the full width half maxima (FWHM) of 520 cm^{-1} decreases as well as intensity of TO peak increases indicating the crystallographic quality of the grain enhances i.e. classical defects like twins and dislocation and stress and strain in the materials are decreased and volume fraction of c-Si component increases with increasing H-dilution and filament temperature.

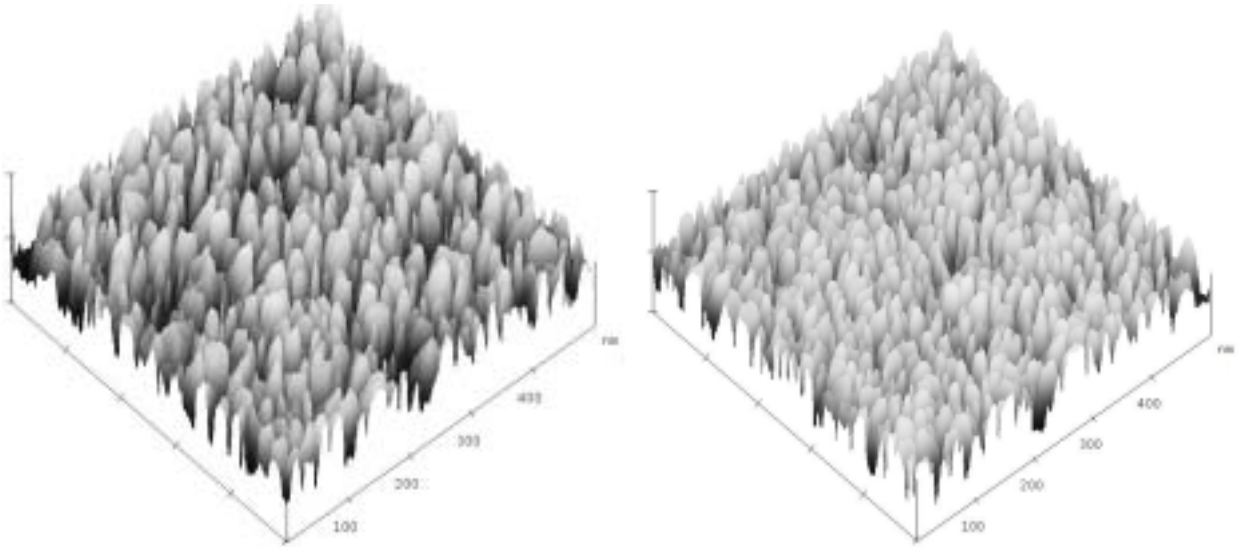

(a) (b)

Figure 44 (a): AFM phase image of poly-Si films prepared with 20:1 dilution.
(b): AFM phase image of poly-Si films prepared with 40:1 dilution.

Thus, we succeeded to synthesize small grain poly-Si films on glass substrate low substrate temperature (~250ºC) and low filament temperature (~1400°C). **Fig. 46** show the comparison of XRD pattern of poly-Si films, prepared with 20:1, 30:1 and 40:1 dilution and 1400°C filament temperature as well as 20:1 dilution and 1800ºC filament temperature. The XRD spectra exhibit all the samples have (111) preferential orientation, the (220) and higher order peaks have also been observed with much lower abundance. The sharp spikes around $2\theta \approx 80^{\circ}$, is most likely originates from noise. On comparison of curves I, II & III, it may be noted that with increasing dilution and filament temperature, the preferential orientation of (111) peak does not change, however (220) and higher order peaks become prominent. The prominent effect of H-dilution and filament temperature is to reduce the line width (FWHM) of (111) peak, i.e. increasing the grain size maintaining the preferential orientation (111). In literature, it has been reported by many groups on formation of microcrystalline and polycrystalline silicon thin films on glass substrate at low temperature (< 450°C) with (220) orientation by RF PECVD and VHF PECVD. However, to the best of our knowledge, there is no reports in the literature on growth μc-Si or poly-Si films with (111) orientation on glass substrate at low temperature. The special environment of film growth in our case, i.e. confinement of thermal radiation from the filament, which is expected to heat the reacting species, may be effective, in addition to substrate temperature (250°C),

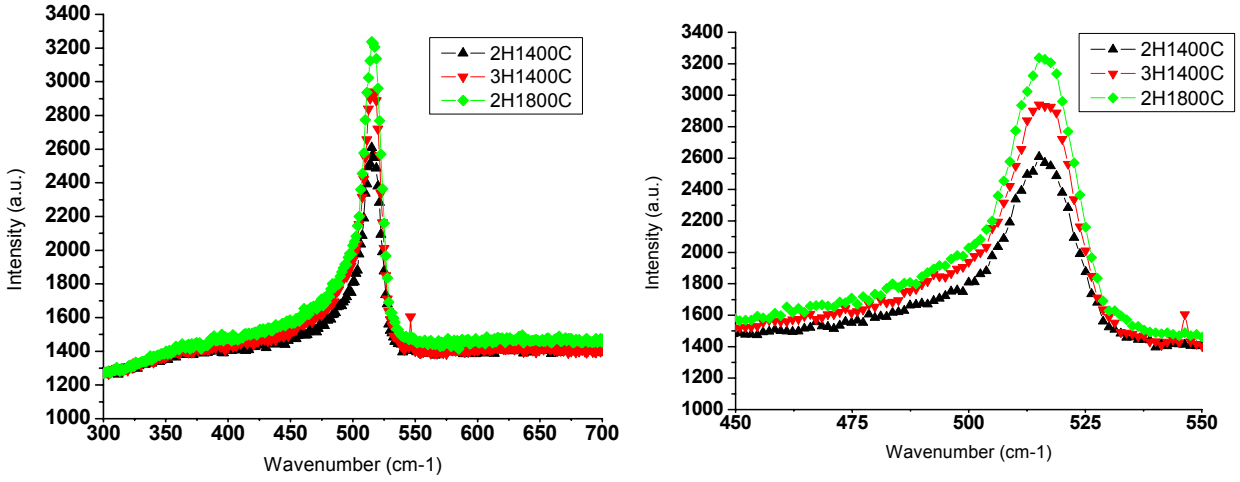

Figure 45 (a): Comparison of transverse optical (TO) bands around 380 cm^{-1} and 520 cm^{-1} of samples prepared with different H-dilution and filament temperature.
(b): Comparison of transverse optical (TO) at 507 cm^{-1} and 520 cm^{-1} of samples prepared with different H-dilution and filament temperature.

in providing sufficient energy during the formation of poly-Si films with (111) orientation. Fig. 46(b) shows the comparison of (111) peak of XRD pattern of same samples corresponding to Fig. 46(a). It may be noted from the Fig. 46(b) that full width half maxima (FWHM) of (111) peak decreases with increasing H-dilution, however, the peak position for all three samples remain same. When the filament temperature increases to 1800ºC, FWHM decreases compared to films prepared with 1400°C and H-dilution 20:1 and peak position is slightly shifted towards higher 2θ. The peak shift towards higher 2θ indicates release of stress and strain in the materials

compared to sample prepared with lower filament temperature and higher H-dilution and decrease of FWHM with increasing filament temperature is due to the increase of grain size, which is consistent with SEM observation [Fig. 42(a) and Fig. 42(b)]. It is interesting to note that for both the samples prepared with 20:1 dilution and 1400ºC and 1800ºC filament temperature, doublet exist in the (111) peak, with increasing H-dilution, the second peak (within the doublet) at higher 2θ diminishes and for sample prepared with 40:1 dilution, (111) peak appears almost as a single peak, maintaining the peak position at lower 2θ. The presence of doublet both for 1400ºC and 1800ºC filament temperature as well as diminishing of peak at slightly higher 2θ, indicates that the origin of doublet is related to the existence of another phase of c-Si, indeed, we observed transverse optical mode at 380 cm^{-1} in addition to 520 cm^{-1} peak in the Raman spectrum of all three samples, indicating presence of second phase of crystalline silicon, Si-XII(r8). The FWHM of (111) or (220) peak is generally used to calculate grain size using Scherrer's formula; however, because of presence of doublet, the grain size calculation will be ambiguous. The effect of H-dilution and filament temperature is clearly observed from the Fig. 46(b). It may be noted that FWHM of sample prepared with 1400°C filament temperature and 40:1 dilution is lower than that of sample prepared with 1800°C filament temperature, which indicates that effect of H-dilution is more pronounced than filament temperature.

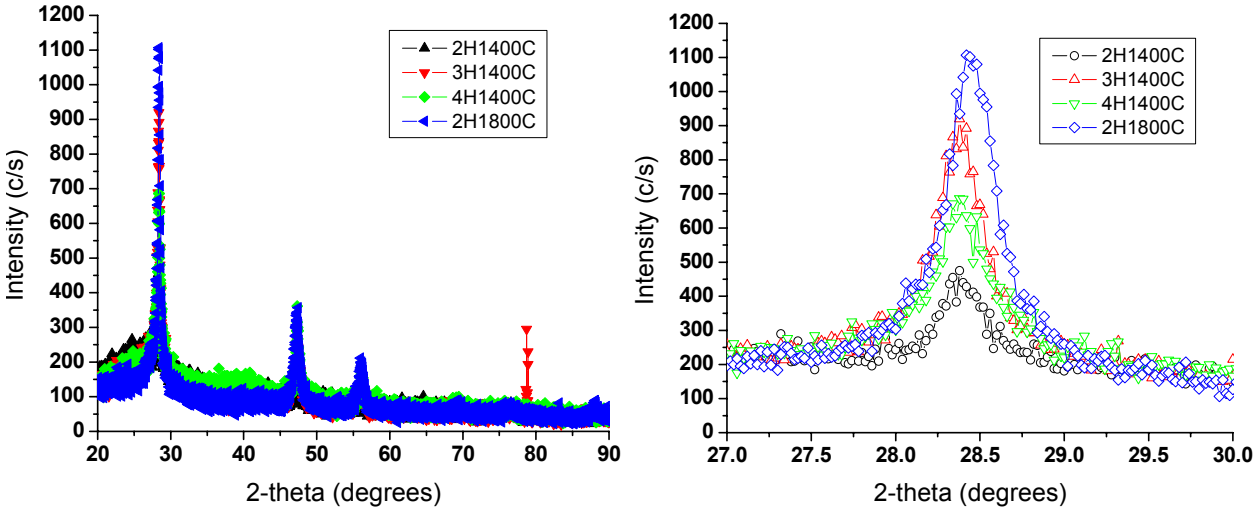

(a) (b)

Figure 46 (a) Comparison of XRD spectra of poly-Si films prepared with different H-dilution and filament temperature, H represents 10:1 dilution.
(b) Comparison of (111) peak of XRD spectra of poly-Si films prepared with different H-dilution and filament temperature.

6.3.2 Impurity analysis of μc-Si and poly-Si films prepared by PECVD and HWCVD

The main drawbacks of hot-wire CVD technology for synthesizing silicon thin films (nanocrystalline, microcrystalline, polycrystalline, epitaxial Si thin films), is incorporation of high level of impurities in the films, particularly metallic, oxygen and carbon impurities. Several

groups reported their efforts to minimize oxygen, carbon and metallic impurities in Si thin films, prepared by hot-wire CVD [21,22]. The key idea behind introducing ceramics filament holder is to minimize metallic impurities by confining the silicon processing zone by ceramics materials.

We have performed SIMS analysis of five different samples, one prepared by RF CVD and other four samples synthesized by hot-wire CVD at different filament temperature. SIMS measurement has been performed at NREL. The reason for analyzing RF CVD sample, is to find out what are the additional impurities incorporate, when filament will turn on in presence of plasma, i.e. when μc-Si and poly-Si films will be prepared by combined process of RF PECVD and hot-wire CVD. **Fig. 47** shows the depth profiling of silicon, hydrogen, oxygen and carbon elements of a μc-Si sample (#083003), prepared by RF PECVD. It may be noted from the figure that H is uniformly distributed throughout the bulk of the materials, except slightly lower concentration at the surfaces (which may be related to surface oxide). The concentration of H in the materials is same order of magnitude to that of Si atom, indicating Si-H alloy has been formed in the μc-Si sample. *It is relevant to mention that, to the best of our knowledge, this is for the first time H atom could be directly detected by SIMS in μc-Si samples*, the analysis show that H is present in the sample in the form of Si-H alloy, instead of percentage level as generally found in μc-Si films by Fourier transformed infrared spectroscopy (FTIR). The concentration of C varies across the thickness in a very interesting way, the level of C impurity drops by more than two orders of magnitude within 0.1 μm thickness from the surface then the level becomes constant in the bulk ~ 10^{19} atom/cm^3. It may be relevant to mention that the chamber wall of our hot-wire CVD system is made of Pyrex glass instead of stainless steel;

There has been a report by a group at Ecole Polytechnique, on large decrease (more than two orders of magnitude) of C content in the SIMS depth profiling of μc-Si sample prepared by a hot-wire CVD reactor with stainless chamber, when an inner vessel is added inside the chamber to minimize impurity [25]. In spite of these two similar observations under the condition of μc-Si films growth with minimum/no outgassing from the chamber wall, the large increase (by two orders of magnitude) of C content towards the surface is not clear. The concentration of oxygen ([O]) ~ 10^{21} atom/cm^3, except in the surface, distributed fairly uniformly in the bulk of the materials. The reliability of measurement of O concentration of the SIMS instrument ~ 10^{21} atom/cm^3. The concentration of Si atom ~ 10^{22} atom/cm^3, which is lower than that in c-Si wafer, the difference may be attributed to the lower density of Si atom in the μc-Si films due to inclusion of a-Si:H component.

Fig. 48(a) and Fig. 48(b) show the elemental analysis as well as depth profiling of the sample prepared by hot-wire CVD at 1400°C filament temperature. It may be noted from the Fig. 48(a) that the concentration of tungsten (W) and Zirconium (Zr) are below the detection limit, however, high concentration of Nickel (Ni), Copper (Cu), Iron (Fe) have been observed. The Chromium (Cr) and Aluminum (Al) have also been detected in the sample. The Ni, Cu, Fe, Cr and Al impurities are most likely originating from the metallic component, used in the filament holder and from the copper wires carrying current inside the reactor. The work is at the early stage of development, the metallic impurities found in the silicon layer can be minimized by suitably modifying the metallic components in the filament holder. Fig. 48(b) show depth profiling of Si, H, C and O, it may be noted that both H and C have characteristics variation across the thickness, which is found to be common for all other samples, indicating some insight about poly-Si films growth in ceramics hot-wire CVD. The level of H-content in hot-wire CVD poly-Si films is lower than that of μc-Si films prepared by RF PECVD, however, the H-content

of hot-wire CVD films ~ 6-7X10^{21} atom/cm^3, which appears to be high although significant amount of H may not be bonded to Si atom. The high bonded H-content in poly-Si films is consistent with low substrate temperature (~250ºC), under which films were grown. The Si level in the sample prepared by hot-wire CVD is significantly higher than that of the sample prepared by RF PECVD, *indicating that poly-Si films of hot-wire CVD is much more compact and homogeneous in density across the thickness than µc-Si films prepared by plasma CVD. This is an important observation and is expected to impact electronic properties of the materials and device performance, particularly solar cells*. **Fig. 49**(a) and 49(b) represent the elemental analysis and depth profiling of metallic impurities of a sample (#120403), prepared with filament temperature ~ 1650°C. The levels of Cu, Fe, Cr, Al and Ni impurities are similar to that of sample prepared with 1400ºC filament temperature; the W and Zr content in the sample are also below the detection limit. When the filament temperature is increased to 1700°C, W impurity significantly increases to ~ 10^{19} atom/cm^3, other metallic impurities also increase significantly. We performed SIMS analysis of poly-Si sample, when filament temperature increases up to 1800°C. The concentration of O increases by a factor of 8 to 9 times compared to that of plasma deposited µc-Si films prepared in the same reactor, when filament temperature is increased to 1800ºC. *Thus SIMS analysis indicates that in order to obtain W free sample, the filament temperature should be below 1650°C.*

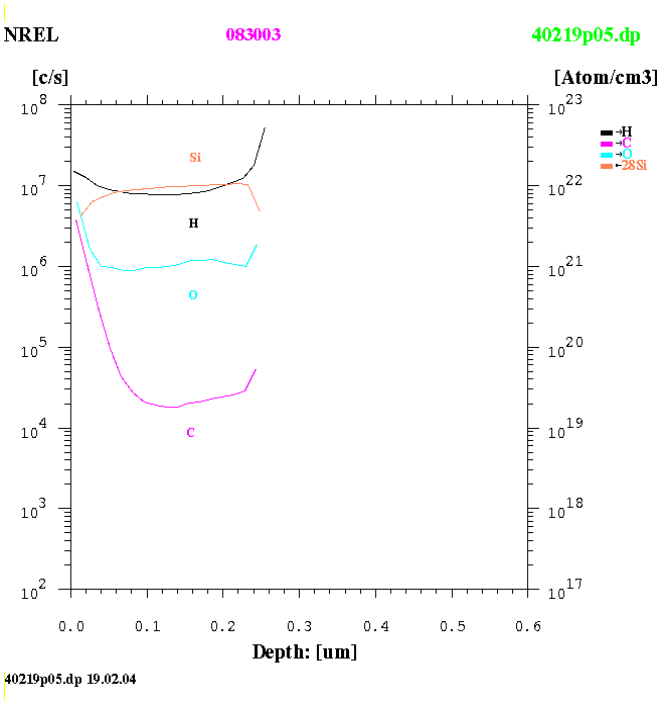

Figure 47 Depth profiling of Si, H, O and C in µc-Si film prepared by plasma CVD.

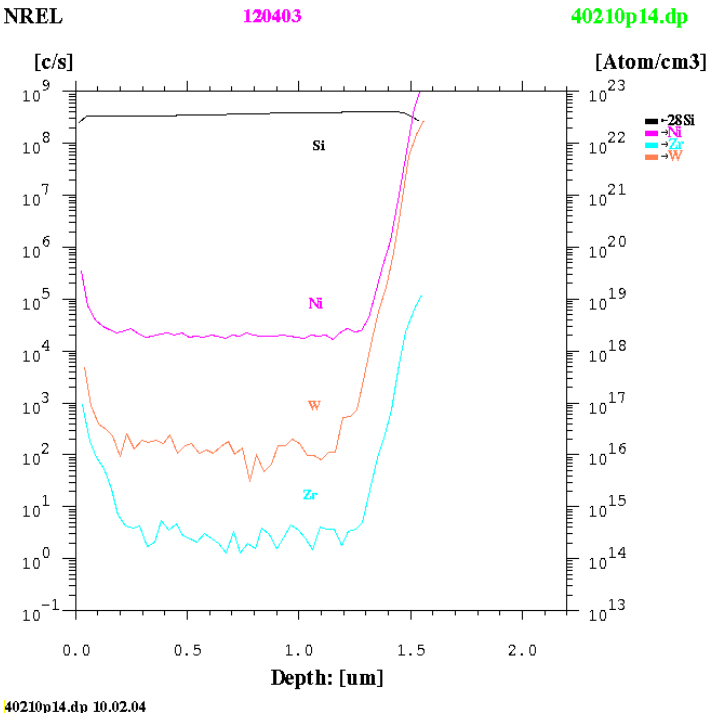

Figure 48 (a): Depth profiling of metallic impurities of poly-Si film prepared by hot-wire CVD filament temperature, $T_f \sim 1400°C$.

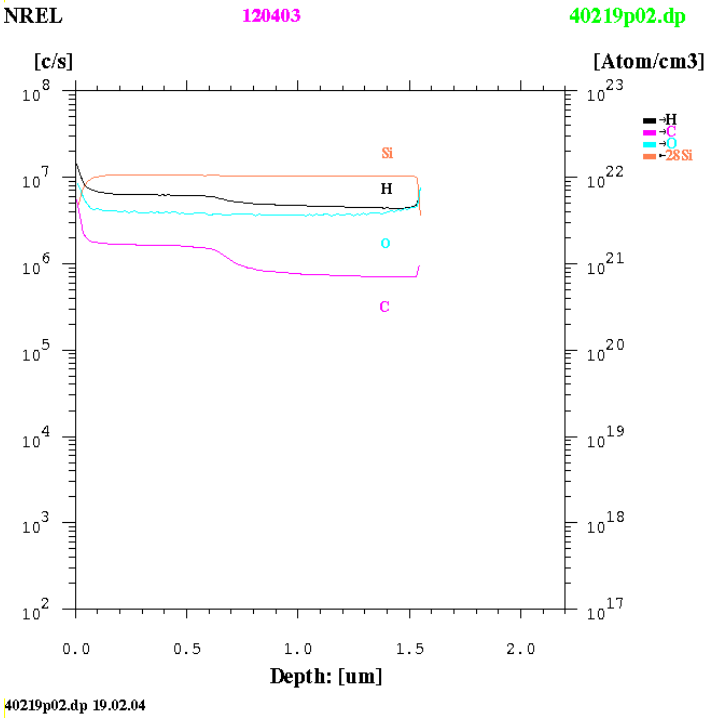

Figure 48 (b): Depth profiling of H, O, C in poly-Si sample prepared by hot-wire CVD for the filament temperature, $T_f \sim 1400°C$.

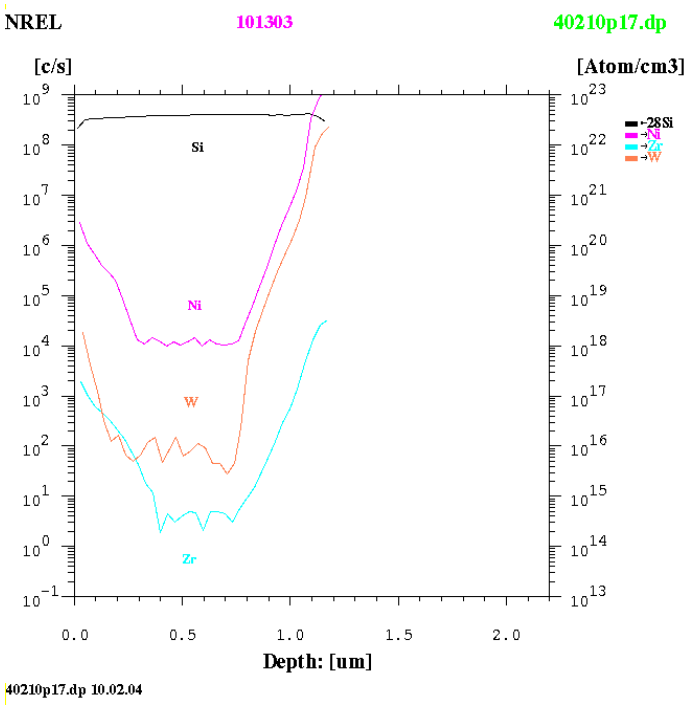

Figure 49 (a): Depth profiling of metallic impurities in poly-Si sample (#101303) prepared with filament temperature, T_f ~1650°C.

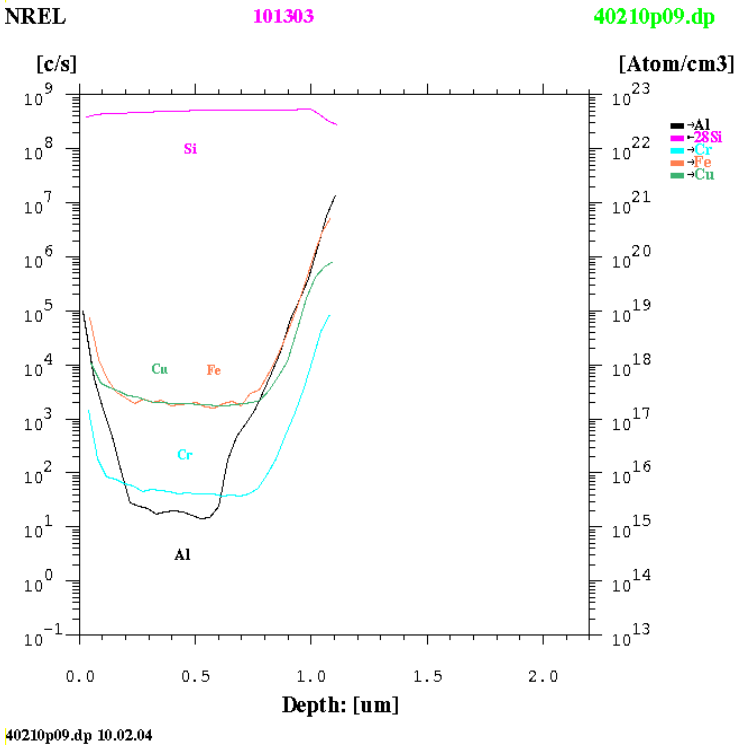

Figure 49 (b): Depth profiling of metallic impurities in poly-Si sample prepared by hot-wire CVD with filament temperature, T_f ~1650°C.

6.4 Comparison of RF PECVD and HWCVD in synthesizing μc-Si and poly-Si

We developed μc-Si films by RF PECVD and poly-Si films by hot-wire CVD in the same reactor. In both cases, we set the substrate temperature 250°C, however, under similar silane to hydrogen ratio and chamber pressure, we obtained poly-Si films in case of hot-wire CVD and μc-Si films for RF PECVD, indicating, under same process condition, atomic hydrogen concentration (causes microcrystalline to polycrystalline transition) is much higher in hot-wire CVD than RF CVD, in other words, process gas silane is fully decomposed in heated filament, creating large concentration of atomic hydrogen. We checked the actual substrate temperature during hot-wire CVD processing for 250ºC setting temperature, by looking at uniformity of the films for with and without setting temperature, the uniformity drastically varies when setting temperature is zero, indicating thermal radiation received by the substrate from the filament is comparable or lower than the heat supplied by the setting temperature. Therefore, the substrate temperature is dominated by the setting temperature. In combined plasma and hot-wire CVD, there will be a competition between heated filament and energetic electron in decomposing silane, our experimental result suggests that nearly 50% of silane is decomposed by heated wire on the other hand gas utilization in RF PECVD is very low 10 to 15%. So, in combined plasma and hot-wire CVD process, it is expected that the thin-film growth will be dominated by hot-wire CVD process. This fact will ensure that combined plasma and hot-wire CVD will be capable of preparing large area uniform thin silicon films since the feasibility of fabricating large-area uniform μc-Si and poly-Si films by hot-wire CVD has already been demonstrated [21]. However, it has been reported by United Solar and EPV, Inc that fabrication of large-area μc-Si thin film solar cells is clearly a problem in case of plasma CVD (RF PECVD and VHF PECVD). In addition, substrate temperature in combined plasma and hot-wire CVD could be significantly lower to prepare μc-Si and poly-Si films, owing to the fact that large concentration of atomic hydrogen is usually available in the combined process. The total concentration of atomic hydrogen in combined plasma and hot-wire CVD process, can be higher or lower compared to either plasma CVD or hot-wire CVD process, depending on chamber pressure, silane and hydrogen flow because of recombination of atomic hydrogen. In addition to large density of atomic hydrogen, ionic species in combined plasma CVD will generate ion bombardment, which, is expected to reduce defect density, compared to films prepared with only hot-wire CVD. Thus, we can conclude that the combined plasma and hot-wire CVD is a promising technique to prepare μc-Si and poly-Si films with high growth rate and low defect density as well as it has capability of depositing large-area thin silicon films.

6.5 Summary and conclusions

1. We have completed the fabrication of combined plasma and hot-wire CVD reactor. The system can operate in three different modes, RF PECVD, hot-wire CVD and combined plasma and hot-wire CVD.

2. We fabricated an innovative design of the ceramics filament holder to minimize impurities in the silicon layer and to create confinement effect of thermal radiation from the filament to lower substrate temperature. Because of ceramics filament holder, we call the hot-wire CVD process as ceramics hot-wire CVD.

3. We developed highly photoconductive a-Si:H films and identified process parameters for amorphous-to-microcrystalline silicon transition regime.

4. We developed optimum process condition to synthesize polycrystalline silicon thin films with (111) orientation on glass substrate at low temperature by ceramics hot-wire CVD.

5. The poly-Si films, we developed have 'pentagonal' and 'hexagonal' rings, distributed throughout the surface morphology (AFM). This type of specific geometrical pattern on the surface morphology of poly-Si films has never been observed before.

6. From scanning electron microscopy, we observed grain size increases with increasing filament temperature and a particular pattern of distribution of grains has also been observed for films prepared with 1800ºC filament temperature and 20:1 hydrogen dilution.

7. We found in ceramics hot-wire CVD, hydrogen dilution and filament temperature are the critical parameters control the nucleation of grains on glass substrate and hence the grain size and crystallographic quality of the grains.

8. AFM phase image also provides grain size and distribution of grains, we observed nucleation density of grains increases and grain size decreases with increasing H-dilution. The apparent contradiction between the observation from SEM and AFM phase is not clear at this moment.

9. X-ray diffraction show preferential growth of (111) peak on glass substrate as well as we observed doublet in the (111) peak and the peak at slightly higher 2θ decreases with H-dilution. The doublet formation at (111) peak position may be linked to the formation of different phase of c-Si or 'pentagonal' and 'hexagonal' rings visible on the surface.

10. Raman spectroscopy reveals there is no amorphous silicon phase in the materials, only peaks at 380 cm^{-1}, 507 cm^{-1} and 520cm^{-1} have been observed. The 507 cm^{-1} and 520 cm^{-1} peaks are transverse optical mode of c-Si which are attributed to the grain and grain boundaries. The 380 cm^{-1} peak indicates presence of second phase of crystalline silicon, called Si-XII(r8). Raman spectroscopy and XRD clearly show that we developed poly-Si films having two phase structure on glass substrate at low temperature (250°C).

11. The 507 cm^{-1} and 520cm^{-1} Raman peak appear nearly equal strength irrespective of growth conditions, in the literature the 507 cm^{-1} peak is assigned to the grain boundary, which seems to be questionable since the volume fraction of grains and grain boundaries varies with H-dilution.

12. The growth of (111) preferential orientation, 'pentagonal' and 'hexagonal' rings, doublet formation at the (111) peak position and the existence second phase of c-Si, i.e. Si-XII(r8), indicates 'confinement of thermal radiation from the filament' by ceramics filament holder is not only effective in thermally energies the reacting species to lower the substrate temperature but also creating environment for the formation new type of poly-Si films.

13. SIMS depth profiling analysis show that chamber wall having no outgassing or minimum outgassing has significant effect on the concentration of carbon across the film thickness. The physics mechanism responsible for this effect is not clear at this moment.

14. If the filament temperature is 1650°C, the tungsten (W) impurity is below the detection limit, however, other metallic impurities like Ni, Cu, Fe, Cu and Al are found in the samples. The work is at the early stage of development, we believe, we can reduce the metallic impurities by modifying the electrical connection between tungsten wire and the current carrying wire.

15. We observed characteristic variation of carbon content across the hot-wire CVD films, providing an insight about the growth process. We also observed high concentration of carbon impurity in HWCVD poly-Si films compared to films by RF-PECVD under similar conditions.

16. The concentration of oxygen (O) increases only by a factor 2 to 3, when hot-wire CVD films are compared with plasma deposited films.

17. We developed infrared photocurrent spectroscopy to estimate defect density in the absorber layers directly in the solar cells. We performed infrared photocurrent measurement to determine the defect density of intrinsic layer in μc-Si solar cells fabricated by EPV and correlated with their solar cells performances.

18. Syracuse University and EPV developed effective collaboration to make progress on μc-Si materials development and to improve solar cells performance.

7. Summary and Outlook

In summary, great strides have been made in the preparation of nc-Si based solar cells in the most demanding environment of low-cost, single chamber system by RF-PECVD on practical, commercially available SnO_2/glass superstrates using mediocre ZnO/Al back contacts. Our R&D activities have not focused on one-of-a-kind, laboratory-only solar cells. Rather, we have been looking for realistic solutions to depositing nc-Si solar cells within the general confines of existing manufacturing processes and equipment established for p-i-n type a-Si PV modules.

Through extensive and relentless experimentation, we have gained detailed knowledge about the seeding processes which are *absolutely critical* to the performance of p-i-n superstrate type, single junction nc-Si solar cells. Seeding is also crucial for a-Si/nc-Si tandem cells. A variety of seeding techniques have been evaluated to work with conventional SnO_2.

We have come to understand, and to able to control, contaminations by residual dopants and impurities during nc-Si solar cell fabrication for improved device parameters and reproducibility. We have evaluated a variety of deposition conditions for nc-Si absorbers in solar cells, and established correlations between cell performance, growth rate, degree of nanocrystallinity, and thickness and efficiency uniformity.

Importantly, we have established the key relationship between nc-Si device performance and the degree of crystallinity of the i-layer. Contrary to earlier popular misconception (which persists even today), nc-Si i-layers capable of high cell efficiency and good stability are made *only* under the 'near-the-edge' conditions, a very narrow processing window for *optimal* nc-Si:H absorber. This 'near-the-edge' requirement severely hinders improvements of nc-Si based PV device performance and uniformity, particularly at the needed high-growth rates.

Relatively efficient p-i-n type nc-Si single junction solar cells with *excellent stability* have been prepared in the low cost single chamber RF-PECVD vessel on inexpensive, commercially viable SnO_2 substrates using mediocre ZnO/Al back contact. The highest efficiency, confirmed by NREL, is 6.5% for a single junction solar cell produced on ZnO-coated SnO_2 superstrate without the benefit of anti-reflection (AR) coating. On bare SnO_2 without thin ZnO over-coat, nc-Si efficiencies approaching 6% have been obtained. Some of the nc-Si solar cells show FF up to 71% and V_{oc} of 500-530 mV, which had been unthinkable values for single chamber processing of nc-Si solar cells until our successful demonstration of its feasibility.

We have examined a variety of effective and non-contaminating tunnel junctions for a-Si/nc-Si tandem cells, and successfully applied the ZnO-interlayer technique to fabricating a-Si/nc-Si 'micromorph' solar cells of good initial and post light-soaking efficiencies (as high as 8.7% after 500 hours of one-sun exposure) on mediocre ZnO/Al back contacts and SnO_2 front contacts. The initial efficiencies measured at EPV are in the neighborhood of 9%. Such good devices have resulted from improvements in tunnel junction, contamination control, and seeding procedure for nc-Si bottom cell. The 'micromorph' tandem cells show reasonable stability against prolonged light exposure. One-sun exposure has been found to be a more reliable test for tandem cell stability than 47-sun accelerated light soaking.

We have evaluated new TCOs, IMO and ITiO (molybdenum or titanium doped tin-oxide), for applications as front contact and back contact in nc-Si related PV devices. Excellent light trapping capability has been demonstrated by the ZnO/ITiO or ZnO/IMO bilayers that are also

resistant to hydrogen plasma. Further improvement in nc-Si solar cells will depend heavily on advanced optical engineering including the use of TCO/Ag back contact and anti-reflection film.

While we are encouraged by the recent nc-Si and a-Si/nc-Si device improvements which have established the viability our unconventional, low-cost approach to synthesizing nc-Si solar cells, we are mindful of the tremendous difficulties that still lie ahead. In particular, we must further validate our approach by improving the 'in-situ' Si based tunnel junctions for a-Si/nc-Si tandem devices with low cross-contamination, improving the uniformity of nc-Si device, obtaining high growth rates, improving optical engineering of the cells, and ultimately demonstrating high efficiency a-Si/nc-Si modules after light soaking. We have only taken the first step in a long and arduous journey. We now reiterate the high-priority areas and key questions for future activities:

- Gain basic understanding to the device supremacy of 'near-the-edge' nc-Si compared to nc-Si materials of higher degree of crystallinity (which often are mistakenly regarded as superior absorbers for solar cell applications). This central question has a direct bearing on small-area cell efficiency and module performance. It governs high-rate, large area (uniform), low-cost manufacturing of multi-junction PV modules containing nc-Si cells.
- Improve nc-Si device uniformity (not necessarily *thickness* uniformity) over large areas. Both seeding and nc-Si i-layer growth determine the properties of the resulting solar cells.
- Find a practical solution to relax the 'near-the-edge' requirement for nc-Si (see above).
- Effective 'in-situ' tunnel junction that satisfies the stringent demand for contamination control for tandem cells (far more difficult than single junction devices in single-chamber operation).
- More sophisticated optical engineering for higher J_{sc}: ZnO/Al or ZnO/Ag back contacts; More-textured front contact; More transparent TCO/glass; ZnO front contact; AR coating.
- Higher deposition rates compatible with good, uniform device performance.
- Study nc-Si materials prepared by alternative plasma chemistry, e.g., containing Cl or F. Plasma chemistry dominated by hydrogen requires too much excitation and too high a dilution ratio of hydrogen to silane in the conventional $H_2 + SiH_4$ gas mixtures.
- Develop VHF-PECVD that can uniformly deposit nc-Si at lower pressure with low defects.
- Develop more stable a-Si top-cells such that higher J_{sc} (thicker cells) can be realized.

At Syracuse University (SU), thin films of microcrystalline Si (and possibly polycrystalline Si) have been prepared by the novel ceramics-HWCVD technique, and μc-Si films have been produced by plasma CVD. The microstructures, morphologies, and compositions of the samples have been characterized. A new phase for silicon, in the 'poly-Si' films deposited by HWCVD at low temperatures, has been proposed. An infrared photocurrent spectroscopy technique has been developed to estimate defect absorption of nc-Si absorber in solar cells. See Section 6 for more detailed summary and conclusions regarding the work performed at SU.

References

[1] J. Meier, P. Torres, R. Platz, S. Dubail, U. Kroll, J.A. Anna Selvan, et al., H. Keppner, A. Shah, K.-D. Ufert, P. Ginnoules, and J. Koehler, *MRS Symp. Proc.* Vol. 420, pp. 3 (1996). For a more recent review, see, e.g., A. Shah, J. Meier, E. Vallat-Sauvain, C. Droz, U. Kroll, N. Wyrsch, J. Guillet, and U. Graf, *Thin Solid Films* Vol. 403-404, p.179-187 (2002).

[2] See, e.g., J. Meier, J. Spitznagel, U. Kroll, C. Bucher, S. Fay, T. Moriarty, and A. Shah, Proc. WCPEC-3 (Osaka, Japan, May 11-18, 2003), p.1544 (published in 2004).

[3] T. Matsui, M. Kondo, and A. Matsuda, *MRS Symp. Proc.* Vol. 808 (2004, in press).

[4] B. Rech, J. Muller, T. Repmann, *et al.*, *MRS Symp. Proc.* 762, A3.1.1 (2003). T. Roschek, T. Repmann, J. Mueller, B. Rech, and H. Wagner, *Conf. Rec. 28th IEEE PVSC*, p.150 (2000).

[5] M. Yoshimi, T. Sasaki, T. Sawada, T. Suezaki, T. Meguro, T. Matsuda, & K. Yamamoto, *Conf. Proc. of WCPEC-3* (Osaka, Japan, May 2003), pp.1566 (published in 2004). Also see an earlier paper by K. Yamamoto, M. Yoshimi, Y. Tawada, Y. Okamoto, and A. Nakajima, *Tech. Digest 11th Internat. PV Sci. & Engineer. Conf.*, Sapporo, Japan, p.225 (1999).

[6] "Massive Parallel Processing for low-cost a-Si Production", Alan E. Delahoy, Yuan-Min Li, J.A. Anna Selvan, L. Chen, A. Varvar, and H. Volltrauer*, Conf. Proc. of "PV in Europe Conference"*, October 7-11, 2002 (Rome, Italy), p.444 (published in 2003).

[7] J.A. Anna Selvan, Yuan-Min Li, A.E. Delahoy, L. Chen, H. Volltrauer, A. Varvar, D. Jackson, N.B. Urli, R. Lyndall, Z. Kiss, *Proc. WCPEC-3* (Osaka, Japan), pp.1899 (2003).

[8] Yuan-Min Li, J.A. Anna Selvan, and L. Li, *Proc. WCPEC-3* (Osaka, Japan), p.1788 (2003). More recent results, including a-Si/nc-Si tandem solar cells, are presented in this report.

[9] J.A. Anna Selvan, "ZnO for Thin Film Solar Cells", published by UFO Atelier fur Gestaltung & Verlag, Germany, ISBN 3-930803-60-7 (October, 1998).

[10] Liwei Li, Yuan-Min Li, J.A. Anna Selvan, A.E. Delahoy, and R.A. Levy, *MRS Symp. Proc.* Vol. 762, p.A5.15.1 (2003).

[11] "Evaluation of Ar Diluted Silane PECVD for Thin Film Si:H Based Solar Cells", J.A. Anna Selvan, Y.-M. Li, Liwei Li, and Alan E. Delahoy, *Mat. Res. Soc. Symp. Proc.* Vol. 808 (MRS Spring Meeting 2004, San Francisco), pp.A9.46.1 (MRS, Pittsburgh, PA, 2004).

[12] V.L. Dalal, P. Sharma, D. Staab, M. Noack, and K. Han, *Mat.Res.Soc. Symp. Proc.* Vol. 808, p.A8.2.1 (2004).

[13] S. Koynov, R. Schwarz, T. Fischer, S. Grebner, and H. Munder, *Jpn. J. Appl. Phys.* 33, Pt.1, No.8, p.4534 (1994).

[14] H. Fujiwara, M. Kondo, and A. Matsuda, *Jpn. J. Appl. Phys.* 41, p.2821 (2002).

[15] "Fabrication and Characterization of Microcrystalline Silicon Solar Cells", Liwei Li, Ph.D. Thesis (Materials Science and Engin.), New Jersey Institute of Technology, January, 2004.

[16] "A new light-trapping TCO for nc-Si solar cells", J.A. Anna Selvan, A.E. Delahoy, S. Guo, and Y. Li, Tech. Digest 14th Int. PVSEC (Bangkok, Thailand), pp.179 (January, 2004).

[17] M. Vanecek, A. Poruba, Z. Remes, J. Rosa, S. Kamba, V. Vorlicek, J. Meier, and A. Shah, *J. Non-Cryst. Solids* 266-269, pp.519-523 (2000).

[18] T. Unold, R. Brueggemann, J. P. Kleider, and C. Longeaud, *J. Non-Cryst. Solids* 266-269, pp.325 (2000).

[19] S. Klein, F. Finger, R. Carius, H. Wagner, M. Stutzmann, *Thin Solid Films*, 305-309 (2001).

[20] J.A. Anna Selvan, Y. Li, S. Guo, A.E. Delahoy, *Proc.19th EPVSEC* (Paris, 5/2004, in press).

[21] A. R. Middya, A. Lloret, J. Perrin, J. Huc, J. L. Moncel, J. Y. Parey and G. Rose, *Mat. Res. Soc. Symp. Proc.* Vol. 377, pp.119 (1995).

[22] A. R. Middya, J. Guillet, R. Brenot, J. Perrin, J. E. Bouree, C. Longeaud and J. P. Kleider, *Mat. Res. Soc. Symp. Proc.* Vol. 467, pp.271 (1997).

[23] "Hot-wire chemical vapor deposition of Polycrystalline silicon thin films", A. R. Middya, J. Guillet, J. Perrin, A. Lloret and Jean-Eric Bouree, Proceedings of the *13th European Photovoltaic Solar Energy Conference*, edited by W. Freisleben, W. Palz, H. A. Ossenbrink and P. Helm (H.S. Stephens & Associates), pp.1704 (1995).

[24] S. B. Concari and R. H. Buitrago, Semiconductor *Scien. and Technol*. 18, pp.864 (2003).

[25] J. E. Bouree, J. Guillet, C. Grattepain and J. Chaumont, *Thin Solid Films* 430, 110 (2003).

REPORT DOCUMENTATION PAGE

Form Approved
OMB No. 0704-0188

PLEASE DO NOT RETURN YOUR FORM TO THE ABOVE ORGANIZATION.

1. REPORT DATE *(DD-MM-YYYY)*	2. REPORT TYPE	3. DATES COVERED *(From - To)*
December 2004	Subcontractor Report	1 May 2002–31 July 2004

4. TITLE AND SUBTITLE
Development of Advanced Deposition Technology for Microcrystalline Si Based Solar Cells and Modules: Final Technical Report, 1 May 2002–31 July 2004

5a. CONTRACT NUMBER
DE-AC36-99-GO10337

5b. GRANT NUMBER

5c. PROGRAM ELEMENT NUMBER

6. AUTHOR(S)
Y.-M. Li

5d. PROJECT NUMBER
NREL/SR-520-37195

5e. TASK NUMBER
PVB55101

5f. WORK UNIT NUMBER

7. PERFORMING ORGANIZATION NAME(S) AND ADDRESS(ES)
Energy Photovoltaics, Inc.
P.O. Box 7456
Princeton, NJ 08543

8. PERFORMING ORGANIZATION REPORT NUMBER
ZDJ-2-30630-28

9. SPONSORING/MONITORING AGENCY NAME(S) AND ADDRESS(ES)
National Renewable Energy Laboratory
1617 Cole Blvd.
Golden, CO 80401-3393

10. SPONSOR/MONITOR'S ACRONYM(S)
NREL

11. SPONSORING/MONITORING AGENCY REPORT NUMBER
NREL/SR-520-37195

12. DISTRIBUTION AVAILABILITY STATEMENT
National Technical Information Service
U.S. Department of Commerce
5285 Port Royal Road
Springfield, VA 22161

13. SUPPLEMENTARY NOTES
NREL Technical Monitor: Bolko von Roedern

14. ABSTRACT *(Maximum 200 Words)*

The key objective of this subcontract was to take the first steps to extend the radio-frequency plasma-enhanced chemical vapor deposition (RF-PECVD) manufacturing technology of Energy Photovoltaics, Inc. (EPV), to the promising field of a-Si/nc-Si solar cell fabrication by demonstrating 'proof-of-concept' devices of good efficiencies that previously were believed to be unobtainable in single-chamber reactors owing to contamination problems. A complementary goal was to find a new high-rate deposition method that can conceivably be deployed in large PECVD-type reactors. We emphasize that our goal was *not* to produce 'champion' devices of near-record efficiencies, but rather, to achieve modestly high efficiencies using a far simpler (cheaper) system, via practical processing methods and materials. To directly attack issues in solar-cell fabrication at EPV, the nc-Si thin films were studied almost *exclusively* in the p-i-n device configuration (as absorbers or i-layers), not as stand-alone films. Highly efficient, p-i-n type, nc-Si-based solar cells are generally grown on expensive, laboratory superstrates, such as custom ZnO/glass of high texture (granular surface) and low absorption. Also standard was the use of a highly effective back-reflector ZnO/Ag, where the ZnO can be surface-textured for efficient diffuse reflection.

15. SUBJECT TERMS
PV : thin film; module; crystalline; solar cells; manufacturer; microcrystalline silicon (μc-Si); seeding procedure; hot-wire chemical vapor deposition (HWCVD); amorphous; infrared photocurrent spectroscopy; impurity; scanning electron spectroscopy (SEM); tandem; radio-frequency plasma-enhanced chemical vapor deposition (RF-PECVD)

16. SECURITY CLASSIFICATION OF:			17. LIMITATION OF ABSTRACT	18. NUMBER OF PAGES	19a. NAME OF RESPONSIBLE PERSON
a. REPORT	b. ABSTRACT	c. THIS PAGE			19b. TELEPONE NUMBER (*Include area code*)
Unclassified	Unclassified	Unclassified	UL		